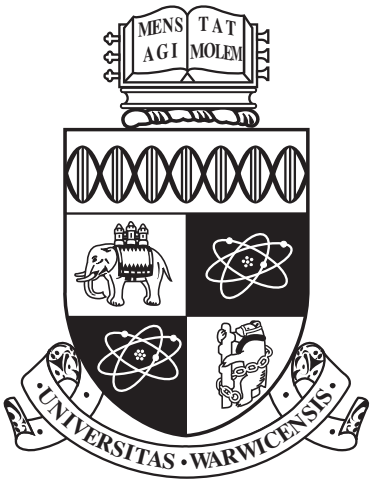

Accurate Free Energy Methods for Model Organic Solids

by

Sally Jane Bridgwater

Thesis

Submitted to the University of Warwick

for the degree of

Doctor of Philosophy

Department of Physics

July 2015

THE UNIVERSITY OF
WARWICK

Contents

List of Tables

List of Figures

Acknowledgments

I would firstly like to thank Dr. David Quigley for his guidance, the insight he has given me into this fascinating subject and from whom I have learned a lot. I would also like to thank Professor Mike Allen; without his help and support this thesis would never have happened.

I have had many interesting discussions about my work and would especially like to thank Dr. Bart Vorselaars for his support and patience.

Getting through my PhD has required more than just academic support and so I would like to thank all the many people who have helped me achieve the necessary caffeination to start, continue and end the day. The main culprits area Aaron Brown, Anja Humpert, Catherine Mackay, Michael Ambler, Sam Brown and Volker Keinhorst. Young Michael, you have learned well. From this point forward, you will be known as... Young Neil. The support of my friends and family has meant a lot to me during this time, especially Benjamin Davis for listening to me and giving me a push (or a beer) when I needed it.

Over the years many people have been and gone but PS1.31 has always been there for me.

Declarations

I hereby declare that the research presented in this thesis is my own work, except where acknowledged with appropriate citations. No part of this thesis has previously been submitted at this or any other university.

Abstract

We discuss existing free energy methods for use with investigation of solid-solid polymorphism. An alternative implementation for phase switch Monte Carlo is introduced which samples from two synchronised Markov chains exploring both polymorphs, using a set of generalised coordinates to transform between Markov chains. This is validated against the existing results for face-centred cubic (fcc) and hexagonal close-packed (hcp) hard sphere crystals.

The extension to more complex crystals including flexibility and constraints is explored. This extension is applied to a hard sphere model of linear alkanes. A phase transition in density is accurately located between two polymorphs of n-butane with increasing density; this is suggested as a rigorous benchmark for free energy methods. We also demonstrate the importance of including anisotropic volume moves when simulating crystalline solids.

Generalised coordinates for any fully flexible molecular system of soft particles are presented. These are used to investigate a coarse-grain model of cholesterol in regards to the polymorphic transition between two anhydrous cholesterol crystals. A phase transition in temperature is found and the limitations in the model are discussed.

Abbreviations

CBMC Configurational-bias Monte Carlo

CG Coarse-grain

CP Close-packed

FCC Face-centred cubic

HCP Hexagonal close packed

MC Monte Carlo

MD Molecular dynamics

MPI Message passing interface

PDF Probability distribution function

PS Phase switch

PSMC Phase switch Monte Carlo

RDF Radial distribution function

TI Thermodynamic integration

Chapter 1

Introduction

The properties of crystalline materials are dependent on small atomic differences between crystal structures. In a system with more than one possible structure, these polymorphs can have completely difference macrostructures and chemistry. When the crystals are biologically relevant, like cholesterol, insight into the phase transition between polymorphs helps our understanding of their role in larger processes such as the crystallisation of cholesterol in cell membranes.

Polymorphism describes the fact that certain substances can exist in different structures; we will only discuss crystalline polymorphism. Polymorphism is relevant to a large number of fields, particularly the pharmaceutical industry. Here much work is done on categorising and detecting polymorphs; it is necessary to check for polymorphism in drugs before they are submitted for registration due to the potential that the drug created is not the most stable phase. Experiments are the major contributor in the field, however, computer simulations can be invaluable in guiding these studies.

To simulate these systems we need a model that describes the system with all the relevant chemistry and physics included. By their nature models are not exact; we approximate interactions between particles to recreate their behaviour. The limit on the accuracy of models is related to the computational effort needed, increases in realism come at the penalty of computational cost. To further investigate polymorphism we must ensure that our model system is accurate enough to include it. Therefore we must explore the polymorphic nature of our model and, if it is not present, the model needs to be iteratively modified until the appropriate behaviour exists.

There has been a lot of investigation into organic crystal structure prediction using computational models. Theoretically from a single molecule and a set of

conditions, we can calculate the lowest energy structure at 0K. This is the most stable crystal structure at the given parameters. However, in the fifth blind test of crystal structure prediction [28], there was only one correct structure predicted for any of the three molecules given. The only structure that was successfully predicted was for the smallest and simplest rigid molecule. This is because the calculations cannot incorporate entropic effects. Hence we need to look at more than just statics to reliably calculate phase transitions and stable crystal structures. Flexibility in the molecules in crystals also incorporate more degrees of freedom and hence increase the complications in calculations.

Crystal nucleation is not very well understood; there is a large gap between theory and experiment in pharmaceutical and organic crystals. It is difficult to experimentally investigate crystal nucleation due to the small nature of the initial nuclei. Once they can be experimentally observed, the nuclei are too large to give much information on the early process. Hysteresis in the transition also presents a problem for experimental calculations. Therefore, computer simulation is a useful tool to probe this problem with. Simulations are used to study pathways and nucleation rates on the atomic level. This gives us more information about the process of solid-solid phase transitions. To apply these techniques we need a model of the system that incorporates: a) all phases under investigation, b) has a known phase transition point and c) is not unreasonably expensive to compute.

Models are fitted to reproduce specific results and behaviour and hence they are not necessarily valid beyond the regime used. Testing is needed to ensure any desired properties exist; re-fitting or perturbing the model may be necessary to ensure this.

Calculating the free energy difference between polymorphs tells us which phase is the most stable under the given conditions. When the free energy difference changes sign, we know that a phase transition has occurred. From this we can map out the solid phase diagram of our model. We need to be able to accurately calculate the free energy difference to ensure our transition point is clearly defined. Free energies are not simple to calculate so we need to employ advanced simulation techniques.

The ultimate aim of this work is to investigate the solid-solid phase transition in anhydrous cholesterol.

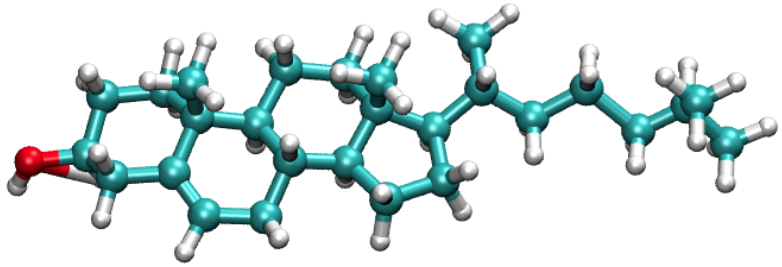

Figure 1.1: Computer graphics visualisation of a cholesterol molecule, Carbon atoms are blue, hydrogen are white and oxygen are red.

1.1 Cholesterol

Cholesterol is an organic, biological molecule with a unique structure and roles in the body, Figure 1.1. It is comprised of a planar multi-ring of carbon atoms, and on one side of these rings methyls are attached. This gives the molecule a smooth and a rough face, which provides directionality. An alcohol, hydrophilic head leads to orientation in bilayers and forms pseudo-symmetric hydrogen bonds in the crystal phases. A flexible tail adds mobility and length. The importance of this molecular structure has been reported in many studies relating to its contribution in bilayers and mammalian membranes.

1.1.1 Experimental research

Cholesterol plays a key role in bilayers, as a rigidity regulator, and in the transfer of molecules across the membrane [120, 54]. As well as its role inside bilayers, cholesterol has been widely studied in human plaques and bile [12, 19, 14, 40–42, 44, 107]. Work by Abela et al. [2] has shown that the crystallisation of cholesterol has a key role to play in heart attacks and strokes [2, 1]. Figure 1.2 shows spikes of cholesterol piercing through plaque layers.

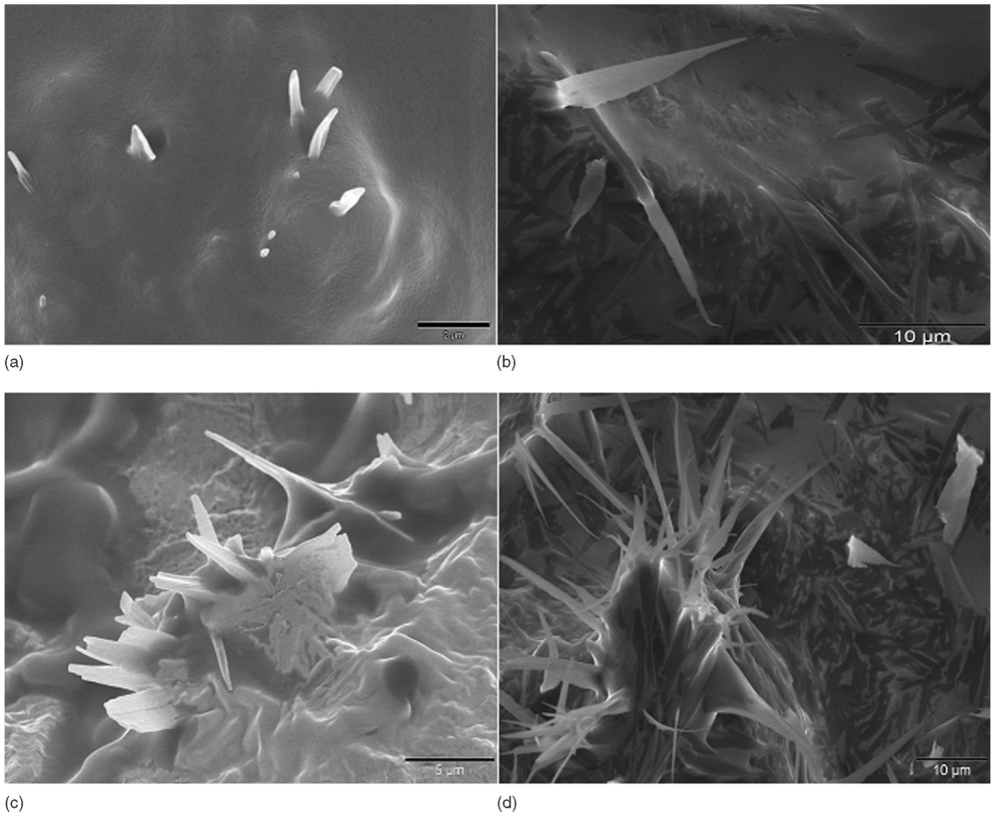

Figure 1.2: Scanning electron microscopy demonstrating perforation of a membrane by single cholesterol crystals following crystallisation (a,b). The sharp tips of cholesterol crystals are seen cutting through and disrupting the membrane. Other examples at other sites demonstrate crystals in clusters protruding through the membrane during an in vitro study (c,d), reproduced from Abela and Aziz [1]

A crystal structure of cholesterol has been known since 1981 when it was fitted to X-ray data by Shieh et al. [95, 94], and this is shown in Figure 1.3.

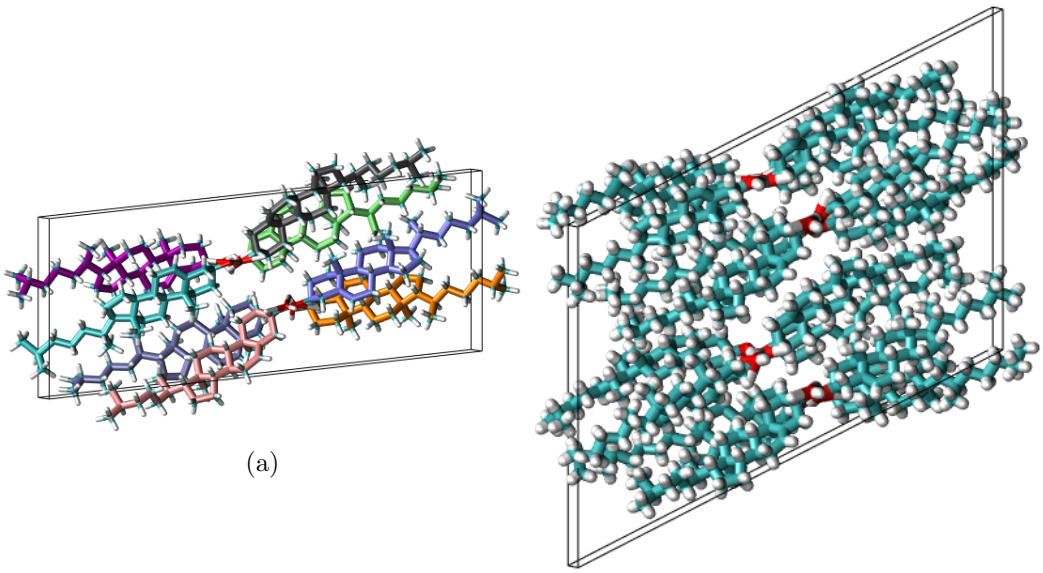

(a) (b)

Figure 1.3: Experimentally derived structures of anhydrous cholesterol: a) low temperature phase; b) high temperature phase.

There is a polymorphic phase transition at 308K. Hsu and Nordman [51] have characterised the structure of this high temperature phase of anhydrous cholesterol [51, 52], as shown in Figure 1.3. The unit cell doubles along the a axis to contain 16 molecules compared to 8 in the low temperature phase; this increase is highly unusual. The study used augmented X-ray data to refine the structure with large amounts of data needed due to the high thermal motion of the hydrocarbon tails. It was shown that there is very little structural difference between the two polymorphs.

1.2 Summary

This thesis is concerned with applying and extending methods to calculate free energy difference between polymorphs. This will be used to investigate polymorphic solid-solid phase transitions.

An introduction to molecular simulation methods will be given in chapter 2. We will critically discuss some of the existing simulation methods for calculating free energy differences in chapter 3.

Then in chapter 4 the phase switch Monte Carlo (MC) method for calculating free energy differences will be explained and our results from implementing a non-standard interpretation of the method will be compared with the existing literature. New work on anisotropic compared to isotropic volume moves will be presented

along with a discussion of stacking of hard sphere crystals.

The phase switch method will be extended to hard sphere molecule systems with internal degrees of freedom, specifically looking at butane crystals in chapter 5. The code Ponders, written by the author, is used to locate the phase transition in the hard sphere butane model that was not known to exist previously.

A discussion of the existing work on the simulation of crystalline cholesterol will take place in chapter 6; this will motivate our investigation of cholesterol.

Next the extension of phase switch Monte Carlo to fully flexible, soft potential models will be discussed in chapter 7 and applied to a coarse-grain model of cholesterol. First our implementation of the model will be validated and then, using the author's code Phlex, we will investigate the stability of the two polymorphic phases of anhydrous cholesterol for biologically relevant temperatures.

Conclusions from the work in this thesis will be analysed in chapter 8.

Chapter 2

Background

This chapter will discuss the background behind molecular simulation. We will focus on how models are created with a specific look at coarse-grained potentials and one common method for obtaining them which is relevant to simulations in chapter 7. Thermodynamics and statistical mechanics will be discussed briefly as the building blocks to later work and as introduction to the Monte Carlo (MC) and molecular dynamics (MD) simulation methods. The chapter will finish by discussing analysis of error and how this will be achieved in the current work.

2.1 Models

When creating a model of our target system, we need to choose what level of detail to represent. The more detail we include, the greater the computational effort of running simulations; depending on the system we are modelling, certain details may be ignored. We must be aware of approximations made during the process of model creation.

We could use first principles quantum mechanics methods to simulate our system; this has the advantage of including the electrons explicitly. Due to this added complexity it is used for static calculations mainly and would be far too computationally intensive for our purposes. Classical methods describe interactions between atoms in terms of the internal potential energy of the system U based upon the configuration of the atoms and their relative distances/orientations and is generally calculated via a model potential in this work.

2.1.1 Potentials

Potentials, $V(\underline{r})$ are used to approximate interactions between particles; they are used in both MC and MD. This approximation is made when *ab initio* methods are too expensive, and where we are not interested in electronic properties and our problem does not depend critically on changes in electronic structure.

Potentials define the interaction energy between two or more particles and hence the energy hyper-surface over which the system moves. They contain implicit approximations and should be kept as simple as possible whilst containing all the relevant complexity. This empirical method depends on the ability to determine a simple set of equations to reasonably describe the local coordination details and interatomic separation between particles.

The potential energy of a system is often written as an expansion of interatomic parts

$$V(\underline{r}_1, ..., \underline{r}_N) = \sum_i V_1(\underline{r}_i) + \sum_{i<j} V_2(\underline{r}_i, \underline{r}_j) + \sum_{i<j<k} V_3(\underline{r}_i, \underline{r}_j, \underline{r}_k) + V_{many}. \qquad (2.1)$$

Self interactions, V_1 are generally ignored. We then must decide on a form for the higher order terms.

One class of potentials, that will be used in this thesis, divides interactions based upon whether the particles are bonded or not. In our work we use a fixed topology, so that if particle i is bonded to j at the start of the simulation it will remain so. Bonded potentials describe an energetic preference for molecules to adopt particular local geometries, i.e. the bond lengths, angles and dihedrals favoured by the quantum mechanics of chemical bonding. Non-bonded potentials describe van der Waals attraction and Pauli repulsion between atoms which are not connected directly in this topology. It is also common to exclude these interactions between atoms indirectly connected via two or three intermediate bonds (1-3 and 1-4 interactions).

Bonded potentials

Bonded potentials describe the interactions between bonded particles in a molecule. There are three common types of bonded potential:

1. Bond stretch : These are defined between two directly bonded particles, and they generally take the form of a harmonic spring with an equilibrium bond length r_0

$$U(r) = \frac{1}{2} K_b (r - r_0)^2, \qquad (2.2)$$

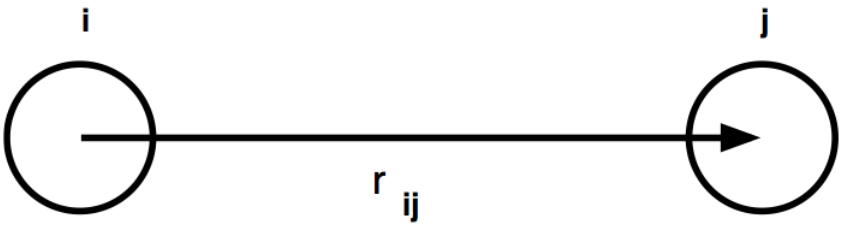

Figure 2.1: The interatomic bond vector

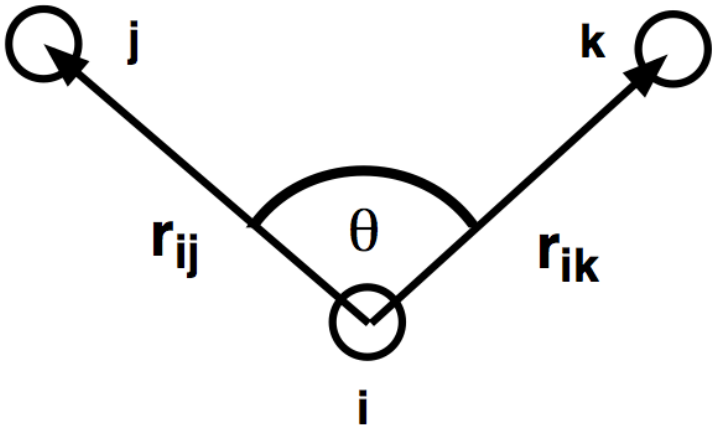

Figure 2.2: The interatomic bond angle and associated vectors

where K_b is the spring constant. This is shown in Figure 2.1.

2. Angle bending: These are defined as a function of the angle between two particles, both involving a common central atom. Again a harmonic energy penalty relative to a preferred bond angle θ_0 is common.

$$U(\theta) = \frac{1}{2} K_a (\theta - \theta_0)^2 \tag{2.3}$$

This is shown in Figure 2.2.

3. Torsional : These involve four particles, and can have multiple forms, with harmonic and cosine potentials being the most common. All based upon a change in angle of the planes described by the four particles, as shown in Figure 2.3.

In this work the breaking of bonds will not be included, since our study is only interested in phase transitions which do not involve bond breaking and only depend

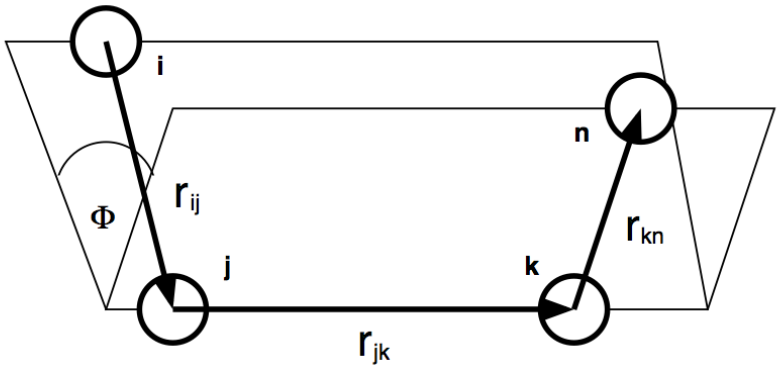

Figure 2.3: The dihedral/torsion angle and associated vectors

on differences in packing and conformation.

Non-bonded potentials

We assume that the interaction depends only upon the interatomic distance. The Coulomb long-range interaction is necessary for inclusion of electrostatics, but in this thesis it will not be included in any of the models studied. This is due to its high complexity because of the long range it acts over. Therefore, it should only be employed when the electrostatics of the system call for it, none of the systems studied in this thesis fall into that category.

Common forms for non-bonded van der Waals potentials are the Lennard-Jones 12-6 and the Buckingham potentials shown in Figure 2.4 and 2.5. The Lennard-Jones potential follows the form

$$V_{\mathrm{LJ}} = 4\epsilon \left[\left(\frac{\sigma}{r}\right)^{12} - \left(\frac{\sigma}{r}\right)^{6} \right], \tag{2.4}$$

where ϵ determines the well depth and σ is the point which the potential crosses the x-axis. The Buckingham potential is of the form

$$V_{\mathrm{Buck}} = A \exp[-Br] - \frac{C}{r^6}. \tag{2.5}$$

Care must be taken when dealing with this potential as it turns over for small r and so may cause problems at short interatomic distances.

Both potentials have parameters that need to be fitted to the model system being studied.

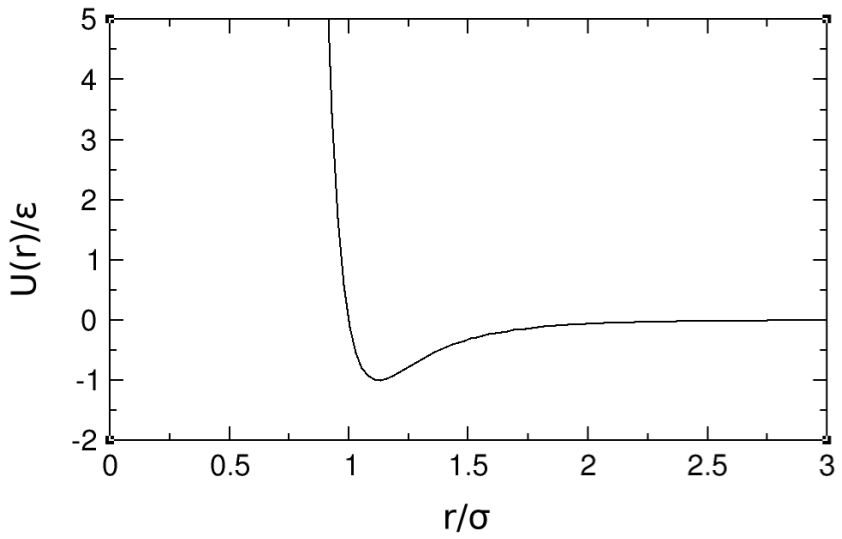

Figure 2.4: Lennard-Jones potential with $\sigma = 1.0$ and $\epsilon = 1.0$, 100 points

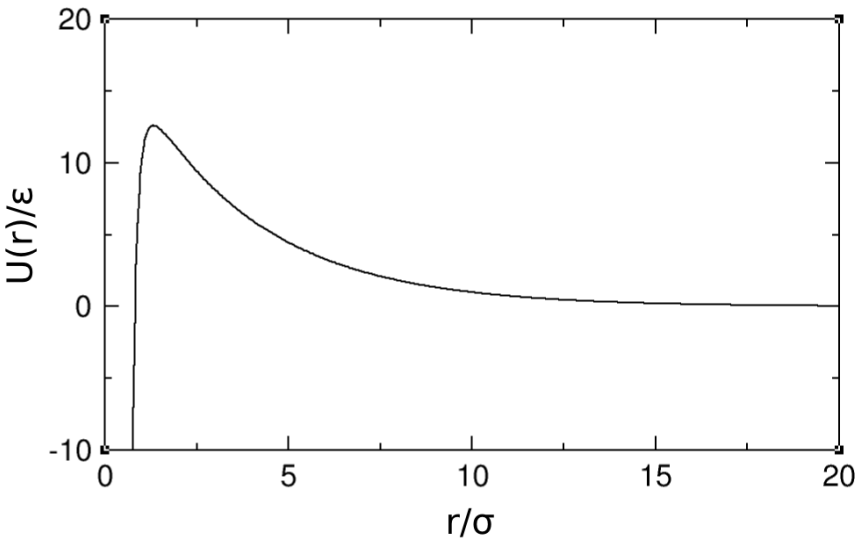

Figure 2.5: Buckingham potential with $A = 20.0$, $B = 0.3$ and $C = 4.5$, 500 points

Cutoffs

The difficulty with using a long-range potential is in the increased calculations needed between all particles that interact. Therefore to increase computational efficiency, reasonably short potentials are used. However, the potentials don't necessarily decay to zero at a convenient length so we employ a cutoff to ignore the potential beyond a certain distance. The simplest approach is to just ignore any interactions after a set distance. However, this can lead to a discontinuous step in the potential and hence the forces may lead to significant unphysical artefacts and influence the results . Therefore, potentials are often smoothed to zero over a short distance to allow the forces to smoothly change as well.

Exclusions

When calculating the energy of a system from the non-bonded potential, it is standard practice to exclude particles that are also part of bonded energy calculations together. There are different forms that these exclusions can take: $1-2$ exclusions only exclude particles that are in bonds only; $1-3$ exclude particles in angles with each other; $1-4$ exclude particles in torsions.

2.1.2 Coarse-graining Methods

One of the overarching problems in molecular computational science is the time-scale and length-scale gap between simulations and experimental methods. Experiments on average cannot resolve detail better than ms in time, whereas the entire length of an atomistic computer simulation will be around 100 ns; simulations are also limited in length to around 100 nm, but are often less.

One way to bridge the gap is to use coarse-grain (CG) models. These models represent an atomic system with a reduced number of degrees of freedom. Due to this reduction and elimination of fine-scale interactions, CG simulations require less resources and run faster than the equivalent all-atom simulation. Therefore, we can achieve orders of magnitude increase in time and length scales using this approach.

The main purpose of coarse-graining is to concentrate our model on essential features and average over the less significant ones. This suggests that we need a way of distinguishing between what is essential and what can be removed or averaged. Also this introduces the issue of how transferable the CG model will be: if we have optimised it at a certain state point, we cannot assume it will be valid for all other conditions. We might have averaged over features that become significant under other conditions.

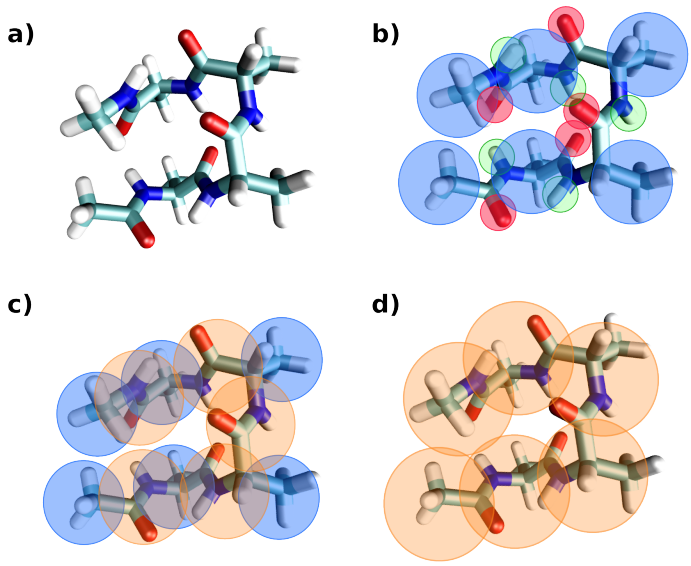

Figure 2.6: Possible levels of coarse-graining for polyalanine: a) atomistic b) coarse-grained hydrogens c) coarse-grained functional groups d) coarse-grained amino-acid residues.

Coarse-graining is particularly prevalent in the biological materials community due to the preponderance of large molecular systems such as proteins and lipids; these molecules cannot easily be simulated with all-atom models. CG models represent molecular systems by using interaction sites that correspond to groups of atoms, also referred to as beads. When coarse-graining a system, the term 'CG mapping' refers to the transformation from atomistic particles to the CG group interaction sites. This coordinate mapping converts between a group of atomistic Cartesian coordinates $\underline{\mathbf{r}}_i$ for particles i in the group to a CG bead site $\underline{\mathbf{R}}_I$

$$\underline{\mathbf{R}}_I = \sum_i c_{Ii}\underline{\mathbf{r}}_i \tag{2.6}$$

where c_{Ii} is some positive coefficient for example the centre of mass or some geometry for the associated group of atoms. Figure 2.6 shows atoms on a polymer being group into CG beads in different ways, and degrees of coarseness.

Coarse-grain models should reflect the 'correct physics' of the atomistic de-

tails that have been averaged over and provide underlying insight and accurate predictions. There are two main paradigms, 'top-down' and 'bottom-up'. The bottom-up approach describes when the CG model is built upon a more detailed model for the same system which may be first principles or, as we will discuss, a classical atomistic potential. The resultant CG model should reproduce the statistical thermodynamics of the original system.

Top-down strategies address the problem from the opposite direction by using experimental and larger scale data to construct a more fine-grained model. Our work will only focus on bottom-up approaches.

There are numerous coarse-graining schemes based upon reproducing different properties of the reference system, e.g. energetics or structural properties. CG potentials take the standard form, already discussed, with bond, angle, dihedral and non-bonded potentials between interaction sites. Each potential is modelled by a function and acts on a degree of freedom,

$$U(\underline{\mathbf{R}}) = \sum_{\xi} \sum_{\lambda} U_{\xi}(\psi_{\xi}(\underline{\mathbf{R}}_{\lambda})) \tag{2.7}$$

where ξ is the interaction modelled by U_{ξ}, a function of ψ_{ξ} which is a function of cartesian coordinates $\underline{\mathbf{R}}_{\lambda}$ for a set of particles λ.

In order to calculate this potential we need to decide what to compare between the CG and the atomistic reference model.

The pair correlation function, also known as the radial distribution function, of a system describes how density varies as a function of distance from a reference particle,

$$g(r) = \frac{\delta(\underline{r}_{ij} - \underline{r})}{4\pi r^2 \rho} \tag{2.8}$$

summed over pairs of particles.

For correlation-function based methods we describe a probability distribution $P_{\xi}(x|U)$ that samples ξ degree of freedom when the CG model has potential U. U_{ξ} is calculated so that the corresponding target, atomistic distribution $p_{\xi}(x)$ is reproduced,

$$P_{\xi}(x|U) = p_{\xi}(x). \tag{2.9}$$

There is no direct method for calculating potentials that are guaranteed to produce this target distribution. Therefore, iterative methods that converge towards the target distribution are commonly used, one of which is the inverse Boltzmann inversion method.

Iterative Boltzmann inversion

This method is relevant to the model studied in chapter 7.

To calculate the potentials for a CG model we require all pair correlations to match the reference. This obviously means that all the pair correlations in our CG model will be correct, but it neglects higher order correlations. The method involves simulating the target system and determining the RDF $g_{\text{ref}}(r)$ between the CG sites. Since the RDF is just the probability of separation which is also proportional to the Boltzmann distribution for that distance (see section 2.3), we can rearrange for the energy; this is for two particles only and ignores many-body correlation terms. Using this we can make a first guess at the CG potential W:

$$W^0(r) = -k_{\text{B}}T \ln(g_{\text{ref}}(r)). \tag{2.10}$$

We run our CG simulation with potential $W^0(r)$ and determine the RDF $g^0(r)$. The potential is iterated such that

$$W^i(r) = W^{i-1}(r) + k_{\text{B}}T \ln\left(\frac{g^{i-1}(r)}{g_{\text{ref}}(r)}\right). \tag{2.11}$$

We keep iterating over the potential and calculating the corresponding RDF until $g^i(r)$ is within some tolerance of $g_{\text{ref}}(r)$.

Since we are only converging our potential based upon pair interactions, this method can have convergence problems, especially for multi-component systems. The inverse Boltzmann method is suitable for dilute liquids as higher order correllations effects come into play at higher densities [87]. Inverse Boltzmann inversion assumes that non-bonded potentials are pair-wise and that all effective potentials are independent of each other. It has also been shown that for heterogenous systems of molecules with multiple interaction sites, directionality must be taken into account [20]. Care must be taken in the order of the optimisation of the potentials as they can affect each other. The suggested method is to start with the stiffest potential and work down in stiffness. This will still not remove the underlying issue.

Summary of coarse-graining

Coarse-graining methods should be used only whilst aware of the limitations and disadvantages. However, they are very useful for allowing us to study systems normally out of reach with standard techniques.

For molecular dynamics simulations we need to numerically calculate the derivative of the non-bonded potentials in order to obtain the necessary the forces

in the system. These can be very jagged and non-smooth, and so we must ensure that the potential goes to zero at the cutoff so there is not a discontinuity in the forces in molecular dynamics. We will see in later chapters that the potentials generated are not guaranteed to be smooth and may have large oscillations.

2.2 Thermodynamics

Thermodynamics describes the equilibrium states of macroscopic systems. The properties of these macroscopic systems can be fully specified by state variables, such as energy E and volume V.

The first law of thermodynamics states that the only way to change the internal energy U of a system in equilibrium is by interaction with the surroundings; that is by application of heat Q and work W.

$$dU = dQ + dW \tag{2.12}$$

This means that the internal energy of an isolated system is conserved.

The first law of thermodynamics has no preferential direction, we know, however, that heat flows from regions of high temperature to regions of low temperature. The second law of thermodynamics defines this preference

$$dS \geq \frac{dQ}{T} \tag{2.13}$$

where dS is the entropy variation in the system involving heat exchange dQ with a reservoir at temperature T. The equality in equation (2.13) occurs only for reversible processes. This shows us that the entropy is maximised at equilibrium with respect to any change of intensive variables, that is the equilibrium state is given by variables that maximise the entropy.

From the first and second laws of thermodynamics a system with a fixed number of particles N has an internal energy U defined as

$$dU = TdS - pdV \tag{2.14}$$

where U is a function of entropy S and volume V, p is the pressure and T the temperature. Using the chain rule, this can be written as

$$dU = \left(\frac{\partial U}{\partial S}\right)_V dS + \left(\frac{\partial U}{\partial V}\right)_S dV, \tag{2.15}$$

giving the following identities defining temperature and pressure of the system:

$$\left(\frac{\partial U}{\partial S}\right)_V = T \tag{2.16}$$

$$\left(\frac{\partial U}{\partial V}\right)_S = -p. \tag{2.17}$$

The Helmholtz free energy of a system is given by

$$\mathcal{F} \equiv U - ST, \tag{2.18}$$

and this corresponds to the energy that can be used as work from the system. Then by differentiating and applying Equation (2.14) we get

$$d\mathcal{F} = dU - TdS - SdT \tag{2.19}$$

$$= TdS - pdV - TdS - SdT \tag{2.20}$$

$$= -SdT - pdV, \tag{2.21}$$

where we can see that $\mathcal{F} = \mathcal{F}(T, V)$. Applying the chain rule similarly to equation (2.15) we see that,

$$d\mathcal{F} = \left(\frac{\partial \mathcal{F}}{\partial T}\right)_V dT + \left(\frac{\partial \mathcal{F}}{\partial V}\right)_T dV. \tag{2.22}$$

Comparing this to equation (2.21) we get derivatives in the free energy as,

$$\left(\frac{\partial \mathcal{F}}{\partial T}\right)_V = -S, \tag{2.23}$$

and

$$\left(\frac{\partial \mathcal{F}}{\partial V}\right)_T = -p. \tag{2.24}$$

Since from the second law (Equation 2.13) we know that entropy must be maximised at equilibrium, combining this with Equation (2.23) this means that the free energy is minimised in equilibrium.

The Gibbs free energy for a system of N particles at a constant pressure p and temperature T is

$$G \equiv F + pV, \tag{2.25}$$

and this quantity is also at a minimum in equilibrium, under conditions of fixed P and T.

2.3 Statistical Mechanics

Statistical physics is the use of statistical methods to study the behaviour of a macroscopic body when the microscopic behaviour cannot practically be described by mechanics alone. One key area of study is the transition of matter between different phases; how and under what conditions this occurs. An ensemble is the collection of microstates that can be realised by a system. At equilibrium the relative probability of each microstate is determined by the way in which that system is coupled to its environment.

Large systems have many microstates so we use probability distributions to sample the systems and calculate average values from them. The most commonly used distribution function is the Boltzmann function which applies to the distribution of molecules in an isolated system at thermal equilibrium. Where

$$B_i = e^{-\beta E_i}, \tag{2.26}$$

is the relative probability of sampling a particular microstate i. $\beta = \frac{1}{k_{\mathrm{B}}T}$ where k_{B} is the Boltzmann constant. Analytically, the behaviour of systems of particles can be studied through the use of the partition function Z from which many properties of the system can be derived

$$Z = \sum_i e^{-\beta E_i}. \tag{2.27}$$

The sum is over the all the microstates in the system with E_i being the energy of state i. The probability of being in state i is given by

$$P_i = \frac{1}{Z}\exp(-\beta E_i), \tag{2.28}$$

which is normalised such that $\sum_i P_i = 1$. The ratio of the probability for two states is

$$P_{ij} = \exp[-\beta(E_i - E_j)] \tag{2.29}$$

and is only dependent upon the difference in energy of the two systems.

The ensemble average of an observable A is

$$\langle \mathcal{A} \rangle_{ens} = \frac{\sum_i \exp(-E_i/k_{\mathrm{B}}T)\mathcal{A}_i}{\sum_j \exp(-E_j/k_{\mathrm{B}}T)}, \tag{2.30}$$

where $\mathcal{A}_i$ is the value of $\mathcal{A}$ in configuration i. This suggests that we can calculate the values for every state and compute the average value of $\mathcal{A}$. However, this is completely unfeasible. The number of states that contribute to the sum is huge

and hence we need to infer this value from a much smaller number of samples, introducing an uncertainty which will be discussed later in section 2.6.

2.3.1 Ensembles

Microcanonical ensemble

The microcanonical ensemble describes a system that is completely isolated from its surroundings, there is no exchange of energy. Therefore, the energy E in this system is constant, the number of particles N is also fixed and so is the volume V. Since the energy is constant, all accessible microstates have the same energy. This ensemble is difficult to achieve experimentally and hence it is not very prevalent. Since all the energies of the states must be the same the probability of being in a certain state is

$$P = \frac{1}{W} \tag{2.31}$$

where W is the number of microstates. This is so that the total probability is one.

Canonical ensemble

The canonical ensemble describes a system that is in contact with a heat bath, that is energy can be transferred between the system and the heat bath allowing microstates with a range of energies to be realised. The number of particles N and the volume V are fixed as well. The probability of being in a certain state of energy E_i for this ensemble is

$$P_i = \frac{1}{Z} e^{-E_i/(k_\mathrm{B}T)} \tag{2.32}$$

where the partition function is

$$Z(N, V, T) = \sum_i e^{-E_i/(k_\mathrm{B}T)}. \tag{2.33}$$

Grand canonical ensemble

In this ensemble the system is in contact with a heat bath and a particle bath. Therefore the energy and the number of particles fluctuate at equilibrium. The energy exchange depends upon the temperature of the heat bath T, and the particle exchange depends upon the chemical potential μ. Particles are exchanged such as to ensure the chemical potential is the same in the system and the particle bath.

The partition function for this ensemble is

$$\Omega(\mu, T, V) = \sum_{i,N} e^{-\beta[E_i(N)-\mu N]}. \tag{2.34}$$

Isothermal-isobaric ensemble

This ensemble is also known as the constant pressure and constant temperature (NPT) ensemble. The system is in contact with a heat bath and can be thought to be in contact with a piston driven by a constant pressure. The partition function of the isobaric-isothermal ensemble Δ is

$$\Delta(N, P, T) = \sum_{i,V} e^{[-\beta(E_i+PV)]} \tag{2.35}$$

2.3.2 Fluctuations

From the ensemble average of a sampled quantity equation 2.30, we can write down the mean squared fluctuation in $\mathcal{A}$

$$\langle \delta\mathcal{A}^2 \rangle = \langle \mathcal{A}^2 \rangle - \langle \mathcal{A} \rangle^2. \tag{2.36}$$

The magnitude of the fluctuations is dependent on the ensemble used.

In the NPT ensemble we can calculate fluctuations in enthalpy

$$\langle \delta\mathcal{H}^2 \rangle_{NPT} = k_{\mathrm{B}} T^2 C_P \tag{2.37}$$

where C_P is the heat capacity at constant pressure. The heat capacity at constant pressure can also be calculated as the gradient of the change in enthalpy versus temperature at constant pressure

$$C_p = (\partial\mathcal{H}/\partial T)_P. \tag{2.38}$$

2.4 Monte Carlo

Monte Carlo simulations sample members of an ensemble according to the Boltzmann distribution. MC simulation is not exact and so to get out any useful results we must take ensemble averages of the values required over many samples, Equation (2.30).

The normal sampling method is to use a stochastic algorithm in the form of a Markov chain, and the most often used is the Metropolis algorithm.

2.4.1 Metropolis algorithm

The Metropolis algorithm simulates a Markov process. In a Markov process, each new state of the system ν is generated in a random manner from the previous state μ creating a 'chain' of samples. The transition probability $P(\mu \to \nu)$ needs to satisfy the following:

1. Does not vary over time
2. Depends only on the properties of states μ and ν
3. $\sum_\nu P(\mu \to \nu) = 1$ for all states including $\nu = \mu$

The general form of the method is to propose a randomly generated move, calculate the change in energy due to this move, then accept or reject the move based upon the Boltzmann distribution. $A(\mu \to \nu)$ is the acceptance probability and determines how often the transition $\mu \to \nu$ is accepted. For this algorithm a Boltzmann distribution is used such that

$$A(\mu \to \nu) = \begin{cases} e^{-\beta \Delta E} & \text{if } \Delta E > 0 \\ 1 & \text{otherwise} \end{cases} \tag{2.39}$$

This is known as the Metropolis acceptance probability with ΔE being the change in energy the system undergoes in a transition from state μ to state ν in the canonical ensemble[75].

Two additional conditions also need to be satisfied by the process if the chain of configurations generated is to be representative of an equilibrium ensemble.

1. **Ergodicity**: It must be possible to reach every state of the system from any other state given enough transitions.
2. **Detailed Balance**: Is satisfied when the transition rates between each pair of states μ and ν are the same in both directions. The system should obey the following

$$\frac{P(\mu \to \nu)}{P(\nu \to \mu)} = \frac{g(\mu \to \nu) A(\mu \to \nu)}{g(\nu \to \mu) A(\nu \to \mu)} = e^{-\beta(E_\nu - E_\mu)} \tag{2.40}$$

   Here $g(\mu \to \nu)$ is the selection probability, with one for each possible transition between states from μ to ν. The Metropolis criterion satisfies this condition.

Since the algorithm depends only upon the energy difference between the current and proposed microstates, we may use unphysical moves on our system, this is the main advantage of Monte Carlo simulations.

2.4.2 Isobaric/isothermal

For the NPT ensemble the volume of the system is not fixed. This ensemble is widely used in our work and is of great importance when simulating crystalline materials under pressure.

The partition function is given by equation 2.35, the Metropolis acceptance criterion is accordingly

$$P(V_{\text{old}} \to V_{\text{new}}) = \{1, \exp[-\beta(\Delta E + P\Delta V) + N \ln(V_{\text{new}}/V_{\text{old}})]\}. \tag{2.41}$$

where $\Delta E = E_{\text{new}} - E_{\text{old}}$ and $\Delta V = V_{\text{new}} - V_{\text{old}}$. The volume acceptance is derived assuming uniform scaling in the volume, $V_{\text{new}} = V_{\text{old}} + \delta V$ where δV is distributed uniformly between $\pm\delta V_{\text{max}}$ which is a fixed extremum.

This acceptance criterion is derived for a system of N particles that are scaled with the volume expansion, such that their fractional positions remain the same, $\underline{s}^N = \underline{r}^N/L$ for cubic box of size L. When we are dealing with molecular systems, we do not want to scale each atom individually because we want to ensure the molecular bonding remains constant. Therefore we choose a consistent coordinate for the molecules and scale that by the volume change instead, keeping all intramolecular positions constant relative to this coordinate; the centre of mass for the molecule is often chosen. This means that our factor of N in the acceptance criterion should be changed to N_{mol} for molecular systems as we have reduced the number of degrees of freedom in the scaling of the positions term and our acceptance becomes

$$P(V_{\text{old}} \to V_{\text{new}}) = \{1, \exp[-\beta(\Delta E + P\Delta V) + N_{mol} \ln(V_{\text{new}}/V_{\text{old}})]\}. \tag{2.42}$$

Anisotropic scaling

When simulating crystalline solids and inhomogeneous systems only changing the box isotropically can lead to stresses in the system. Therefore we introduce an anisotropic isobaric/isothermal ensemble [79]. This will always be used in this work for simulating solids for the NPT ensemble, unless otherwise stated.

We work in terms of the cell matrix $\mathbf{h}$ defining the lattice vectors of the system. The cell matrix $\mathbf{h}$ is a 3×3 matrix $\mathbf{h} = ((a1, a2, a3), (b1, b2, b3), (c1, c2, c3))$, where the vectors $\mathbf{a} = (a1, a2, a3)$, $\mathbf{b} = (b1, b2, b3)$ and $\mathbf{c} = (c1, c2, c3)$ correspond with the three axes of the system. We want to ensure that one edge of the system is fixed, to simplify calculations. We ensure that the cell matrix has zero entries above the diagonal, a2, a3 and b3 and we only change the non-zero elements. This makes sure that the a vector is fixed along the x axis, that the b vector lies in

the $x-y$ plane and the c vector is free to move. This removes three degrees of freedom, which just correspond to rotations of the simulation cell and do not affect the free energy difference between polymorphs. The volume of the simulation box is $V = |\det \mathbf{h}| = (a1b2c3)$. Since only diagonal matrix elements will affect the volume, when we tweak one of these we use equation 2.42 as we are making a normal volume move, however, when we change any other element we are making a constant volume change and hence apply equation 2.39 instead.

2.5 Molecular Dynamics

Molecular dynamics (MD) involves classically integrating Newton's equations of motion to evolve coordinates $\mathbf{r}$ and momenta $\mathbf{p}$ in time and calculating forces from a model describing inter-particle interactions. A useful (for our purposes) implementation of MD will visit microstates with the same equilibrium probability as MC, allowing its use to compute ensemble averages.

A good integrating algorithm is crucial for molecular dynamics, Newton's equations of motion are time reversible and so the algorithm should be too. A very good algorithm is the velocity Verlet algorithm. The algorithm advances the co-ordinates and moments (velocity) by one timestep Δt,

$$\mathbf{p}(t + \frac{1}{2}\Delta t) = \mathbf{p}(t) + \frac{1}{2}\Delta \mathbf{f}(t) \tag{2.43}$$

$$\mathbf{r}(t + \Delta t) = \mathbf{r}(t) + \Delta t\ \mathbf{p}(t + \frac{1}{2}\Delta t)/m \tag{2.44}$$

$$\text{force calculation}$$

$$= \mathbf{r}(t) + \mathbf{p}(t)\Delta t + \frac{1}{2}f(t)/m\Delta t^2 \tag{2.45}$$

$$\mathbf{p}(t + \Delta t) = \mathbf{p}(t + \frac{1}{2}\Delta t) + \frac{1}{2}\Delta t\ \mathbf{f}(t + \Delta t). \tag{2.46}$$

$$\tag{2.47}$$

This algorithm preserves the area of phase space accessible, before and after a move, that is it is symplectic. We do not need to create special move sets for MD simulations, it is more general, but limited to physical pathways.

2.6 Error analysis

When reporting simulation results we need to include the uncertainty in the data. The simplest way to do this is to repeat our calculation many times and look at

the spread of the results. The average value is likely to be closer to the true value than an individual measurement. The standard deviation σ_s gives us a measure of the spread of our results and is often used to represent the uncertainty from a set of separate calculations.

$$\sigma_s = \sqrt{\frac{1}{N}\sum_i (x_i - \bar{x})^2} \tag{2.48}$$

Here x_i is sample i, $\bar{x}$ is the mean value of x and N is the total number of samples.

The standard error,

$$\sigma_e = \frac{\sigma_s}{\sqrt{N}} \tag{2.49}$$

measures the uncertainty in our estimate of the true mean of an observable, and this will converge to zero as we increase the number of samples to infinity and our sample mean converges exactly with the true mean.

When we average our data, we need to be aware of the correlation in our samples. If we sample too often, then our data will still be correlated and we will end up over counting the number of independent samples and hence underestimating the uncertainty. We can calculate the correlation function of our samples, defined as

$$G(t) = \langle x(t)x(0)\rangle - \langle x(t)\rangle\langle x(0)\rangle. \tag{2.50}$$

From this function we can fit it to an exponential and estimate the correlation length τ

$$G(t) \approx e^{\frac{-t}{\tau}}. \tag{2.51}$$

τ gives us a measure of the range over which fluctuations at one point are correlated with those in another region. If we only take every τ samples for our data set we can be sure that they are uncorrelated.

Chapter 3

Introduction to free energy methods for solids

Calculation of fluid-solid and solid-solid phase boundaries for a given molecular model has long been a difficult undertaking. The intuitive approach of locating this transition point by setting the system up in one phase and then heating/cooling across the transition is dominated by hysteresis. This obviously puts large bounds on the accuracy of the values that can be calculated since starting from each of the two phases will give highly variant results.

The hysteresis is due to the first-order nature of the phase transition and the resulting high free energy barrier between the two phases near coexistence. This barrier is caused by the free energy penalty for having a mixed-phase region due to the interfacial free energy from the interface between the two phases. This means that there is a cost for forming a mixed-phase region due to the need to form an interface between the two phases which disrupts the intermolecular bonding of both domains. Hence, for direct simulation of phase transitions we either need to start with a simulation that already includes the interface or eliminate the interface entirely. If an interface already exists then there is no new interfacial penalty for growth of one phase over the other, unless the interface expands or contracts. This means that the free energy barrier to mixed-phase coexistence has already been overcome and hysteresis should no longer be an issue.

When looking at solid-solid phase transitions, the creation of an interface is neither a simple nor obvious task. The boundary conditions that fit one phase are highly unlikely to match up with the other phase and so it is more general and widely applicable to use a method where no interface is needed. Also, when interfaces are present one must take into account the possible presence of more than

one crystallographic orientation that the interface can lie along. These differences would need to be fully investigated due to possible anisotropy between faces.

To calculate phase transitions we must look more closely at why a transition occurs and what makes one phase more stable than another.

Using the second law of thermodynamics, eq (2.13) we know that entropy must always increase which leads us to the Helmholtz free energy always being a minimum in equilibrium with respect to unconstrained variables; analogously for the Gibbs free energy at constant pressure. This implies that for a certain state point whichever phase has the lowest free energy will be the equilibrium state of the system. So we can define the point of transition as the point where the free energy difference between the phases changes sign.

The free energy of a system cannot be directly measured during a simulation as it cannot be calculated via an average of a thermodynamic observable as shown in section 2.3. This is due to it being directly related to the partition function Z and the volume of phase-space accessible to the system. However, the derivatives of the free energy can be calculated as an ensemble average from simulations, hence a set of methods exist where the free energy is obtained via integration over a path from a known reference state. This method forms the basis of thermodynamic integration upon which many methods are based.

Many methods used to calculate free energies in liquids and gases generally will not work for solids. The main branches of methods that cannot easily be applied to crystal phase transitions are methods involving an interface between phases and methods involving insertion and deletion of particles. The overriding reason for this inapplicability is due to the close packing and crystalline form of the solid phases.

In the grand canonical ensemble methods, particles need to be exchanged between two phases. The removal of a particle from a crystal introduces a vacancy in the structure, but the normal concentration of vacancies in solids is very low (of the order of 1 in 8000 particles) depending upon temperature and the vacancy formation energy; one would need a huge crystal for the number of vacancies to be reasonable.

One could also use a set of methods known as 'lattice dynamics' and treat the crystal as a harmonic solid [31]. However, this is a rather large approximation and only works well for very simple crystals at low temperature. Due to the nature of the approximation these methods do not work with large scale anharmonic motions at thermal energies; this is a major disadvantage. One advantage of these methods is the trivial inclusion of quantum effects, e.g. zero point energy. However, quantum effects can be ignored when classical length scales are reached. Similarly,

the computation cost in simulating an atomic system with a quantum treatment of nuclear dynamics included is exorbitant. For example, the unit cell of cholesterol has close to 1200 atoms. Soft matter comprises of physical systems that are strongly affected by thermal fluctuations and stresses, unlike hard crystalline systems, i.e. silicon, which are very resistant to permanent structural changes. Due to this, the approaches used when studying soft compared with hard solids are very different.

3.1 Thermodynamic integration

Thermodynamic integration in general can be applied to a wide range of systems. The main theme of the method is to integrate along a reversible path from a reference state to the state of interest.

As mentioned in section 2.2, the derivatives of the free energy can be calculated as ensemble averages from a computer simulation, such as

$$\left(\frac{\partial F}{\partial V}\right)_{NT} = -P \tag{3.1}$$

and

$$\left(\frac{\partial F/T}{\partial 1/T}\right)_{VN} = U. \tag{3.2}$$

To calculate the free energy from these derivatives we need to create a reversible path in the $V-T$ plane that connects our phase of interest to another phase of known free energy. We then integrate equations (3.1) and (3.2) along this path to get the change in F along the path; hence we need a state of known free energy to integrate from to be able to calculate absolute free energy. The path must also be reversible, so it cannot cross a phase transition because this would cause hysteresis. One reference state that can be used is the ideal gas, and this is most often used for liquid free energy calculations. However, if used as the reference state for a solid phase, one would need to cross the first-order phase transition solid$\rightarrow$ liquid to create a path to the ideal gas and hysteresis would be a problem. This is obviously not a problem for liquids due to the existence of the critical point in the liquid-gas transition. It is important to note that the system is assumed to always be in equilibrium and so either separate simulations must be used for each sample along the path or the parameter must be varied slowly enough for the system to be in equilibrium.

The methods are discussed chronologically and show how thermodynamic integration has evolved and compared in terms of their performance in computing the relative stability of face-centred cubic (fcc) and hexagonal close-packed (hcp)

phases.

3.1.1 Single occupancy cell, Hoover and Ree

First suggested in 1967 by Hoover and Ree [50], a path is created linking the solid under investigation and a dilute lattice gas. The dilute lattice gas has the same pressure as the ideal gas at the same density and its free energy can be calculated exactly. Each solid particle is assigned a lattice point and is allowed to move within its cell about this lattice point. The solid is constrained to the cell via an artificial constraint. The cells are then expanded and translational order is not lost as the density decreases. The low density limit the system coincides with the dilute gas. The single occupancy cell model can be expanded uniformly without melting, so the issues of reversibility should not be a problem and we can calculate the free energy. The free energy of the lattice gas at high densities coincides with the free energy of the corresponding unconstrained solid, provided the cell walls have negligible effect on the displacements. The free energy is found by computing

$$F_{\text{solid}}(V_2) - F_{\text{lattice gas}}(V_1) = -\int_{V_1}^{V_2} P(V)dV \tag{3.3}$$

at constant temperature. The numerical integration involves evaluating the pressure at many state points due to cell walls constraining the particles.

This method was stated as the first to be able to definitely show that face-centred cubic systems have lower free energy than hexagonal close-packed [118]. However, the error was very great so no numerical value could be accurately obtained. Another issue with the single-occupancy cell method is that there is evidence that the expansion of the lattice cells may not actually be free of hysteresis. There appears to be a weak first-order transition when the cells reach the density at which the solid would become mechanically unstable. Therefore calculations using this method may not be very accurate and integration in each direction is not likely to give the same result.

3.1.2 Einstein crystal method

This methodology was pioneered by Frenkel and Ladd [38] and is based upon the construction of an unphysical, reversible path from a state of known free energy, an Einstein crystal with the same structure as the solid being investigated. The solid under consideration is coupled to its lattice sites by gradually turning on harmonic springs, and when the coupling is sufficiently strong, the solid is indistinguishable

from an Einstein crystal. In an Einstein crystal, each atom is an independent harmonic oscillator, all oscillating with the same frequency and with a potential energy function given by

$$\mathcal{U}_{\text{Ein}} = \frac{1}{2}\sum_{i=1}^{N} \alpha_i (\underline{r}_i - \underline{r}_{0,i})^2 \tag{3.4}$$

where $\underline{r}_{0,i}$ is the associated equilibrium lattice position of particle i at position $\underline{r}_i$ and α_i is the corresponding coupling parameter. The Helmholtz free energy can easily be calculated, as needed for a reference state [39, p.253–254].

The Einstein crystal has the same structure as the solid being investigated, hence the path is very likely to be reversible, i.e. not pass through any phase transitions.

The path is constructed by adding to the unperturbed hamiltonian $\mathcal{H}_{\text{Model}}$ the hamiltonian corresponding to the Einstein crystal, $\mathcal{H}_{\text{Ein}}$

$$\mathcal{H}(\lambda) = \lambda\mathcal{H}_{\text{Ein}} + (1-\lambda)\mathcal{H}_{\text{Model}}. \tag{3.5}$$

The free energy of a real crystal is related to that of the Einstein crystal with spring constant λ. For a value of $\lambda = 0$ we retain the original solid hamiltonian and for $\lambda = 1$ the path goes exactly the hamiltonian of the Einstein crystal.

The derivative of the free energy with respect to the spring constant λ is

$$\frac{\partial F}{\partial \lambda} = -k_{\text{B}}T\frac{\partial}{\partial \lambda}\left(\ln \int ... \int \exp[-\beta(\mathcal{H}(\lambda)]\right) \tag{3.6}$$

$$= \langle V \rangle_\lambda \tag{3.7}$$

this leads to the free energy of the crystal ($\lambda = 0$) as

$$F(\lambda = 0) = F(\lambda) - \int_0^1 \langle V \rangle_{\lambda'} d\lambda'. \tag{3.8}$$

The implementation requires simulations to find the optimal spring constant and then further simulations to sample the free energy derivative at varying λ-points. Quantifying the error from these calculations can be very expensive. The obvious, and most common, way is to repeat the calculation many times and look at the variance in the results. This will take up a lot of computer time and will also give no handle on systematic errors. There is no easy or smart way of calculating the error from these simulations or how the errors get propagated through simulations to the final result.

Absolute free energies are generally very large quantities, but the difference in free energy between crystal polymorphs close to a phase transition can be extremely small $\sim 10^{-5} k_{\mathrm{B}}T$. This is often smaller than the typical error in an Einstein crystal calculation.

This method also depends on a lot of parameters that need to be chosen and optimised in order to get an accurate result. Hence, it is not the most reliable way to find small free energy differences.

This method was first applied to the hard sphere system to calculate the free energy difference between face centred cubic (fcc) and hexagonal close packed (hcp) phases. Calculations were made at a reduced density $\rho/\rho_{cp} = 0.7360$, which is the density of solid-fluid coexistence, and at a density of $\rho/\rho_{cp} = 0.7778$.

For each simulation Frenkel and Ladd performed ten runs for different values of λ. The chosen values of λ were different for each density. The free energy of the Einstein crystal was approximated by a cluster expansion. Eq. (3.8) was adapted so that the integrand is a slowly varying function of the integration variable.

$$\Delta F = -\int_0^{\lambda_{max}} \langle r^2 \rangle_\lambda (\lambda + c) \frac{d\lambda}{(\lambda + c)} \tag{3.9}$$

$$= -\int_{\ln(c)}^{\ln(\lambda_{max}+c)} \left\{ \langle r^2 \rangle_\lambda (\lambda + c) \right\} d\ln(\lambda + c). \tag{3.10}$$

where $\langle r^2 \rangle$ is the mean square particle displacement, λ_{max} is the maximum spring constant used, decided for each system separately. c is a constant, chosen to be $c = \exp(3.5) \approx k_{\mathrm{B}}T\sigma^2/\langle r^2 \rangle$ where σ is the hard sphere diameter. The centre of mass needs to be constrained to ensure that the mean square displacement does not diverge. Without this constraint, the mean square displacement would become of order L^2, where L is the box length, as $\lambda \to 0$. The integrand in eq. (3.10) would sharply peak about $\lambda = 0$ and greatly affect the accuracy of the result. This constraint of the centre of mass involves difficult computation, and especially for MC simulations it is not trivial.

To implement this constraint Frenkel and Ladd expressed all coordinates relative to the centre of the periodic box. One needs to keep track of the displacement of the centre of mass of the system by updating and changing the entire box coordinates after every move. This makes it a costly undertaking, yet necessary for this method. One must also take into account this constraint in the centre of mass with a $(\ln V)/N$ term to the free energy.

The system sizes studied were chosen so that perfect stacking of the crystals was ensured. It was found that the excess free energy depended on the shape of

the system box and so there is significant difference between the free energy of a $54 = (3 \times 3 \times 6)$ system and a cubic $216 = (6 \times 6 \times 6)$ system. One also must compare with results from studies that have taken this into account in the same way. When looking at finite size effects this extrapolation can have a huge effect on the results, as seen in the work of Frenkel and Ladd at a density of $\rho/\rho_{cp} = 0.7360$. The value calculated for the free difference between fcc and hcp hard sphere crystals put the free energy difference in the interval $-0.001 < \Delta F^{\infty} < 0.002$, where $\Delta F = F_{hcp} - F_{fcc}$ for both system sizes.

This shows that the method is not accurate enough to fully resolve the free energy difference. The error is of the same order as the difference between the absolute values, for example at a density of $\rho/\rho_{cp} = 0.7360$ the free energy difference is $\Delta F = 0.0009$ and the error on the absolute free energy for the fcc phase is 0.0010.

In summary, the errors are very large and uncertain, and the final result doesn't even definitively determine the most stable phase. This shows that the method is not best used for such small free energy differences.

Polson et al. [82] corrected the formulas in this method, showing that the true free energy of a crystal is $(2/N)\ln(N)$ lower than that in the original paper. Even though this tends to zero as $N \to \infty$, for the finite sizes studied this will have a non-negligible effect. Polson et al. [82] only calculated results for the free energy of soft spheres, which cannot be directly compared with the hard sphere results. Nevertheless, the error in their calculations was given as an order of magnitude lower than that quoted in the original Frenkel and Ladd paper. No explanation of where this reduction in error came from was given. Their final value for the free energy difference is $\Delta F_{\text{hcp-fcc}}/(Nk_{\text{B}}T) = 0.0028(8)$, showing that the fcc crystal phase is more stable.

3.1.3 Einstein molecule method, Vega and Noya

The Einstein crystal approach was extended by Vega and Noya [108] to make it simpler and easier to apply to a variety of systems. The underlying method is the same, except a reference particle is chosen from the two systems in order to fix the centre of mass, and all other particle positions are in terms of the fixed reference particle.

Let us consider a system of three hard disks confined to move within a segment of length L. The partition function of this system (once the momenta have

been integrated out) is given by

$$Z = \frac{1}{3!\Lambda^3} \int_0^L \int_0^L \int_0^L e^{-\beta U(x_1,x_2,x_3)} dx_1 dx_2 dx_3, \tag{3.11}$$

were Λ is the de Broglie wavelength. The potential energy of the system is a sum over pair potentials,

$$U(x_1, x_2, x_3) = u(x_1, x_2) + u(x_2, x_3) + u(x_1, x_3). \tag{3.12}$$

Let us define each of the positions of the particles in terms of x_1,

$$x_1 \rightarrow x_1, \tag{3.13}$$

$$x_2 \rightarrow x_2' = x_2 - x_1, \tag{3.14}$$

$$x_3 \rightarrow x_3' = x_3 - x_1. \tag{3.15}$$

Due to the periodic boundary conditions one must use the minimum image convention to find the smallest distance between two particles, that is the distance between closes images. The partition function can be written as

$$Z = \frac{1}{3!\Lambda^3} \int_0^L dx_1 \int_0^L \int_0^L e^{-\beta[u(x_2')+u(x_3')+u(x_3'-x_2')]} dx_2' dx_3' \tag{3.16}$$

$$= \frac{1}{3!\Lambda^3} \int_0^L dx_1 \kappa', \tag{3.17}$$

where κ' is the integral over x_2' and x_3'. Since there is no dependence on x_1 the integral over x_1 can be calculated exactly and the equation can be rewritten as

$$Z = \frac{1}{3!\Lambda^3} L\kappa'. \tag{3.18}$$

This can be extended to a system of N particles and three dimensional space as

$$Z = \frac{1}{N!\Lambda^3} V(N-1)\kappa'', \tag{3.19}$$

where V is the volume of the system and κ'' is the integral over the positions of the $(N-1)$ particles in the system with particle 1 fixed, as in the three particle system.

Therefore, when calculating the free energy of a solid, one only needs to compute κ''.

The Einstein molecule method uses this result, in that one particle is defined as the 'carrier' which is the reference atom. The other atoms in the system vibrate

harmonically about their lattice positions. The lattice positions are defined in terms of the reference atom. Without any pair potentials between particles this is defined as the ideal Einstein molecule crystal. The reference atom is allowed to move, it just does not vibrate. The free energy of this Einstein molecule crystal is just the free energy of the ideal Einstein crystal with one particle fixed, which gives it an extra free energy of $k_{\mathrm{B}}T\ln(V/\Lambda^3)$.

The Einstein molecule method defines a path from the ideal Einstein crystal, to the Einstein crystal with a fixed particle to the hard sphere solid with one fixed particle and from there to the full hard sphere solid, as shown in Figure 3.1

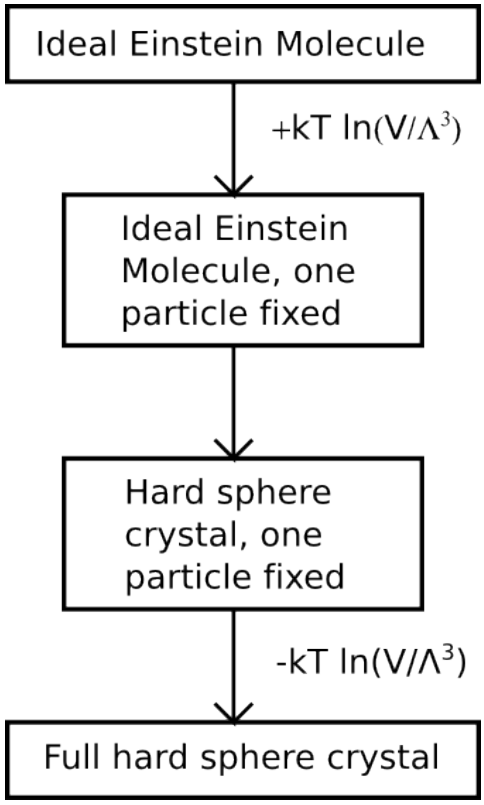

Figure 3.1: Flow diagram of the Einstein molecule method

The terms corresponding to having one particle fixed will cancel out. Therefore we can calculate the free energy of the hard sphere solid by adding the free energy of the ideal Einstein crystal with the free energy of the Einstein crystal with one particle fixed and the hard sphere solid with one particle fixed. We slowly turn on the harmonic springs from the hard sphere solid, and since the position of atom 1 is fixed, the system behaves well even as $\lambda \to 0$. This implementation is equivalent to fixing the centre of mass, as in the original Frenkel and Ladd paper. However, the methodology is much simpler as there is cancellation of the contre of mass constraint

in the results, also since one of the particles is fixed there is no need to recalculate the lattice site positions.

Vega and Noya tested the radial distribution functions for the system with and without a fixed particle and found them to be identical; this shows that fixing a particle will not affect the configurational properties of the system.

Vega and Noya presented results for the free energy of the face centred cubic hard sphere phase that were in agreement with the work of Polson et al. [82] to within the statistical error. The shapes of the systems used by Vega and Noya [108] were not specified in this work and, as shown in [38] this can have a large effect on the calculation of finite size effects. From the system sizes used, they could not have compared with cubic systems like used by Polson et al. [82]. Vega and Noya calculated the free energy for only the fcc hard sphere solid and only compared with work at a single density. Again the errors quoted are of the same order as in the original work by Frenkel and Ladd [38] $\approx 10^{-3} k_{\mathrm{B}} T$.

Overall this method has a much simpler implementation than the original Frenkel and Ladd method, but the resolution of this method is no better and so suffers the same issues for calculating very small free energy differences.

3.2 The self-referential method

The self-referential method was developed by Sweatman [103]. In most other methods the free energy of the system is calculated from an ideal reference state, for example, the Einstein crystal or the ideal gas. In the self-referential method the crystalline solid of interest with a different number of unit cells is used as the reference state. This method was tested on hard sphere and Lennard Jones solids.

The main difference and advantage to this method is that the reference state is exactly the same as the state of interest, except for a different number of particles. This is an advantage because a path between the two will not cross a first order phase transition. The main disadvantage is that the method, as stated by the author, is not very efficient as one needs to continually double and halve the system size with relaxation time in between. The errors quoted on the results are slightly higher than for the thermodynamic integration methods, and so this method does not have the accuracy needed for calculation of small free energy differences.

3.3 Conclusion of methods

Thermodynamic integration is conceptually simple but its application can be very complex. Parameters for each different sized system need to be set, also the centre of mass needs to be constrained and accounted for correctly. Then one slowly turns on the harmonic springs; even this seemingly simple stage has many hidden complexities. Also one must deal with translational and orientational order and ensure that the system is in equilibrium throughout. If model couplings to springs are to be turned off, the question of when this should happen is non-trivial as it can affect the results. All of this ensures that the method, although conceptually simple, needs great insight and experience to utilise effectively and accurately.

The main problem with all these methods is the same: high numbers of simulations are needed for each result; parameters must be numerically optimised for each result; and the error is on the order of the free energy differences we are likely to be interested in for the present work. Systematic errors may come from the reference state via finite size effects, and statistical errors from each simulation along the path and the numerical integration itself. Therefore, a completely different approach is needed that does not require an interphase path to reference states. Optimally, the result would be calculated from a single simulation and with a higher degree of precision.

Chapter 4

Hard sphere phase switch Monte Carlo

The phase switch Monte Carlo method was first reported by Bruce et al. [16], when it was applied to a system of hard spheres to investigate the free energy difference between the face-centred cubic (fcc) and hexagonal close-packed (hcp) structures. This is a challenging application due to the very small free energy difference between the two phases. Previous calculations had been made using other methods, the most common being thermodynamic integration, and specifically the Einstein integration method [38]. However, Frenkel and Ladd could not resolve the free energy difference between the two phases to a high enough degree of accuracy to determine its sign and hence find which is the most stable structure. As discussed in chapter 3 the computational cost to acquire a significantly small error on such a tiny value is very great using this method.

The phase switch method showed good agreement with the previous work and a much smaller error on the result, showing that fcc is the most stable hard sphere structure. The method was later extended to work with the Lennard-Jones potentials and also for solid-liquid phase transitions [34].

The Ehrenfest classification of phase transitions labels the transition based upon the behaviour of the free energy as a function of thermodynamic variables. A phase transition is classified as first-order when there is a discontinuity in the first derivative of the free energy with respect to a thermodynamic variable; for example, a discontinuous change in density during a solid-solid transition. Second-order phase transitions occur when the first derivative is continuous, but the second derivative is discontinuous.

This section will discuss the original methodology of [16, 17]. and our inter-

pretational and computational differences in implementation. We will validate our results against previous work.

4.1 Statistical Mechanics for phase switch Monte Carlo

The Helmholtz free energy of system of N identical particles at volume V and temperature T is

$$F(N, V, T) = -k_{\mathrm{B}} T \ln Z, \tag{4.1}$$

where Z is the partition function.

The difference in Helmholtz free energy between two systems $1, 2$, given by $\Delta F_{1,2} = F_1 - F_2$ can be written as

$$\Delta F_{1,2} = -k_{\mathrm{B}} T \ln(Z_1/Z_2). \tag{4.2}$$

The probability of picking states within a set α is the ratio of the partition function of the states contained in α compared with the partition function for the whole system

$$\begin{aligned} \mathcal{P}_\alpha &= \frac{Z_\alpha}{Z} \\ Z_\alpha &= \mathcal{P}_\alpha Z \end{aligned} \tag{4.3}$$

Applying equation 4.2 then gives us

$$\Delta F_{1,2} = -k_{\mathrm{B}} T \ln(\mathcal{P}_1/\mathcal{P}_2) \tag{4.4}$$

so the free energy difference can be calculated from the ratio of probabilities of the two sub-systems without the need for the full partition function.

In order to calculate these probabilities one must sample the configuration space corresponding to both sub-systems enough to build up sufficient statistics. When the two systems are both crystalline, major structural reorganisation is needed to change phase and so advanced techniques should be used to facilitate the sampling.

Umbrella sampling is one of the simplest methods of this type, and it was first introduced by Torrie and Valleau [105]. The main idea is to sample configuration space associated with two different systems of N particles where an energy barrier exists to hinder ergodicity. Sampling will be poor, or completely fail, when the probability of overcoming the barrier is statistically insignificant. To overcome this, one biases the simulation using some energy penalty function. The ideal choice for

this biasing function would be one that completely cancels out the barrier, such that the probability distribution is flat. However, *a priori* knowledge of the barrier is necessary and an iterative approach would be needed. Since the biasing function is known exactly, unbiased statistics can be recovered in post-processing analysis.

This method is still not sufficient to deal with systems with restricted configurational space, e.g. solid-solid transitions where the crystal structure limits the configurational space of that system and there is limited capability for major structural rearrangement. Therefore, to deal with the difficulty arising from working with small unit cells of solids, a more refined approach is needed.

One option, that has been used widely and successfully for fluids and spin lattice systems, is the interface method, when two coexisting regions of each phase are simulated beside each other separated by an interface [10, 114]; this interface removes the high barrier, as shown in Figure 4.1. However, application of this approach to two crystalline phases is obviously not straightforward as major physical restructuring would be needed between the two phases. Currently this can only be done for trivially simple cases; if we guess an interfacial structure the timescale for rearrangement to more realistic configurations is too large to simulate.

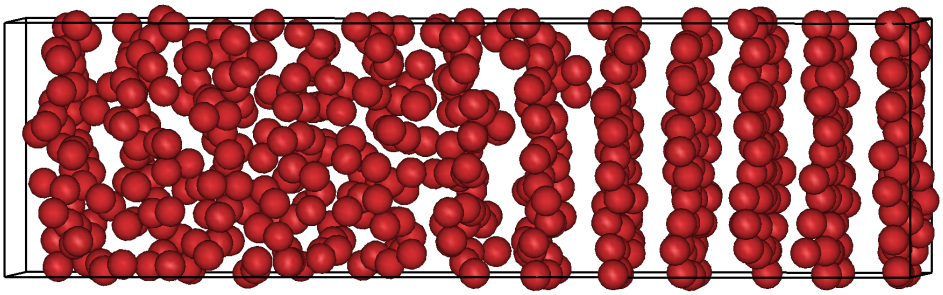

Figure 4.1: System of solid and liquid Lennard-Jones particles set up for the interface method.

This suggests that a path traversing inhomogenous, mixed phase regions would be intrinsically slow and susceptible to ergodic trapping. Hence a method that only samples single phase crystals would have a great advantage.

Phase switch MC is exactly such a method that explores an un-physical interphase path in a single simulation. Since the path is un-physical it removes the issue physical interphase paths have of huge energy barriers to structural changes since there is never a physical interface between the two phases. The method will comprise of an un-physical move-set, therefore, Monte Carlo simulations are the obvious choice, and this advantage is further compounded by the many methods

available to extend and enhance sampling in a MC context.

Since a Monte Carlo trial move has no dependence upon the system or configuration of the system, it has equal probability of being attempted in any system. The only configurational dependence arises in the acceptance criterion when the energies of the configurations are evaluated

$$P_{acc}(o \to n) = \min\{1, \exp[-\beta \Delta E]\} \tag{4.5}$$

with $\Delta E = E_{\text{new}} - E_{\text{old}}$. This means that if the same move is proposed for two different configurations, or even two different phases, only the acceptance criterion will be different, leading to the different behaviour and favoured structures/moves.

Attempting a move $A \to C$ has probability of acceptance

$$P(A \to C) = \exp[-\beta(E_C - E_A)]. \tag{4.6}$$

If that move is split up in to moves $A \to B \to C$ then the probability of the separate moves is

$$\begin{aligned} P(A \to B) &= \exp[-\beta(E_B - E_A)] \\ P(B \to C) &= \exp[-\beta(E_C - E_B)] \\ P(A \to B) \cdot P(B \to C) &= \exp[-\beta(E_B - E_A)] \cdot \exp[-\beta(E_C - E_B)] \\ &= \exp[-\beta(E_B - E_A + E_C - E_B)] \\ &= \exp[-\beta(E_C - E_A) \\ &= P(A \to C). \end{aligned}$$

This shows that the the only determining factor in the acceptance of an MC move is the initial and the final state and it is independent of any states in between.

A Monte Carlo move may be created where the proposed transformation is a change of crystal structure; as with any MC move there is an acceptance criterion which depends on the Boltzmann factor. This proposed move is to jump directly from the current configuration in phase α to the equivalent configuration in phase γ. That is to recreate all the moves that have been applied to phase α to a representative state of phase γ. Most moves that would be accepted in phase α are unlikely to be accepted if applied to a completely different configuration. However, there exists a subset of configuration space of phase α that, when mapped onto phase γ would be accepted; these states are henceforth known as gateway states. This 'switch' move allows us to map realisable configurations of one phase onto the other phase and

allows a transformation between the two whilst only simulating single crystals far away from a mixed phase region. The subset of configurations that can be switched between is not necessarily of high enough statistical weight to be sampled sufficiently often and hence the system will generally need to be biased towards it. This use of biased MC will be discussed in greater detail in section 4.4.

Assuming one can push the system into these gateway states, we now have a MC move to directly transform between crystal phases and hence, can calculate the ratio of the configurational weights of the two phases and from that calculate the free energy difference between them.

The switch move can be considered in more than one way, either as a geometric transformation of one phase into the other or as a logical switch between two concurrently simulated phases. The difference between these two approaches determines only the implementation of the method. Bruce et al. [16] constructed a geometric switch to transform between the two systems in their simulations. A different implementation approach was taken in the current work where a logical switch is employed in our custom Monte Carlo code Ponders.

4.2 Phase switch theory for hard spheres

For N hard sphere particles with a diameter σ in a box of volume V, the configurational energy is

$$E(\{\underline{r}\}) = \begin{cases} 0 & \text{if } r_{ij} \geq \sigma \ \forall i,j, \\ \infty & \text{otherwise,} \end{cases} \tag{4.7}$$

where $r_{ij} = |\underline{r}_i - \underline{r}_j|$.

The coordinates of the particles can be split into reference vectors which correspond to the ideal lattice site, and the particle's displacement from the reference vector,

$$\underline{r}_i = \underline{R}_i^{\alpha} + \underline{d}_i \tag{4.8}$$

where $\underline{R}_i^{\alpha}$ denotes the ideal reference vectors associated with crystal α, $i = 1, \ldots, N$. The displacement of a specific particle is the same in both systems $\underline{d}_i$, but the reference vectors differ $\underline{R}_i^1 \neq \underline{R}_i^2$, as shown in Figure 4.2.

For a system of hard spheres at constant volume, the partition function is

$$Z(N,V,T) = \sum_s \exp[-\beta E_s] \tag{4.9}$$

where s is over all the microstates in the system. Since all realisable configurations

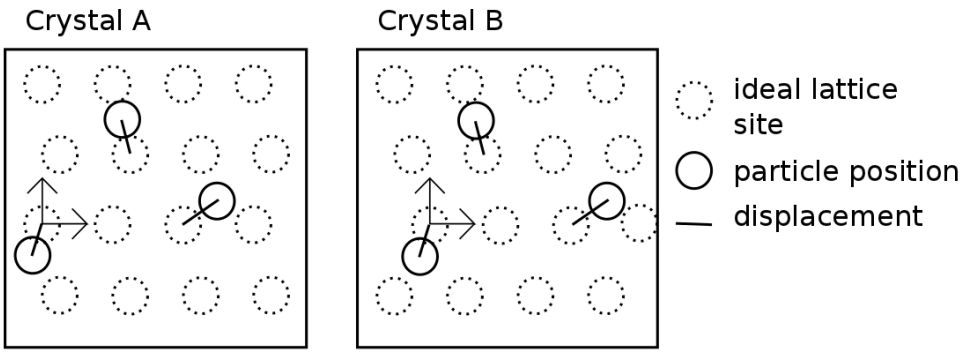

Figure 4.2: Coordinates are the displacement from ideal lattice site

of hard spheres have zero energy, any difference in free energy comes purely from entropy. The probability of occupying microstate s is

$$\mathcal{P}(N, V|s) = \frac{1}{Z} \exp[-\beta E_s], \tag{4.10}$$

hence, all realisable microstates are equally probable for a hard sphere system.

Using equation 4.4 the free energy difference for a system of N hard sphere in a constant volume V is

$$\Delta F_{\alpha,\gamma} = -\ln\left(\frac{\mathcal{P}(N, V|\alpha)}{\mathcal{P}(N, V|\gamma)}\right). \tag{4.11}$$

This can be extended to the isobaric-isothermal ensemble for a system at constant pressure P.

The Gibbs free energy is obtained from the partition function $\Delta(N, P, \alpha)$, as standard,

$$G(N, P, \alpha) \equiv -k_{\mathrm{B}} T \ln \Delta(N, P, \alpha) \tag{4.12}$$

so a difference in Gibbs free energy between phases α , γ can easily be shown to be given by

$$\Delta G_{\alpha,\gamma} = G(N, P, \alpha) - G(N, P, \gamma) = -k_{\mathrm{B}} T \ln \mathcal{R}_{\alpha\gamma}(N, P) \tag{4.13}$$

where

$$\mathcal{R}_{\alpha\gamma}(N, P) = \frac{\Delta(N, P, \alpha)}{\Delta(N, P, \gamma)} = \frac{\mathcal{P}(N, P|\alpha)}{\mathcal{P}(N, P|\gamma)}. \tag{4.14}$$

Since the probability that a system will be found to have structure α is provided by a measure of the associated partition function

$$\mathcal{P}(N, P|\alpha) = \frac{\Delta(N, P, \alpha)}{\Delta(N, P)} \tag{4.15}$$

where $\Delta(N,P) \equiv \sum_{\alpha} \Delta(N,P,\alpha)$.

Hence, to calculate the Gibbs free energy, only a ratio of the probabilities of being in each structure is needed. Accordingly, it is imperative that all configuration space, of both structures, is explored, especially the *gateway* states where both structures are feasible.

The interphase path maps one structure onto the other ($\alpha \leftrightarrow \gamma$), so it is necessary to understand what makes a configuration belonging to a certain structure. The definition used in this method is the set of configurations that are accessible from some member of the set within a nominal time range. This has the advantage that it should be independent of the time frame, given enough time to fully sample configuration space; this is also how standard simulation methods operate already.

Theoretically, one can map the moves made by configurations belong to phase α onto phase γ by building up a probability of how likely these moves are to belong to phase γ as well. In order to do this one needs to switch between the two phases by applying the set of accepted moves of one to the other. Obviously this will only be accepted if the move set results in an allowable configuration, and for hard spheres this means a system without overlaps.

Due to the discrete nature of the hard sphere model there is no differentiation between forbidden states; a system with hundreds of overlaps has the same energy as a system with just one overlap. In standard hard particle MC simulations, there is no need to differentiate between these two forbidden states. However, with phase switch Monte Carlo, since the probability of the interphase moves being allowed is very low we need to bias the system towards these states. An order parameter is needed to describe how 'far away' we are from a zero overlap system. This order parameter can simply be chosen as a function of the overlaps in both systems

$$\mathcal{M}(\mu|\alpha,\gamma) \equiv \mu(\alpha) - \mu(\gamma) \tag{4.16}$$

where α and γ corresponds to the crystal structures and μ is a measure of the number of overlaps in that configuration. Consequently, $\mathcal{M}(\mu)$ is a measure of how 'close' to being feasible each configuration is; for very large values of μ (negative or positive) the system is very far from being energetically allowed, and there are also a lot more ways of having 100 overlaps than 5 so there is a higher entropy. For $\mu = 0$ only, the configuration is feasible for both structures as this means that there are zero overlaps in both, and this is the only allowed MC state for the hard-sphere model, and hence these are the gateway states. Figure 4.3 shows an example calculation of $\mathcal{M}$.

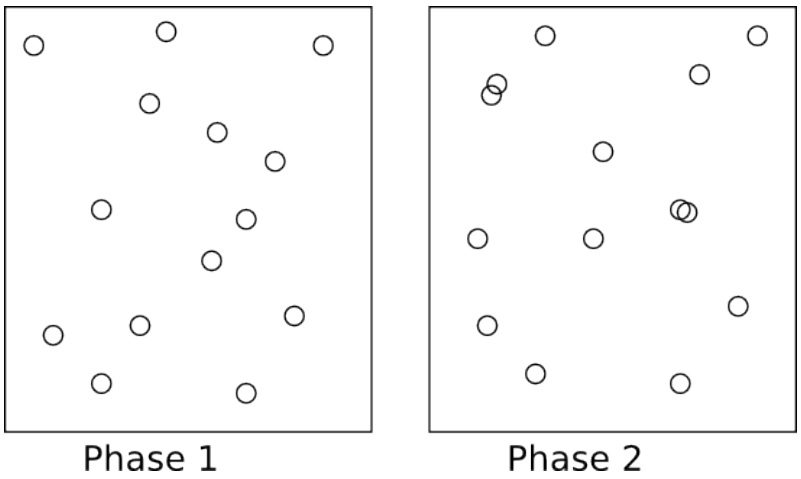

Figure 4.3: Phase 1 has zero overlaps, $\mu(\alpha_1) = 0$ in and phase 2 has two overlaps $\mu(\alpha_2) = 2$, this gives us an order parameter value of $\mathcal{M}(\mu) = \mu(\alpha_1) - \mu(\alpha_2) = 0 - 2 = -2$.

In the constant pressure ensemble, it is often useful to include the volume change into the order parameter

$$\mathcal{M}(\mu) = \mu(\alpha) - \mu(\gamma) + P(V_\alpha - V_\gamma) \tag{4.17}$$

with P as the external pressure and V_α is the volume of the system in phase α.

4.3 Biased Monte Carlo

The aim of the biasing technique is to uniformly traverse the order parameter and hence frequently visit the gateway states.

The phase switch method was first published in 1997 and used the visited-state (VS) technique and the transition probability method to bias their Monte Carlo simulations [98]. Wang and Landau [110] published their paper on an efficient algorithm for producing flat sampling across an energy range in 2001. The Wang Landau (WL) algorithm uses the fact that if a random walk is made with probability proportional to the inverse of the density of states, $\frac{1}{W(E)}$, then a flat histogram will be generated. To actually implement this we would need knowledge of the property that we are trying to find. Therefore, an estimate of the density of states is used and iteratively modified to converge on the true value.

At the beginning of the random walk the density of states is a completely unknown quantity so is initialised to have a value of $W(E) = 1$ everywhere. The

acceptance probability of a move is adapted to include the biasing

$$P_{\text{acc}}^{\text{biased}}(E_1 \to E_2) = \exp[W(E_1) - W(E_2)]. \tag{4.18}$$

Each time a move is attempted the estimate of the density of states is incremented by a modification factor $f > 1$, $W(E) \to W(E) \times \ln(f)$, and concurrently a histogram is incremented by a constant $h(E) \to h(E) + 1$. Care must be taken to include rejected moves as a new increment of the weighting and histogram to get correct sampling.

Whenever the histogram is deemed to have reached a critical flatness, chosen to be when all points are within 0.95% of the mean in this work, the f value is reduced as $f \to \sqrt{f}$ and the histogram zeroed, so as to flatten and smooth the weighting function. Once a predetermined minimum value of f has been reached, or a maximum time, the simulation is stopped. Since the weighting, and hence the acceptance criterion, is not constant throughout the simulation the weighting must be fixed for production runs to obey detailed balance. As the f value goes to zero the non-fixed simulation approaches detailed balance.

The definition of critical flatness is not unique: if it is too loose the system may quickly converge to an incorrect weighting that will take a long time to change; if it is too tight then the time taken to converge will be unfeasibly long. The definition of a 'flat histogram' used in this work is that the minimum value in the histogram is within a chosen percentage, p_{WL}, of the mean $\langle h(E) \rangle$.

The algorithm has been shown to be efficient and accurate over a wide range of temperatures and system sizes and doesn't suffer from the systematic errors and substantial deviations at large system sizes that other methods encounter [9, 36, 29, 111].

In this work we adopt the Wang Landau algorithm to generate a flat histogram in the overlap parameter; this works as the algorithm is not confined to energy space. The function energy of a given configuration, augmented with a bias function eta, replaces the density of states in equation (4.18). This changes to

$$P_{\text{acc}}^{\text{biased}}(\text{old} \to \text{new}) = P_{\text{acc}}^{\text{metropolis}} \times \exp[\eta(\mathcal{M}_{\text{old}}) - \eta(\mathcal{M}_{\text{new}})] \tag{4.19}$$

$$= \exp[-\beta(E_{\text{new}} - E_{\text{old}}) + \eta(\mathcal{M}_{\text{old}}) - \eta(\mathcal{M}_{\text{new}})]. \tag{4.20}$$

We increment the element of the biasing and histogram functions corresponding to the order parameter value of the current state of the systems, k.

A biasing function $\eta(\mathcal{M})$, in units of $k_{\text{B}}T$ is constructed across the order parameter space, $\mathcal{M}$. The algorithm is

1. Set $\eta(\mathcal{M}) = 0$ and $h(\mathcal{M}) = 0$ for all values of $\mathcal{M}$, set f to the chosen starting value.

2. Make MC moves with adapted probability $P_{\text{acc}}^{\text{biased}}$ eq. (4.20).

3. Update after every move, $\eta_k \mathrel{+}= \ln(f)$ and $h_k \mathrel{+}= 1$.

4. Check flatness of histogram, flat if $h_{min}(E) > p_{\text{WL}} * \langle h(E) \rangle$. If flat then $f \to \sqrt{f}$, repeat from number 2. until f reaches a defined minimum value.

5. Unbias histogram to recover equilibrium distribution, see Equation (4.21).

To recover the equilibrium probability distribution we must remove the effect of the bias from the histogram. Since the Wang-Landau algorithm is non-Markovian, we should only use this result on simulations run with fixed weighting rather than whilst the weighting is being converged.

$$h_{unbias}(\mathcal{M}) = h(\mathcal{M}) \times \exp[\eta(\mathcal{M})]. \tag{4.21}$$

4.3.1 Discretising order parameter space

The order parameter space defined for hard spheres is naturally discrete, with only integer values of overlaps. This means that when storing the biasing function we have a natural scale with which to work; we use the discrete nature of our order parameter to ensure no loss of information. This means that we can have a number of bins corresponding to the number of order parameter values and the difference between each bin will be one. However, for large system sizes the range of data to store can become very large, and this will take up a lot of memory and be inefficient when implemented in our simulation. It would also increase the noise in our system and take longer to converge to a good weight. Therefore, we need to further discretise the space and have larger bin widths to minimise the total number of bins, and hence memory, needed. This is also an issue due to the noise that will be produced from having such a large number of bins, and so in order to get good statistics many more samples and hence much longer simulations times would be needed. Care must be taken when further discretising the order parameter space as this coarse-graining can cause a loss of information, especially where the weighting function varies rapidly; there can be no biasing towards values within the same bin. This means that we must not make the bins too large otherwise the system will be very slow to traverse the order parameter space as biasing will have minimal effect. For efficiency of interphase switches we have a bin solely for the gateway states, $\mathcal{M} = 0$, which ensures that the biasing will be the most effective.

All of this suggests non-uniform discretisation of the order parameter space to be the best approach, so that we increase the efficiency and reduce memory issues whilst having increased resolution only where needed. Due to the non-uniform bin widths the amount the weighting function should be incremented by now depends on the width of the bin; this ensures that the incremented area of the bins remain the same. Each crystal structure is likely to equilibrate to a different value of $\mathcal{M}$ in an unweighted simulation, so we must be able to deal with non-symmetric order parameter spaces.

Non-uniform bins are implemented via a geometric progression of bin width. A geometric progression or geometric sequence is a sequence where the next term is found by multiplying the previous term by a common ratio r. The nth term in the sequence, with initial value a is given by $a_n = ar^{(n-1)}$.

In Ponders the width of the bins is described by a geometric sequence. The zero weighting (middle) bin is always of width 1. The number of bins is set as an input parameter and is the same for either side of the weighting. However, the number of overlaps to be covered by these bins need not be the same. This leads to the need for two separate geometric progressions, one for the positive side (structure α) and one for the negative side (structure γ).

An initial guess for the common ratio of the geometric progression is found by using the standard formula for the sum of a geometric sequence

$$\sum_{k=0}^{n} ar^k = \frac{a(1-r^{n+1})}{1-r}, \tag{4.22}$$

where n is the number of terms (in this case bins), a is the initial width of the bin, always set to always be 1, and r is the ratio of the geometric progression. Because the number of overlaps is discrete for hard spheres, the bin widths should be integer values. This causes problems because the ratio has been calculated assuming real values.

To get around this issue an iterative method was used to calculate the ratio. The first guess from Equation 4.22 is used to calculate the actual sum of the series with rounding to the nearest integer. This is then adapted by finding the difference from the desired number of overlaps and multiplying the ratio by a factor of this difference. The actual sum is then iterated until the value has converged and the remaining overlaps are fewer that the width of the last bin in the series. Any extra overlaps are added into the final bin. This process is done for both the positive and negative sides separately, and leads to two separate series. In order to speed up calculations in Ponders, arrays are stored with the corresponding overlap and

bin values, for easy conversion between the two. That is, for a given overlap $\mathcal{M}_i$ it will return the bin number which the overlap relates to and vice versa. This implementation of adaptive resolution grids for Wang-Landau multicanonical iterative biasing with phase switch Monte Carlo is thought to be unique.

4.4 Implementation for hard spheres

Translation moves In the Ponders code the MC sampling of displacements selects a sphere at random and trial changes to the displacement of this sphere, δr are picked from a uniform distribution $-\Delta r \rightarrow +\Delta r$ that is tuned by the acceptance rate required, but kept fixed for an entire simulation. There is a trade off between small moves being accepted often but giving slow sampling of configuration space versus large moves having a low probability of acceptance but giving faster sampling of configuration space. A value of 30% acceptance rate was used in this work even though this may not always be optimal. The acceptance of this change in displacement is determined by the standard Metropolis criterion [75],

$$P_{\text{acc}} = \min\{1, \exp[-\Delta\tilde{E}]\} \tag{4.23}$$

where $\Delta\tilde{E}$ is the change in energy between the two configurations, and is related to the biasing method (Equation 4.20). A random number ξ in $[0, 1]$ is chosen and if $\xi < P_{\text{acc}}$ the trial move is accepted. Otherwise, the particle is returned to its original position. Trial moves that lower the bias energy of the system are always accepted, and trial moves that raise the energy are accepted according to their Boltzmann weight. We must ensure that the number of moves is incremented even after a rejected move to ensure correct sampling. N such trial moves are commonly referred to as a MC cycle or sweep.

To actualise phase switching, two separate simulations are used, one for each structure. One system is arbitrarily denoted as the *active* system and the other as the *passive*. MC moves are only undertaken in the active system and, if accepted, the displacement of the move is applied to the passive, irrespective of overlaps caused, see Figure 4.4.

This application of a single move to both systems is used due to the need to know the order parameter value after every MC move for biasing purposes.

The methodological application presented by Bruce et al. [17] differs from our interpretation. A representation of the Markov chain for the original implementation is shown in Figure 4.5a. There is only a transformation between colour, representing phase, in the chain. Figure 4.5b shows a representation of the Markov chain for our

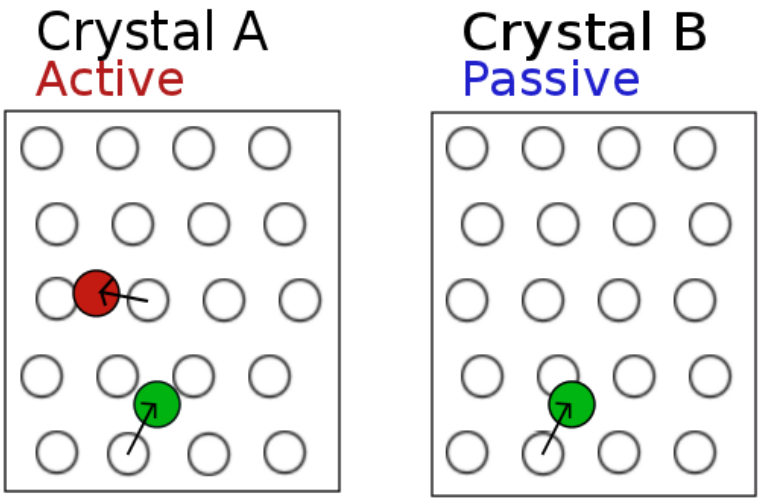

Figure 4.4: A move accepted in the active (denoted by green) is also made in the passive (irrespective of energy penalties within the MC model), a rejected move (denoted by red) is not applied

implementation, where there are two concurrent chains and the solid line is the Markov chain that switches between the two paths.

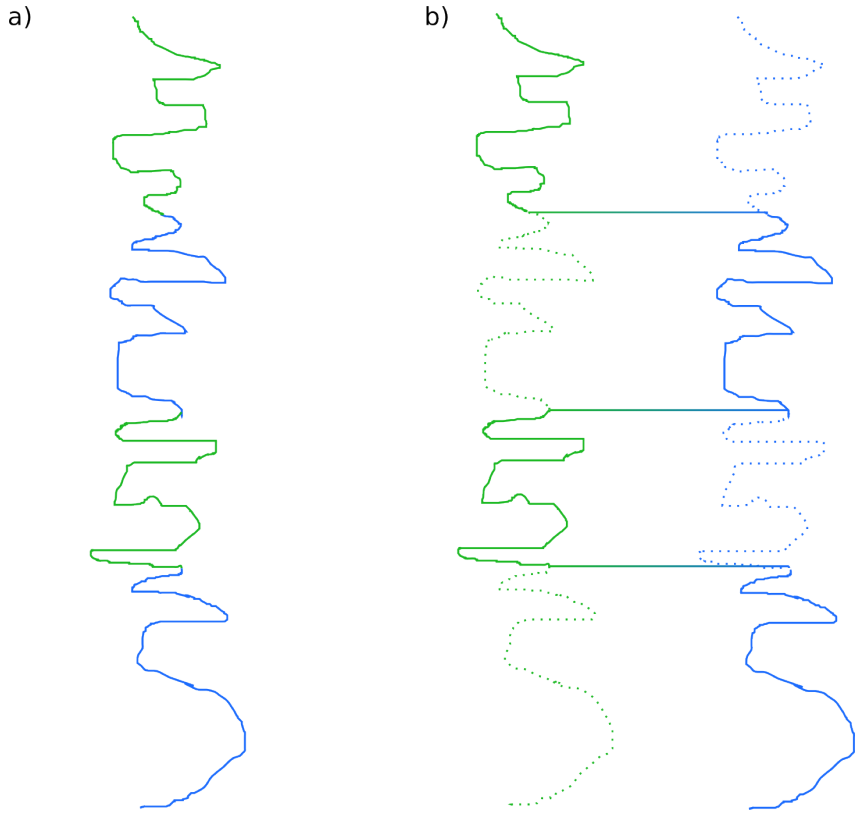

Figure 4.5: Representation of the Markov chain for a) the original implementation of the phase switch method, and b) our new implementation. The two colours denote different phases and the solid line is the sampled Markov chain.

In the work of Bruce et al. only one phase is simulated at each time, and a transformation is created that will map one set of lattice vectors onto the other. This, obviously, is very system dependent and requires insight into the structures to utilise the most efficient mapping. When dealing with two structures that are very similar this is not a major issue, however, when applying this method to more complex systems much insight and thought would have to be taken in this step. This transformation never changes but must be applied to each move in order to calculate the order parameter value. Since there are many possible transformations available, the efficiency of the chosen transformation will be important. One aim would be to match the energies of the two linked configurations as much as possible, hence reducing the barrier to a switch move. However, it was shown that there is not much of an advantage gained for the effort involved. Overall this implementation is very specific to the system under study; it works well for simple and very similar systems but does not generalise well to more complex systems. Our implementation does not suffer so much from the problem of generalisation as a generic transformation is

used. There is also an overhead due to the cost of simulating two systems at once but this gives us free calculation of the order parameter and of the switch move.

4.4.1 Constant pressure

For constant pressure simulations trial moves in the lattice vectors are updated, on average once per MC cycle with a fixed probability of $1/N$. The cell is scaled isotropically by δV and the fractional coordinates of the particles are kept fixed. We have also implemented anisotropic volume moves described in section 2.4.2. The order parameter needs to be recalculated fully after each successful volume move. An attempted resize $V \to V'$ is accepted with probability

$$P_{\text{acc}}^{\text{metropolis}}(V \to V') = \min(1, \exp[-\beta\{\Delta E + p(V' - V)\} + N \ln(V'/V)]). \quad (4.24)$$

Since the volume of the system changes during a move, so does the statistical weight of the configurations, and this is taken into account in the logarithm term in the acceptance criterion.

4.4.2 Interphase switch move

The phase switch move swaps which system is active (+) and which is passive ($\oslash$). This can only occur in gateway states, that is for hard-spheres when $\mathcal{M} = 0$. This is because for all other values of order parameter, the energy of the passive system will be infinity due to overlaps. We cannot switch to a system that has an energy that is not allowed and also it would never be accepted. In summary, the active system is a normal MC simulation with the inter phase switch move added as an extra MC move. The passive system is used to keep track of the order parameter value and to make calculation of the interphase switch probability simple. The value of the order parameter $\mathcal{M}$ is stored after every particle move and then, if the acceptance criterion is met, the phase switch move is accepted. This ensures that both positive and negative values of $\mathcal{M}$ are explored. Since the order parameter value is already known the phase switch move is essentially free as no other calculations are needed.

The probability for accepting an interphase switch move at constant density, is

$$P_{\text{acc}} = \min(1, \exp[-\beta(E_{\oslash} - E_{+})]), \quad (4.25)$$

where $E_{\oslash}$ is the energy in the passive system (switching to) and E_{+} is the energy in the active system (switching from). For this move to be accepted in a hard sphere system, both energies must be zero and hence no calculation is needed.

At constant pressure, the probability for accepting an interphase switch move is

$$P_{\text{acc}} = \min(1, \exp[-\beta\{\Delta E + P\Delta V\} + N\ln(V_{\oslash}/V_{+})). \tag{4.26}$$

This involves calculating the change in volume between the two systems. If they have the same volumes then this calculation also reduces to zero and will always be accepted for a system with zero energy.

4.4.3 Synchronisation

Our implementation of phase switch Monte Carlo does not include the system dependent mapping that Bruce et al. [17] utilise, since our implementation is to concurrently run the two phases with the same Monte Carlo moves applied. Due to the finite nature of computational storage, there will always be rounding errors accumulating, and these errors will cause our two systems to diverge. In order to counteract this divergence we periodically recalculate the change that has occurred due to the Monte Carlo moves in the active system and synchronise the other system to this value. These rounding errors will be discussed later in this section.

In order to do this we must have a way of calculating the sum of all Monte Carlo moves that have been applied to a system. Our implementation for this is to use the initial, also referred to as reference, configuration and the current configuration and calculate the changes between them. When calculating the changes we need to be aware of what degrees of freedom we have in the system and what the Monte Carlo moves change.

In a constant volume simulation, our only Monte Carlo moves are translations. This gives us a very simple calculation in order to ensure the two simulations are synchronised. We need only compare the cartesian displacement vector between the initial and final states. We calculate this displacement vector $\underline{R}$ for each particle i

$$\underline{R}_{\alpha,i} = \underline{r}_{\alpha,i} - \underline{r}^{\text{ref}}_{\alpha,i} \tag{4.27}$$

where $\underline{r}_{\alpha}$ are the coordinates for particle i in phase α and $\underline{r}^{\text{ref}}_{\alpha,i}$ denote the reference coordinates for the same particle. This can be seen to be equivalent to the alternate definition of the particle positions as

$$\underline{r} = \underline{R} + \underline{u}, \tag{4.28}$$

where $\underline{r}$ are the current coordinates of the particles, and $\underline{u}$ are the lattice vectors for the phase, when in our case we use an arbitrary $\underline{r}^{\text{ref}}_{\alpha,i}$ configuration from the

equilibrium distribution as a reference.

The procedure for the synchronisation of the two systems is to calculate the displacement vector for each particle for the phase that is currently active and then apply those displacement vectors to the reference configuration of the passive phase. This newly calculated configuration is then set as the new configuration of the passive system. The order parameter must then be recalculated and the weighting function updated.

When simulating at constant pressure we have to include volume moves as well. Therefore we need to calculate the difference in volume between the active and passive systems and set the passive accordingly.

Since we are only accounting for a small build up of errors with synchronisation process, we need only apply it to the system infrequently. In all simulations the synchronisation of the two systems only occurs every 1000-10,000 Monte Carlo cycles.

Floating point numbers

Floating point is a method to represent an approximation of real numbers on a computer using a fixed, discrete amount of memory that covers a wide range of values; 64 bits is the amount for double precision. In general numbers are represented approximately to a fixed number of significant digits (the mantissa), and this can then be scaled using an exponent. The base used for scaling is usually base 2, so a typical number is represented as

$$significant\ digits \times base^{exponent}. \tag{4.29}$$

This allows the resolution to be adapted to the numbers, and no space is wasted on unnecessary zeros. A wide range of numbers can be stored, however, there is a trade off between range and scale implicit in this definition. This is where thermodynamic integration can have problems if the two absolute free energies are much larger than the difference, as this means the difference will only be accurate to a few digits.

The most common representation is the IEEE Standard for Floating-Point Arithmetic (IEEE 754) which is a technical standard for floating-point computation established in 1985 by the Institute of Electrical and Electronics Engineers.

Since we are trying to fit infinite numbers into a finite space, the values must be rounded to fit the finite representation. There is obviously an error associated with this necessary rounding, and it also implies that what may be an exact calculation for the full numbers will be a rounded calculation for the approximate values.

This can be seen most easily for a decimal number, 0.1, that has a finite representation in decimal and yet an infinite representation in binary. Therefore, when one adds two of these numbers together rounding errors will occur in the calculation.

Due to the finite nature of computers and the infinite nature of real numbers we must be aware of the possibility of rounding errors and approximations when doing arithmetic on data many times. These errors are only of the order of the significant digits of the computer, however when doing billions of operations they add up.

4.5 Computational considerations

4.5.1 Order parameter space

The width of the order parameter space to use in a simulation should be determined from the width of the corresponding, unbiased probability distribution. It is computationally inefficient to simulate a larger range than necessary. The position of the distribution in order parameter space can be calculated by running simulations initialised with phase α as active and γ as passive, with phase switch moves turned off and the histogram bins made very wide. This set up ensures that the quasi-stationary probability distribution, corresponding to the currently active system, is calculated and so the distribution in the order parameter is known. This is also calculated the other way round so the the distribution for phase γ as active is known as well. The distributions are not equilibrated with respect to each other however.

These distributions show us what the range of order parameters values for each phase are, Figure 4.6 shows one side of the distribution for the hard sphere system. When calculating the free energy we will be comparing these distributions and so it is necessary to know how far along the order parameter space we must push our system to ensure that we include enough of their tails to compute accurate probabilities. The width of the order parameter space is taken as slightly larger than the end of the distribution for each phase; this gives us the upper and lower bound for the order parameter. Since we are only interested in the relative probability distributions, it is unnecessary to push the system out further, and we must only ensure that we include all the relevant area. This also shows that the probability of being in a state with an order parameter value of zero is extremely low, and this validates our need for biasing.

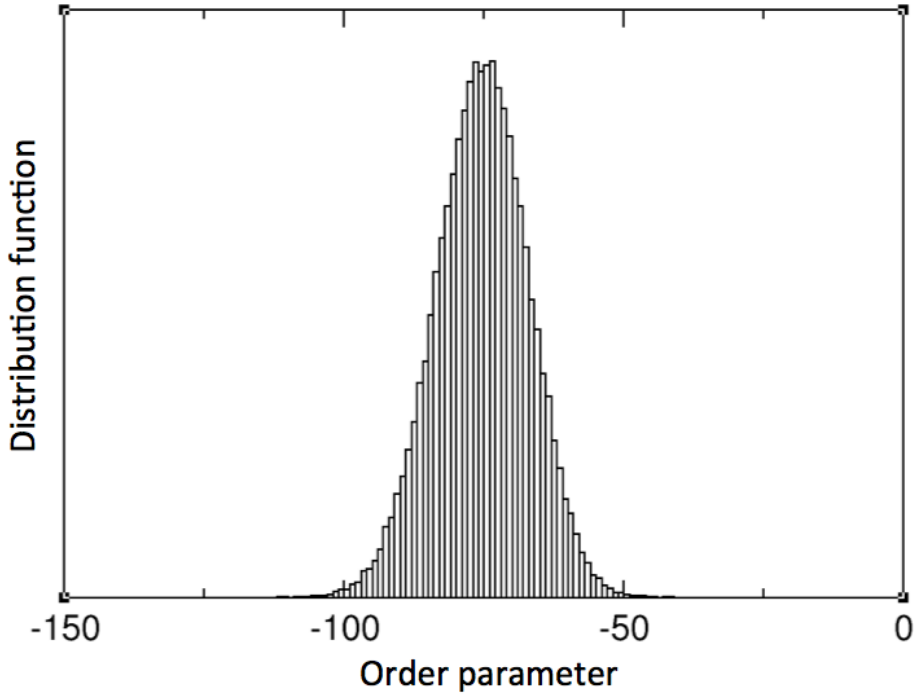

Figure 4.6: Quasi-stationary probability distribution in order parameter space with no biasing for a system of 216 hard spheres.

4.5.2 Neighbour lists

The energy of the system needs to be calculated many times in a simulation, for example before the move acceptance is checked and after a volume move; this is the most expensive part of the simulation. The naïve approach to energy calculations is to loop over all pairs of particles and check for overlaps between them. This means that for a system of N particles $N(N-1)/2$ interactions between pairs must be evaluated. This can obviously become very time consuming as system sizes increase because it scales on the order of N^2. Especially with a hard sphere system, many of these particles may not even be close together, hence we should use an algorithm to separate out the close particles from the far particles and reduce our computational effort. There is a minimum system size below which it will no longer be efficient to create and maintain these algorithms, however for any system above 100 particles it is considerably more efficient to use the algorithms. For crystalline systems neighbour lists are particularly effective because the need to re-calculate them is reduced due to the fixed nature of the structure.

Verlet neighbour list

If our simulation box is larger than our cutoff r_c, which for hard sphere is the diameter, many particles will not contribute to the energy of particle i. Therefore, excluding these particles from the calculation is very advantageous and will greatly reduce the cost of the energy calculation. A second cutoff r_v is created so that $r_v > r_c$ the potential cutoff. A list of particles that are within r_v of each other is created and used for the purpose of energy calculation. This has reduced our calculation from order N^2 to order N, see Figure 4.8. However, as soon as one of the particles has moved more than $r_v - r_c$ the whole list needs to be recalculated, which is of order N^2. For solid systems, the movement of most particles from their lattice site is minimal and so the neighbour list should be robust if initialised with large enough width. The Verlet list can be used with both Monte Carlo and molecular dynamics, with only slightly different implementations.

Cell lists

The system is split up into domains of length slightly larger than the cutoff; for soft systems four-times the cutoff is a reasonable amount. This ensures that particles will only interact with other particles in their own cell or neighbouring ones, as shown in Figure 4.7. This reduces the number of particles to loop over when calculating the energy of the system and scales with N. The allocation of a particle to a cell scales with N and the number of neighbour cells that need to be considered is independent of the system size. This method obviously is not very effective when the number of cells is less than three in any direction, because then no cells are being excluded from calculations. There is also the cost of adding and removing particles from cell lists periodically.

4.5.3 Multicanonical bias parameters

When creating and using our bias function there are many options available to us in regards to the implementation. The most obvious choices are the initial value of the refinement factor and our choice for the flatness criterion. The choice of flatness criterion, especially, can have a large effect on the simulation. Many studies have looked at the error between the calculated density of states from a Wang-Landau simulation compared with the real density of states for that system. However, some articles show that the method converges to the real result [122, 32, 76] while other work shows a saturation in the error [119, 112]. This contradiction in literature on the convergence of this method is somewhat clarified by Belardinelli and Pereyra

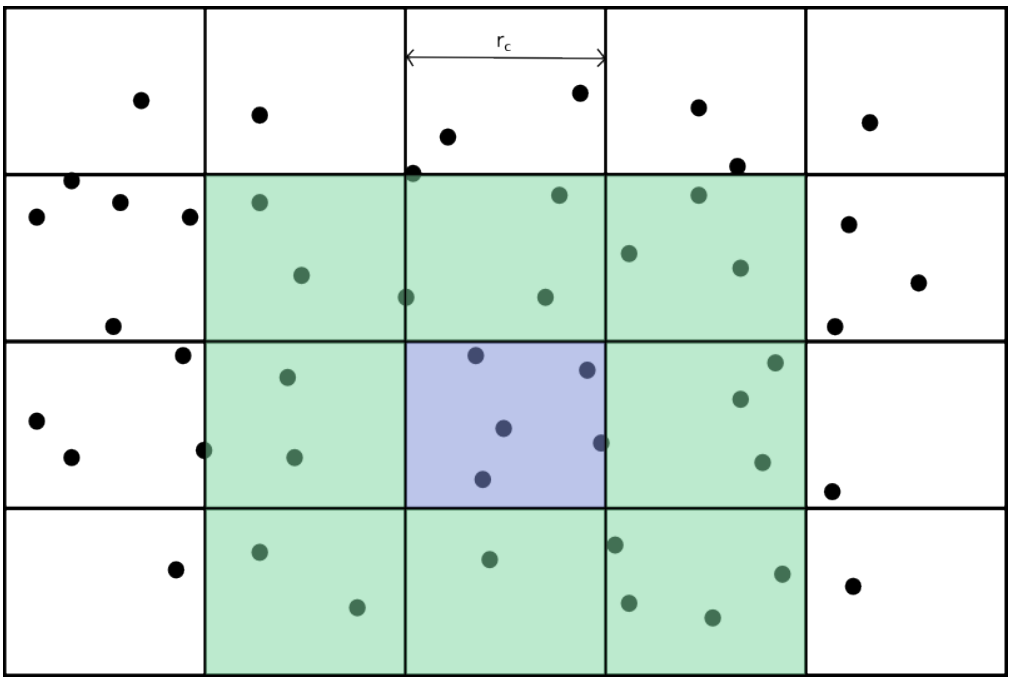

Figure 4.7: The simulation box is divided into cells of with r_c, particles in the blue shaded cell will only interact with particles in that cell and the green shaded neighbouring cells.

[7] who showed mathematically that if the refinement parameter reduces faster that $1/t$, where t is the Monte Carlo time, then the error will saturate; this could explain some of the discrepancies between the work on this subject.

The difficulty with continuous systems is the lack of exact densities of states with which to compare the simulation results. Most work on error saturation is done on discrete Ising-like models; these are a long way from continuous simulations and are much more simplified. However, Li et al. [63] suggested the application of the Wang-Landau method to numerical integration, which is the simplest continuous system available. Belardinelli et al. [8] looked at the saturation of error in continuous numerical integration systems and confirmed that the $1/t$ adaptation is more accurate for all systems studied. They also showed that the bin width used for storing the density of states introduces a saturation of error in the $1/t$ algorithm as well as the original algorithm.

For the hard sphere systems we have a discrete order parameter due to the discrete nature of the hard sphere system. This means that we can avoid this saturation of error if we stick to the natural resolution of our system, that is we have a bin width of one. We also must be aware of the possibility of a saturation

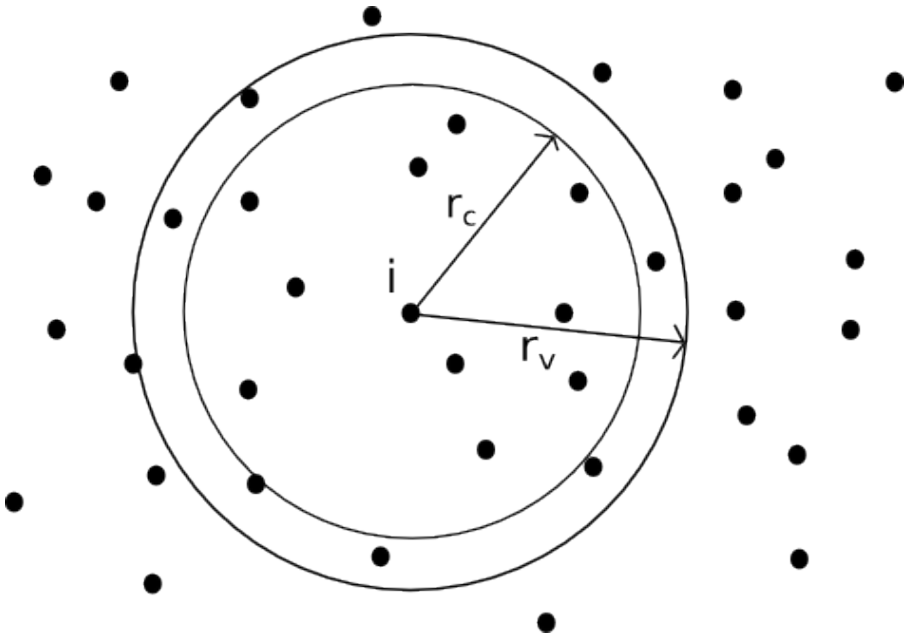

Figure 4.8: The Verlet list contains all particles within a distance r_v of particle i, particles within r_c of particle i will interact with it.

of error in the method, and we can reduce this error by increasing the strictness of our flatness criterion. We can also test the error in our calculations against previous work from different methods and if the error between them is too great then this is a possible cause and could be alleviated by using the $1/t$ adaptation. We only need to ensure that our biasing function is good enough to allow us to sample the full order parameter space during a simulation with fixed biasing function; the more accurate it is though, the shorter our production runs can be.

Schulz et al. [92] discussed issues in regards to the treatment of the boundaries of the order parameter or energy range with Wang-Landau style multicanonical methods. When a boundary is reached a choice is made about how trial moves, that would take the simulation outside of the allowed range, are treated.

In the original Wang-Landau method they rejected the trial move without updating the current histogram or density of states function. It was shown that this leads to a systematic underestimation of the density of states at the boundaries. Instead, when proposing a trial move that would take the simulation outside the allowed range, we should reject the move and then update the histogram and biasing function for the current order parameter value; this was shown to produce no systematic errors.

This is especially important when using a variant of the Wang-Landau method

where the order parameter range is split up in to 'windows' with overlapping sections, Figure 4.9. Separate simulations are run in each window and this means that the range for each simulation is smaller and more manageable. These windows are then joined together to form the complete function or density of states. If there are lots of boundaries then more care is needed when dealing with possible errors in the boundaries. Even though Schulz et al. [92] showed that there was no systematic error in the boundaries once they updated the histograms when a rejection occurred, this was only for a simple Ising model system and it may be more complicated for complex, continuous systems.

Cunha-Netto et al. [26] suggested that having fixed windows was the issue and led to a build up in error around these fixed boundaries. They suggested a method with adaptive windows where the boundaries change whenever the refinement parameter is reduced. They showed that this was an effective method for large continuous systems such as polymers [27].

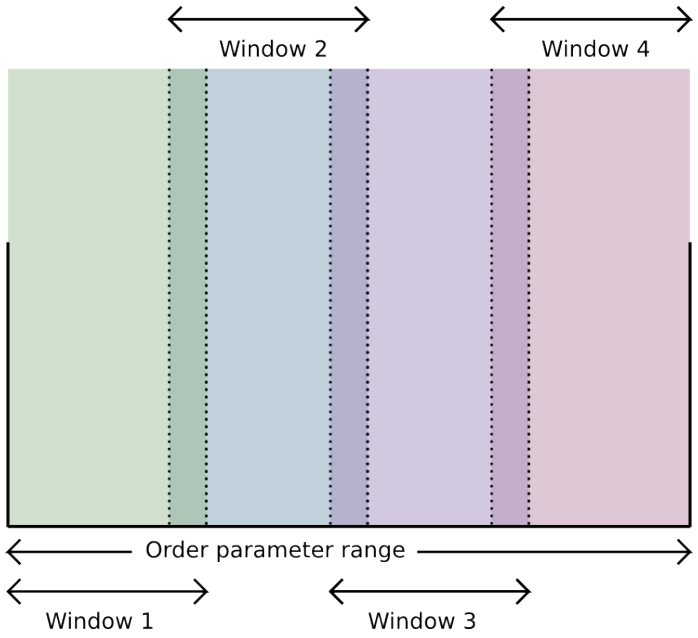

Figure 4.9: The allowed order parameter range is split into overlapping windows, labeled in different colours in the diagram. A separate simulation is run within each window.

However, since the hard sphere system is so simple, these extensions of the multicanonical method may not be necessary.

When using the multicanonical biasing in the hard sphere system, the initial order parameter is at the gateway state that we want to bias towards. This is

because both crystals are initialised to allowed configurations and hence the order parameter is zero. Therefore we let the system equilibrate to higher order parameter values for 1,000 MC cycles before building up the weighting. This ensures that the gateway states are not over sampled at the beginning leading to long convergence times as this is corrected.

Another possible option to speed up the early parts of the convergence is whenever a new bin is visited, that has never been visited in this simulation before, we increase it by the smallest non-zero value in the weighting [60]. This should speed up the coverage of the entire space, but obviously this does not affect the simulation once all the range has been explored. However, this is more useful when there is not a fixed range of order parameter space or it is very hard to traverse. Neither of these situations occur in our simulations, and it was deemed an unnecessary computational effort as the simulations run fast enough without it.

The final parameter that needs to be decided upon is the initial value to use for the refinement parameter. The larger the starting value the faster the simulation will be pushed around the space but the longer it will take to get to a small enough value to say that the simulation is converged. However, if we start with a very small refinement value then the time taken to build up enough bias to push the simulation around the entire space will be very long. Therefore, a balance needs to be struck between these two factors.

4.5.4 Mapping between phases

When we create our two crystal structures, we have a choice in how we number the particles: either we can randomly assign each particle in each structure an index from $1 \rightarrow N$, or we can give similar particles in the two phases the same index.

The advantage of a good mapping of the particle numbers between the two phases is that the range of order parameter space that needs to be sampled will be narrower and this means that convergence of the weighting function will be faster; also less memory will be needed to store the arrays. The free energy difference is independent of the mapping chosen.

4.5.5 Validation

The obvious validation of the code is to apply it to find the free energy difference between fcc and hcp crystals of hard spheres. This is a good validation as this system has been studied by phase switch MC previously [17] and also by thermodynamic integration methods [38, 84, 82]. Another reason it is a good test system is that

the free energy difference is very small between the two phases and so it fully tests the method and will be sensitive to any irregularities. Fcc and hcp phases are very similar structurally: they are both close-packed hard sphere phases made up of layers stacked on top of each other; the difference comes from the stacking of the layers (Figure 4.10).

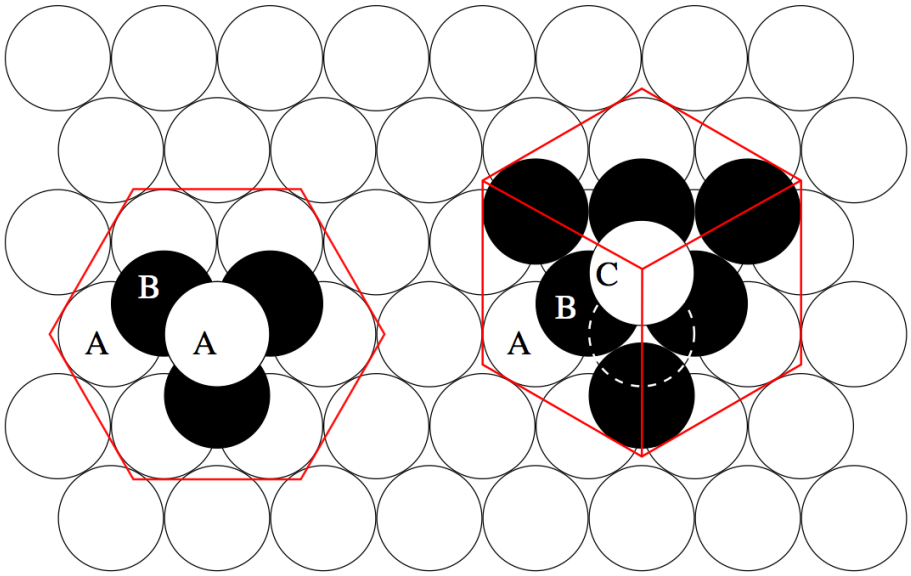

Figure 4.10: The build up of layers in hcp (left) and fcc (right) crystals, obtained from Wiki Commons in the public domain.

There are three different ways of stacking close-packed hard spheres into layers: A, B or C. Fcc stacking repeats layers in the pattern ABCABC and hcp stacking repeats the pattern ABAB.

4.6 Simulation details

In order to ensure comparible crystal phases without stacking faults, our systems must be a multiple of three and two in the z-direction. For this reason we chose to simulate systems of size $6^3 = 216$, $12^3 = 1728$ and $18^3 = 5832$ in order to calculate finite size effects. All densities of the hard sphere system are quoted in terms of the reduced density,

$$\tilde{\rho} = \frac{\rho}{\rho_{cp}} \tag{4.30}$$

where $\rho_{cp} = \sqrt{2}\pi/6$ is the density of the close-packed system and $\rho = V_{ex}N/V$, where V_{ex} is the volume of a sphere. Simulations were performed at a range of constant densities from near the melting density towards close-packings, $\tilde{\rho} = 0.736 \rightarrow 0.85$ at a spacing of roughly 0.025. A value of $\tilde{\rho} = 0.7778$ was used for comparative purposes due to its prevalence in the literature.

A maximal move displacement of 0.12σ was chosen for all system sizes at $\tilde{\rho} = 0.7778$ to produce an efficient acceptance ratio. As the density was increased this displacement was reduced to retain a similar acceptance ratio.

Weights were generated until the value of f was reduced so that $|f - 1.0| < 1 \times 10^{-10}$; this resulted in $\sim 1 \times 10^8$ MC sweeps for $N = 216$. All simulations were run in serial on university workstations. The free energy differences were then calculated from simulations run using these calculated weights of fixed value. A series of runs were made for each system size to give independent estimates of the free energy difference. The standard deviation of these results was used as a basis for the statistical uncertainty in the results.

4.6.1 Initial conditions

The code was written so that both crystal structures are automatically generated for a given number of particles in the x, y and z directions, where z is taken to be the layering direction. In order to avoid stacking faults in the periodic images of our system the number of z layers must be a multiple of 6. The structures generated are the perfect crystal structures isotropically scaled by $\sqrt[3]{1/\tilde{\rho}}$ to produce the desired reduced packing fraction. The mapping chosen for numbering equivalent atoms between the two phases utilises the similarity between layering in the two phases. The particles are numbered so that the particles in both phases have the same index in x, y, and z directions.

4.7 Results for hard sphere system

Whether the fcc or hcp phase is lowest in free energy was unknown until 1997 when Woodcock presented a paper in Nature [118]. With an estimated error of $\sim 20\%$ the actual value of the result could not be relied upon, just the conclusion that fcc is the most stable.

This result has been substantiated and more exact numerical values found in various simulations [84, 73, 17, 82]. Hence, this is a well documented, yet difficult and small value to validate against, and to test the accuracy and computational expense of our adaptations and alterations.

Therefore we calculated this result using our new implementation of phase switch MC. The change in order parameter value with MC cycles should be checked to ensure full coverage of the allowed space, as shown in Figure 4.11. The phase switch move occurs at an order parameter value of zero and so it can be seen from this figure that many switches occur and hence our biasing technique can be assumed to be working effectively. The number of accepted phase switch moves can be seen to be a linear function of Monte Carlo cycle in Figure 4.12. This shows that there are a constant number of switches with time and our system is not getting stuck in a single phase for long periods of time, showing that our sampling is good and our biasing effective.

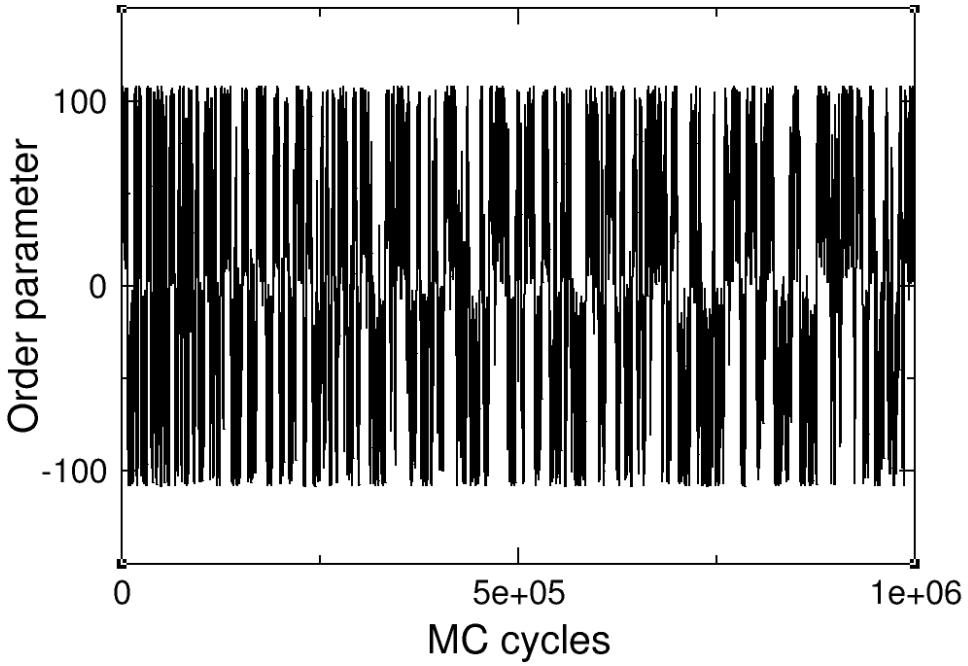

Figure 4.11: The order parameter value as a function of MC cycles, between $\mathcal{M} = \pm 108$.

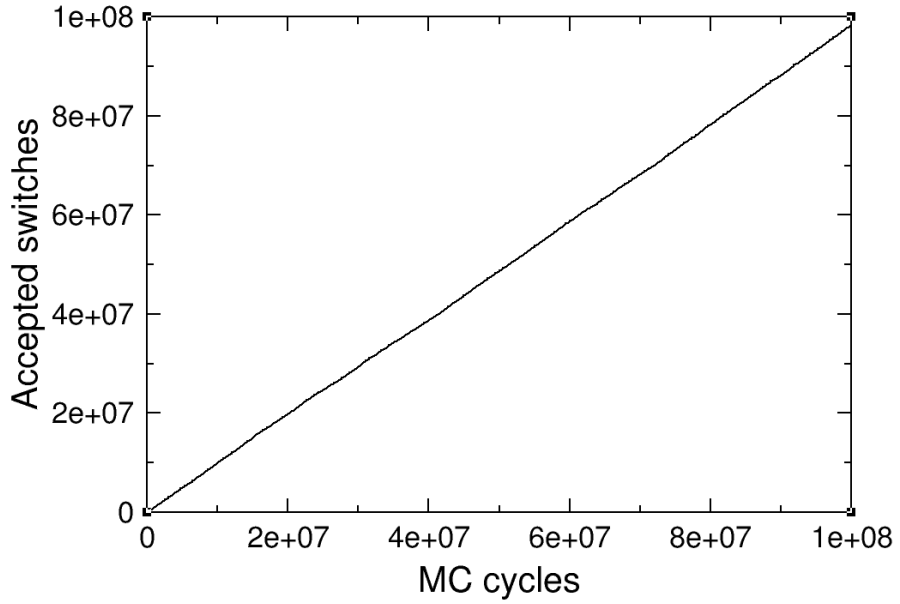

Figure 4.12: The number of accepted interphase switch moves as a function of MC cycles for hard spheres, fcc-hcp.

The biasing function converging with the number of Monte Carlo cycles is shown in Figure 4.13. The simulation initialises with an order parameter value of zero, so in Figure 4.13(a) an initial weighting has been built up as the simulation starts to move towards higher order parameter values. This then builds up on one side pushing the weighting further from the gateway state at $\mathcal{M} = 0$ in Figures 4.13(b, c). A similar process occurs after the simulation switches to the opposite sign of order parameter in Figures 4.13(d, e). The weighting function is still very rough at this point, but it smooths out as the simulation progresses. A larger weighting on one side than the other indicates that that side of the order parameter has been visited more often than the other and hence will have a higher probability. In Figures 4.13(e, f, g) we can see that the two sides oscillate about their final value while the weighting function is converging. The final result in Figure 4.13(h) shows the positive and negative sides of weighting function with nearly identical heights and areas, signifying how close in free energy the two phases are. The negative side favours fcc and the positive side favours hcp.

To converge the biasing function our increment factor, $\ln(f)$ is reduced when the histogram is sufficiently flat. A plot of this reduction in $\ln(f)$ gives us a measure of how fast our simulation is; see Figure 4.14. It can be seen that some of the decreases in $\ln(f)$ vary between lots of reductions close together and occasionally there will be a few long gaps. However, if we look at just the general curve of the

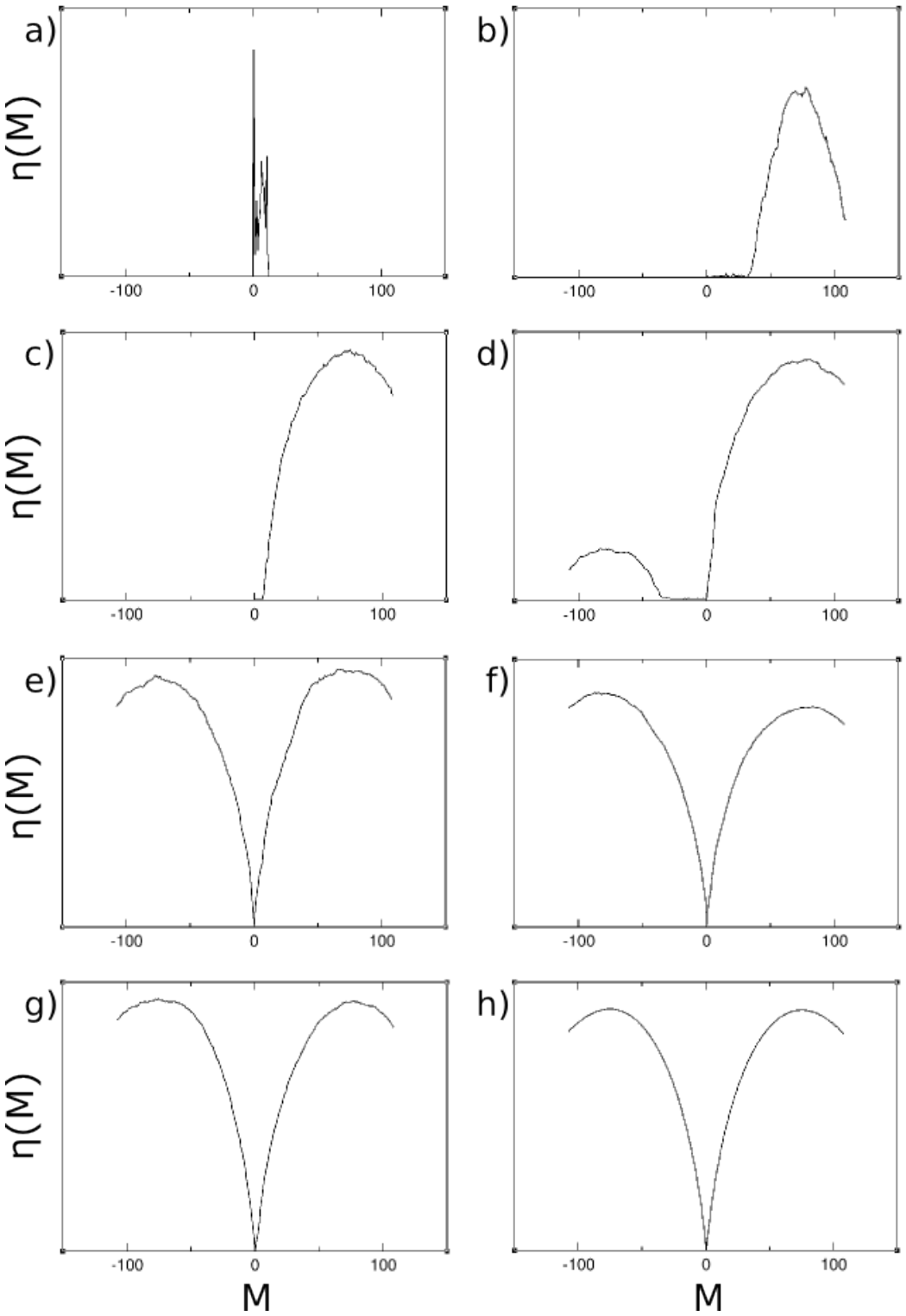

Figure 4.13: The biasing function $\eta(\mathcal{M})$ for $N = 216$, at a reduced density of $\tilde{\rho} = 0.7778$ for increasing numbers of MC cycles: a) 0, b) 1,000, c) 5,000, d) 9,000, e) 20,000, f) 80,000, g) 100,000, h) 100,000,000

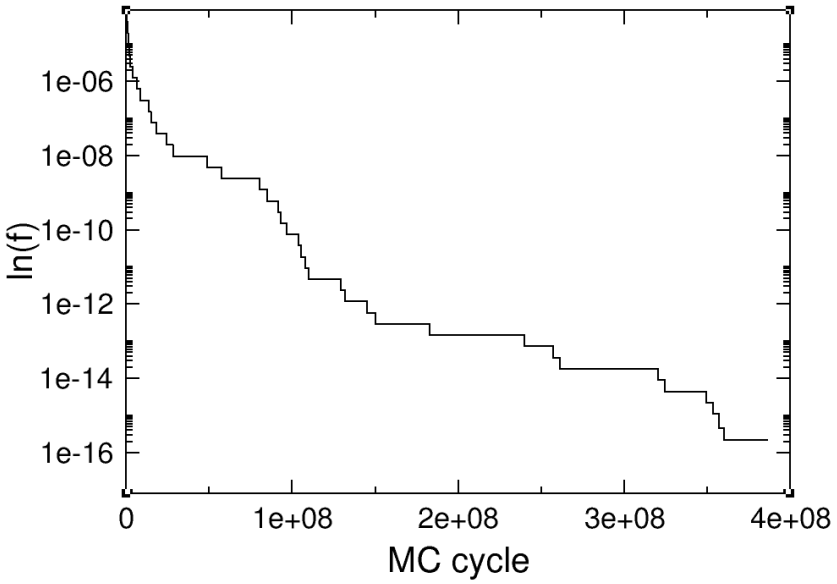

Figure 4.14: The reduction of the log of the biasing increment value as a function of MC cycles for $N = 216$ at $\tilde{\rho} = 0.7778$ with a flatness criterion of 0.95%.

reduction in $\ln(f)$ we can see a very quick initial drop which then oscillates about a linear line for the rest of the simulation.

As well as the weighting function, we also store a histogram of visits, and this is used to check the flatness of the distribution in order to reduce the increment value, $\ln(f)$. A histogram while creating the biasing function is shown in Figure 4.15. It can be seen that the minimum value is not within 0.95% of the mean, however, this is not an issue because the weights are converging in this simulation.

A histogram from a simulation run with fixed weights is shown in Figure 4.16. The minimum of this histogram is well above 0.95% of the mean value, showing that the weighting function is working very well as the histogram is much flatter than the criterion used.

4.7.1 Helmholtz free energy

The normalised probability distribution functions of the overlap-order parameter for a range of isotropically increasing system sizes at constant density where the bias has been unfolded is shown in Figure 4.17. From Equation (4.11) we can calculate the free energy difference between the two phases using the ratio of the areas of the two peaks. It can be seen from Figure 4.17 that the free energy difference between the two phases must be very small for these distributions to be of the same order of magnitude. The mapping between the two phases is the same for all system sizes,

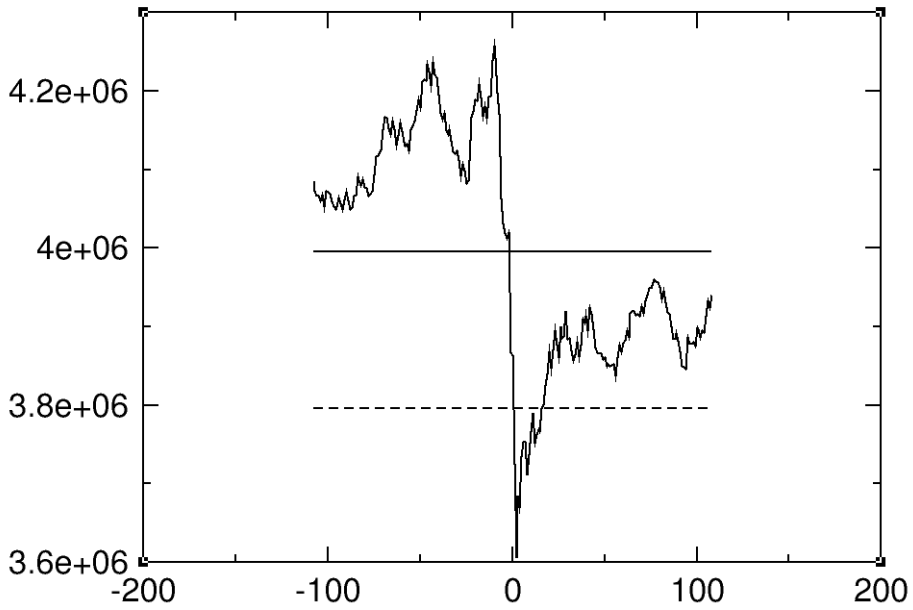

Figure 4.15: The histogram generated during creation of the weights for $N = 216$ at $\tilde{\rho} = 0.7778$. The straight solid line indicates the mean value and the dashed line is 0.95% of the mean, which is the flatness criterion.

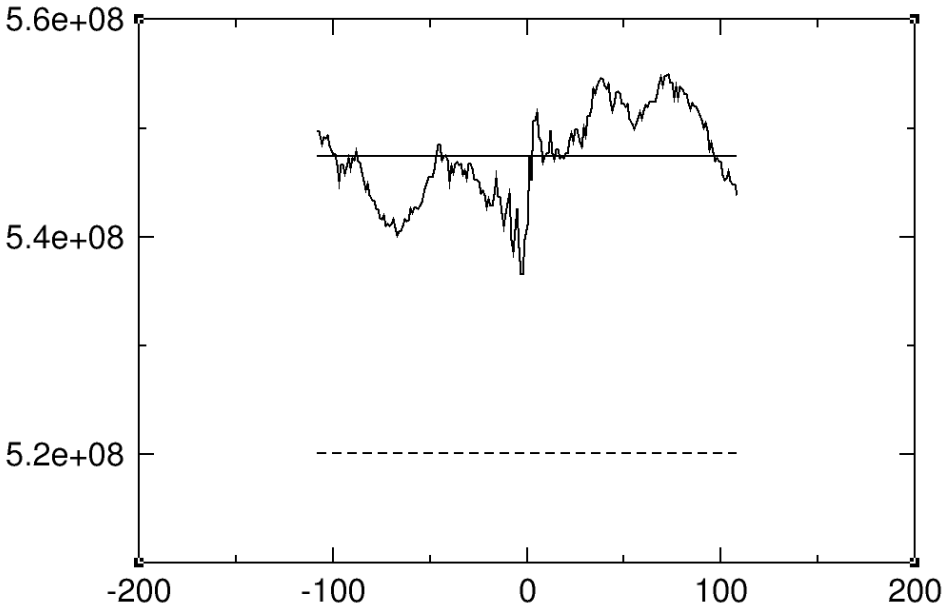

Figure 4.16: The histogram from using the fixed weights for $N = 216$ at $\tilde{\rho} = 0.7778$. The straight solid line indicates the mean value and the dashed line is 0.95% of the mean, which is the flatness criterion from making the weights.

which is why the peaks are all centred on the same value of $m = \mathcal{M}/N$.

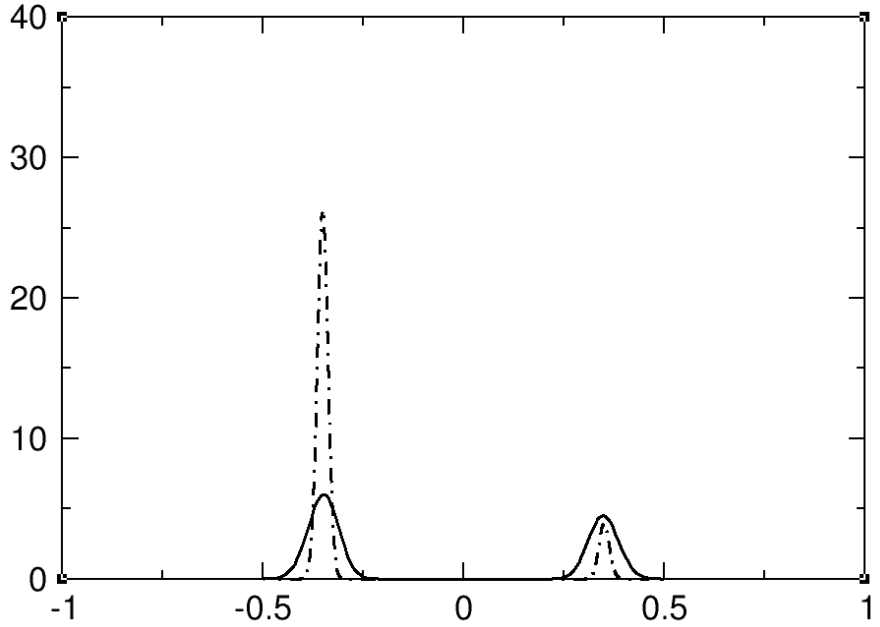

Figure 4.17: The probability distribution for $N = 216$ shown by the solid line, and $N = 1728$ shown by the dashed line.

These results for the Helmholtz free energy difference between fcc and hcp crystal structures are shown alongside existing data in Table 4.1. Positive values favour the fcc structure since a lower free energy means that structure is the most stable, and $\Delta F_{hcp,fcc} = F_{hcp} - F_{fcc} > 0$ because $F_{fcc} < F_{hcp}$.

N	$\Delta F(10^{-5} k_{\mathrm{B}} T)$	Method	Reference
216	133 ± 2	LS	CW
1728	112 ± 2	LS	CW
5832	112 ± 3	LS	CW
216	132 ± 4	LS	[84]
1728	112 ± 4	LS	[84]
1728	113 ± 4	IM	[84]
216	133 ± 3	LS	[17]
1728	113 ± 3	LS	[17]
5832	110 ± 3	LS	[17]

Table 4.1: The Helmholtz free energy difference (hcp - fcc) per particle (Equation 4.16, 4.11). The results are all for systems at a reduced density of $\rho/\rho_{cp} = 0.7778$. CW denotes the current work, LS is lattice/phase switch method and IM is integration method.

This result confirms that the fcc crystal structure is lower in free energy. It can also be seen that our results have very good agreement with the existing data, even from different methods. Our errors are equivalent, as is expected and could be reduced further via longer simulations. It is taken that $N = 1728$ is representative of the thermodynamic limit as larger system sizes do not affect the result significantly. The errors were calculated from the standard deviation of the averages of a series of runs.

The convergence of the Helmholtz free energy difference for a system with $N = 6^3 = 216$, is shown in Figure 4.18, and it can be seen that our result is well within the errors from previous work. The longer the simulation, the more converged our resulting value of $\Delta F_{hcp,fcc}$ is.

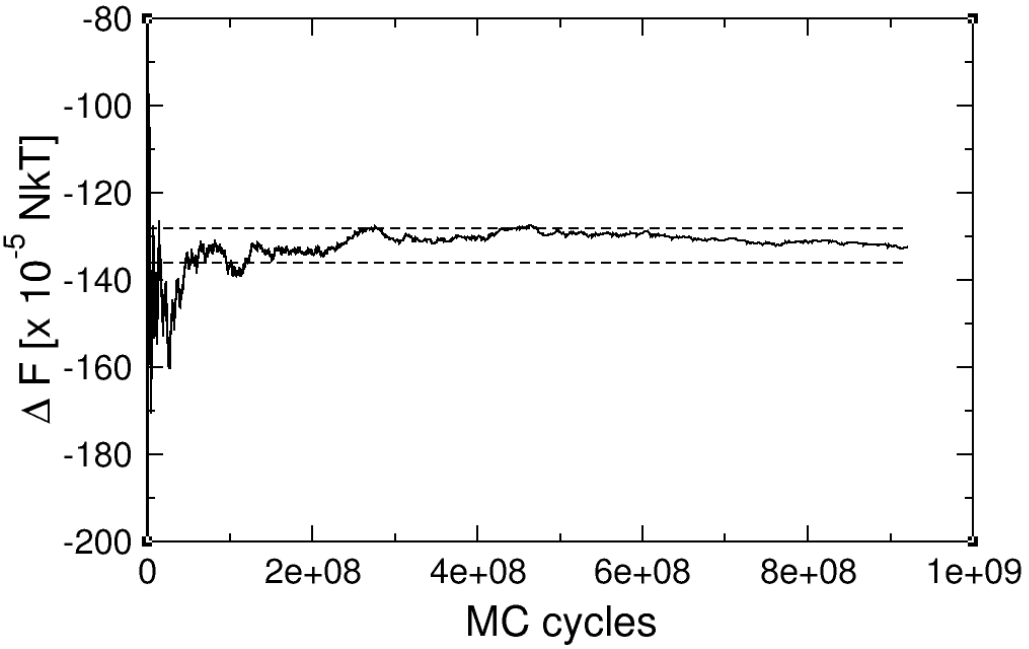

Figure 4.18: The value of $\Delta F_{hcp,fcc}$ per particle for $N = 216$ at a reduced density $\rho/\rho_{cp} = 0.7778$: black dashed lines denote the error bar in previous work [84].

We have calculated the Helmholtz free energy differences for a range of reduced densities as shown in Figure 4.19; the trend is compared with previous calculations.

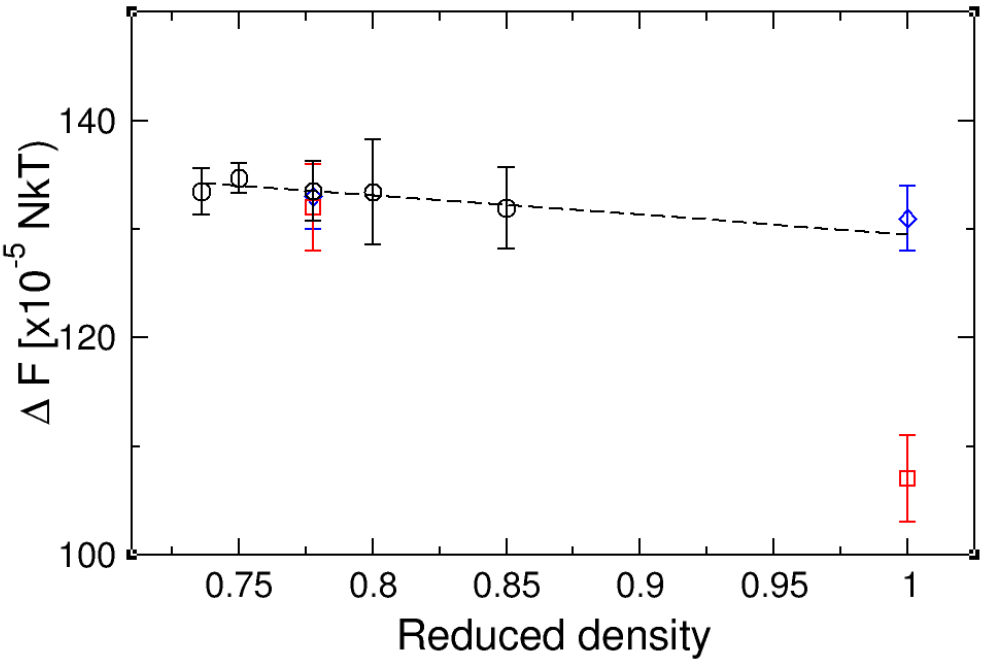

Figure 4.19: The value of ΔF per particle for $N = 216$ at a range of reduced densities: black circular points are from the current work, blue diamond points from reference [17], and red squares from Mau and Huse [73]. The black dashed line is a linear fit to our data.

$\tilde{\rho}$	$\Delta F(10^{-5} N k_{\mathrm{B}} T)$
0.736	133 ± 2
0.75	134 ± 2
0.7778	133 ± 2
0.80	133 ± 5
0.85	131 ± 4

Table 4.2: The Helmholtz free energy difference (hcp - fcc) per particle (Equation 4.16, 4.11). The results are all from the current work at a system size of $N = 6^3 = 216$.

It can be see that our results, shown in Table 4.2, compare very well with existing work and our extrapolated value at $\tilde{\rho} = 1.0$ matches very well with the work done by Bruce et al. [17], shown in Figure 4.19. There is also very little change in free energy difference with density. We did not calculate the free energy difference for reduced densities above 0.85 because the acceptance ratio became exceedingly

small, even with a small move attempt size. $\tilde{\rho} = 0.736$ is the melting temperature so we did not simulate below there as the crystals might melt. Our data are also compared to work by Mau and Huse [73] and although the data points at $\tilde{\rho} = 0.7778$ are in very good agreement, their calculated value at $\tilde{\rho} = 1.0$ is much lower that our estimate. The results at $\tilde{\rho} = 1.0$ are both from calculations and not simulations.

Finite size effects

Modelling infinite systems via a finite simulation box upon which periodic boundary conditions are applied is often the only feasible way to approximate bulk properties. However, the finite simulation cell introduces an independent particle finite size effect. This is an error in the energy per particle between the finite and infinite system due to artificial periodicity which leads to different structure. As the finite system size increases this error decreases. It is necessary to calculate results for a variety of sizes and from these the value for an infinite system can be extrapolated. The standard way is to plot $\frac{1}{N}$ versus the result of interest, extra care must be taken with anisotropic expansions of the system [82]. A regression line is then calculated through the points and extrapolated to $\frac{1}{N} = 0$ to give the value for an infinite sized system.

For the hard spheres we chose isotropic expansion by a factor of 3, in all directions, each time. This ensures comparison with previous work and that the stacking layers are perfect for both systems.

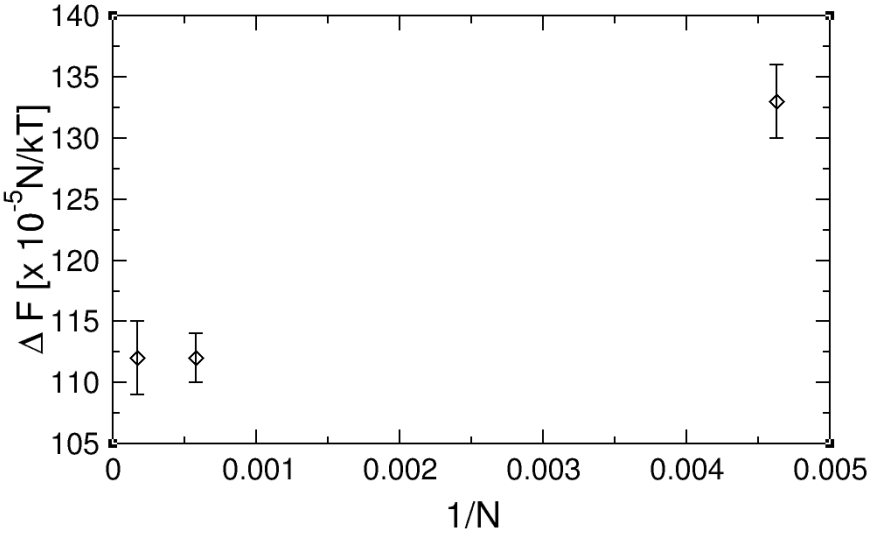

Figure 4.20: The Helmholtz free energy $\Delta F_{hcp,fcc}$ per particle at $\tilde{\rho} = 0.7778$ against $1/N$.

In Figure 4.20 it can be seen that a system size of 1728 is large enough to be representative of the thermodynamic limit, so we have chosen this as the largest system to simulate for other calculations. The $\frac{1}{N}$ fit only accounts for the dominant contribution to the finite size error and other higher order terms are likely to be exposed by our highly accurate calculations.

4.7.2 Stacking arrangement

Hard sphere crystals have three layering options for their stacking, A, B, or C Figure 4.10. fcc and hcp crystals differ only in how the layers of spheres are arranged: an fcc layer has two different layers on either side of it whereas a hcp layer has the same layer above and below it. We can arrange the layers of a crystal to form a mixture of fcc and hcp layering. Mau and Huse [73] investigated the stacking via simulations and fitted to an Ising model. They found that it was necessary to look at the second nearest neighbours as well when calculating the entropy of the system. This means that it is not just the number of each type of layer that affects the entropy but how they are arranged. It is not possible to compare our simulation results with their Ising-like model because it is equilibrated for a different density.

In order to look into this further we simulated two crystals with no overall stacking defect and with the same number of fcc (c) and hcp (h) layers, but with different arrangements of the layers. The two layerings are shown in Table 4.3. We are looking specifically at the free energy difference between alternate and grouped layers.

N	layers	stacking	label
$1728 = 12^3$	ABCACACACABC	ccchhhhhhccc	D
$1728 = 12^3$	ABCBABCBABCB	hchchchchchc	E

Table 4.3: The layers and stacking of the two crystals we are calculating the Helmholtz free energy difference between: c denotes a layer with fcc stacking and h a layer with hcp stacking.

We ran at a constant density of $\tilde{\rho} = 0.7778$ and the weighting function was reduced 20 times from a starting value of $f = 1.0005$, the results are shown in Figure 4.21.

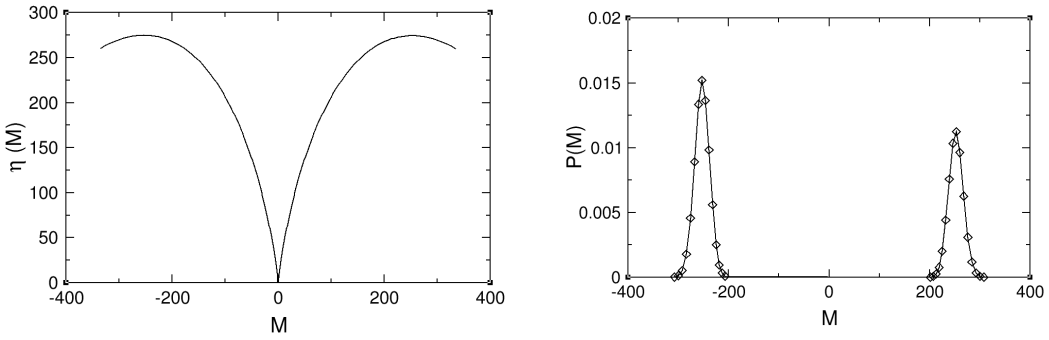

(a) (b)

Figure 4.21: a) The weighting function after 20 reductions of the increment factor and b) the probability distribution function from the weighting function for varying stackings of hard sphere crystals.

It can be see in the probability distribution, derived from the weighting function $P(M)$, that there is a slight free energy difference between the two crystals. We then ran on top of the fixed weighting function and calculated the free energy difference, Figure 4.22.

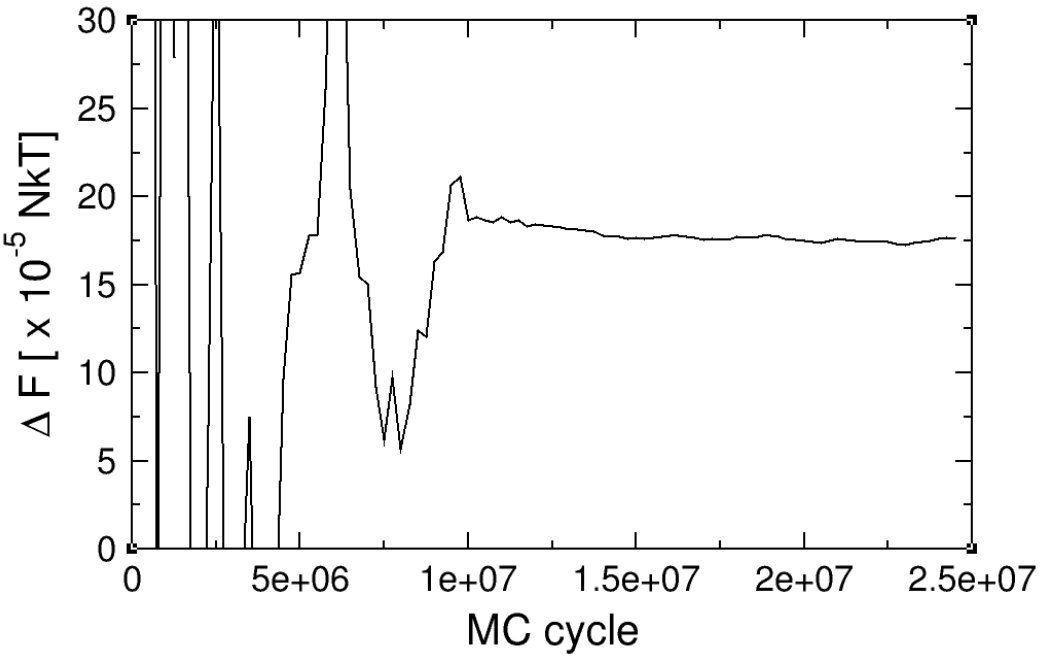

Figure 4.22: Convergence of the Helmholtz free energy per particle between stackings at a density of $\rho = 0.7778$.

Our final value for the Helmholtz free energy difference per particle between the two stacking arrangements is $\Delta F_{E-D} = 17.7 \pm 0.2 k_{\mathrm{B}} T$ per sphere. This is a very

small free energy difference but it is significant and confirms that the arrangement of the layers and not just the number of each type is important. This means that stacking D, where the same-type layers are grouped together in domains is more stable than when layers are alternated. This could be caused because pure cubic (fcc) layers are the most stable. Therefore, to group them together is more stable than to separate them as there will be an entropy penalty not just for having the hexagonal layers but also for separating the cubic ones. Mau and Huse [73] investigated similar stackings, but the system sizes they used initially do not seem to be commensurate with the periodicity of the layers. However, the periodic boundaries they apply ensure that the periodicity and layering is correct by including the in-plane layering shift directly; this means that they can simulate a much wider range of system sizes. They investigated at a different density, close to the melting density and at close packing. Their closest simulation to ours was between $F_{cchhcchh}$ and $F_{chchchch}$ which was calculated to be $\Delta F/k_{\mathrm{B}}T = 13.7 \pm 2.9$. This is of the same order of magnitude as our result, but with a much higher error in the value and they have not actually calculated, like we have, the penalty for splitting up the crystals into separate layers rather than domains.

4.7.3 Gibbs free energy

When simulating in the constant NPT ensemble at a pressure of $P = 14.58$, our value of the Gibbs free energy in Table 4.4 lies well within the quoted error bounds of the previous work [17]. As shown by the convergence of this value in Figure 4.23, our result has a high degree of accuracy. A longer simulation would increase this accuracy further but is not necessary. These results are all for isotropic volume moves.

We are calculation the difference in Gibbs free energy between the fcc and hcp phases, when the fcc phase is stable, $G_{fcc} < G_{hcp}$ and $\Delta G_{fcc,hcp} = G_{fcc} - G_{hcp} < 0$.

$P\sigma^3/k_{\mathrm{B}}T$	N	$\Delta g_{fcc,hcp}(10^{-5}k_{\mathrm{B}}T)$	Reference
14.58	216	-113 ± 4	[17]
14.58	216	-135 ± 3	CW
14.58	1728	-112 ± 3	[17]
14.58	1728	-113 ± 4	CW

Table 4.4: The Gibbs free energy difference per particle (fcc - hcp) (Equation 4.16, 4.13). The pressure is in units of $k_{\mathrm{B}}T/\sigma^3$, and CW denotes the current work

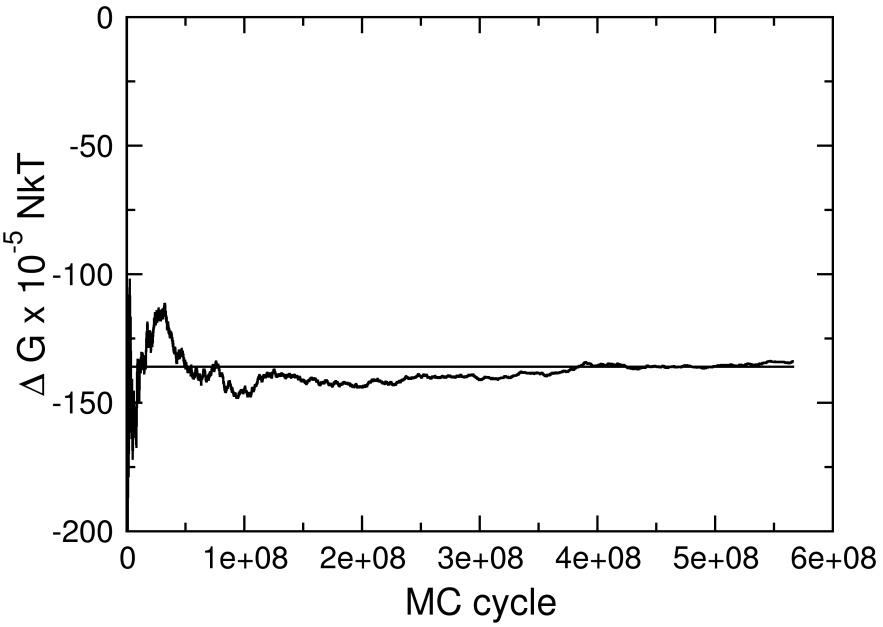

Figure 4.23: The value of ΔG per particle for $N = 216$ at $P = 14.58$ with fixed weighting function, straight line at our final value of $\Delta G = -135$.

The calculated value at a size of $N = 1728$ agrees well with existing work, however, our calculated value for $N = 216$ is significantly different. However, ours is much closer to the value for constant density simulations at the same system size, otherwise there is a 20% change in the value of the small system size, which seems unrealistic when there is a negligible change in the larger system result. Bruce et al. [17] state that the magnitude of $\Delta F_{fcc,hcp}$ and $\Delta G_{fcc,hcp}$ agree within error, so we think there is an error in their table.

Anisotropic volume expansion

The existing work has only looked at the Gibbs free energy with isotropic volume fluctuations, but we implemented anisotropic volume moves as well that scaled a sub-diagonal element of the volume cell matrix instead.

We found that the free energy difference calculated is within the error bounds of the isotropic value for fcc-hcp free energy difference, as shown in Table 4.5. This is not too surprising since the two systems have the exact same cell matrices, and it is still unclear whether anisotropic volume moves should result in different values.

$P\sigma^3/k_{\mathrm{B}}T$	N	$\Delta g_{fcc,hcp}(10^{-5}Nk_{\mathrm{B}}T)$	Volume move type
14.58	1728	-112 ± 3	Iso
14.58	1728	-109 ± 3	Aniso

Table 4.5: The Gibbs free energy difference per particle (fcc - hcp) (Equation 4.16, 4.13). The pressure is in units of $k_{\mathrm{B}}T/\sigma^3$, for isotropic (Iso) and anisotropic (Aniso) volume moves from the current work.

This is the first time that anisotropic volume moves have been compared with isotropic volume moves for the calculation of the Gibbs free energy difference between fcc and hcp crystals. We have shown that the difference is negligible for this system.

4.7.4 Errors

We can calculate the error in our results by looking at the spread from separate simulations, but this does not tell us of systematic errors in the simulation, just statistical ones. To get more information on systematic errors we can run a simulation for which we know absolutely what the result should be. The obvious example is to calculate the free energy difference between the same crystal phases. We randomise the mapping between the systems and then calculate the free energy difference. This also shows that the mapping does not affect the free energy calculation.

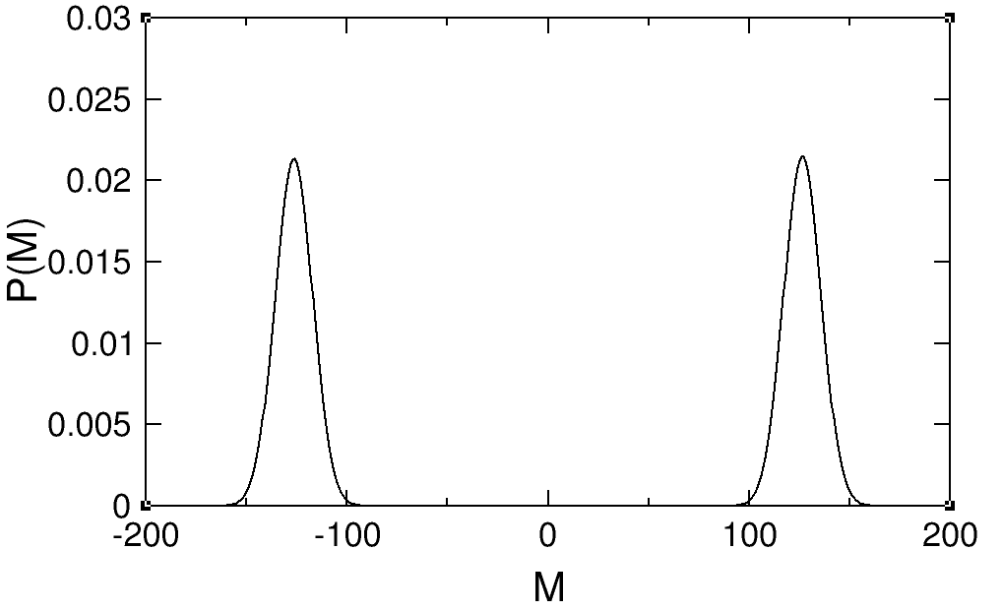

Figure 4.24: The probability distribution function for fcc vs. fcc, $N = 216$ at $\tilde{\rho} = 0.7778$.

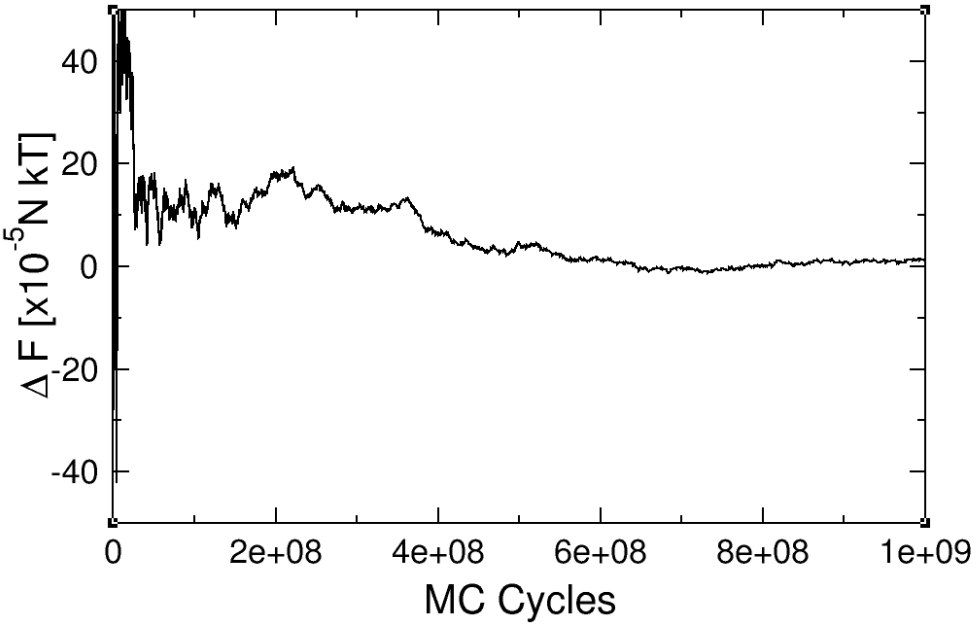

Figure 4.25: The convergence of Helmholtz free energy difference for fcc vs. fcc, $N = 216$ and $\tilde{\rho} = 0.7778$.

In Figure 4.24 it can be seen that the two peaks of the probability distribution

function are extremely close in area. This shows that the free energy difference between the two systems must very exceedingly small, which is what we would expect. Figure 4.25 shows the convergence of the free energy difference between fcc and fcc systems for $N = 216$ particles. The free energy difference is slightly non-zero intially and plateaus off to value of about $1 \times 10^{-5} kT$. This is for a finite sized run length with a fixed level of convergence for the multicanonical biasing function. The error from zero is well below the quoted error of $\pm 4 \times 10^{-5} kT$ for previous work on free energy calculations. This shows us that the limiting factor is not an inherent inaccuracy in the phase-switch method.

4.7.5 Summary

In summary, we have shown that our change in implementation of phase switch Monte Carlo and our code produce valid and accurate free energy differences. We have validated against existing work and our calculated values fall within the error bounds of [17].

The need for anisotropic compared to isotropic volume moves was investigated and found to be unnecessary for this system. Stacking variations were investigated and it was shown that domain packing is lower in free energy that alternating layers; this also emphasises the need for further than nearest neighbour interactions to calculate the entropy of these systems in Ising-like stacking models.

We have also looked at the inherent accuracy of the model, by calculating the free energy difference between the same crystals, and have shown it to be well below the errors quoted in previous works. It was surmised that the error in our work comes from a large number of factors, mainly based upon our finite convergence and run lengths. However, this error value, for any reasonable run length, is much smaller than the precision needed for us to use phase switch Monte Carlo to probe free energy differences of interest.

This allows us to confidently work on extending the phase switch method for use with flexible molecular systems.

Chapter 5

Extending phase switch Monte Carlo to flexible molecular hard spheres

As has been discussed already in chapter 4, phase switch Monte Carlo has been applied to hard spheres looking at the free energy difference between fcc and hcp crystals. It has also been used to study fcc/hcp stacking defects [73, 84] and confirmed that whatever the stacking, fcc is always lowest in free energy. The method has been used to look at the hard sphere freezing transition [116] and soft potentials, for Lennard-Jones particles [34, 56, 74].

Wilms et al. [117] studied confined and imperfectly ordered two-dimensional colloidal systems. They calculated the free energy difference between differently confined colloids, using thermodynamic integration (TI) and the phase switch (PS) MC method. The methods agreed well with each other, but TI was found to have an uncertainty at least an order of magnitude higher than that of PSMC. Due to the size difference between the absolute and relative free energies, it would be hard to reduce the error any further using TI. A comparison was also made between the computational time taken by both methods. PSMC took about 16.5 CPU days to compute each point on the free energy difference curve. TI required calculation of the absolute free energy for each phase along the path of TI, and roughly 250 CPU days was necessary for each phase, giving a total of 500 CPU days required. This is a factor of 30 difference in computational effort between the two methods.

Jackson and Ackland [55] further extended PSMC to binary systems of hard spheres. They showed that the AB(CsCl) structure was not entropically stable at the conditions it is found experimentally, which means that packing effects are not

enough to describe this effect. Raiteri et al. [85] used this method to calculate the free energy difference between solid phases of calcium carbonate when validating their new force field. They worked with molecules as rigid bodies and fixed C-O bond length. This fixed bond length was chosen to be the experimental value of the calcite polymorph. However, there is some variation in the bond length between the polymorphs. This suggests that if the model included more flexibility the phase diagram could be more accurate.

To date this method has only be applied to systems of hard spheres, Lennard Jones particles, and small rigid molecular systems; obviously there is a wide area of research which would benefit from the extension of this method for flexible molecules.

When dealing with flexible molecules, as opposed to independent atoms, the complexity vastly increases. In order to apply phase switch MC to molecules we need to ensure that the basic idea of the method is the same; that is we want to sample both phases to calculate the ratio of the probabilities. However, we no longer have solely translation and volume moves. We also have to include rigid rotation of the molecule and internal MC moves within the molecule, which depend upon the model used. This means that we need to extend our mapping between the two phases.

An important change is the ability to include intramolecular motions of degress of freedom which will allow a much wider range of systems to be investigated. The difference between internal and whole-molecule moves is that the conformation of the molecule is no longer fixed and this can cause some extra complication. For example, if we decide to locate a molecule using its centre of mass, then its position will change if an internal degree of freedom is changed. In order to test out our extension we need a basic system to work with, and for simplicity's sake we will use a hard sphere model which minimises the difference from our existing implementation. We also must include internal flexibility, and the system should exhibit polymorphism. This narrows down our choice of system greatly, especially when we try to minimise the size and complexity of the molecules as well.

The simplest molecule to study is a chain of beads bonded to their neighbours, and if the chain has four or more beads then there is a torsion angle. Alkanes are not the simplest chain-like molecules, as they are zig-zags rather than linear chains. However, *n*-butane is the alkane with four carbon atoms chained together and has the advantage of having three known polymorphs. If we use an united-atom model then we will incorporate the hydrogens and be left with a chain of four units. This is exactly the system that we would like to study; we only need to decide on model parameters.

In this chapter we will discuss the possible models for butane and the reasons for our choices. Next the increase in the degrees of freedom compared to single particles and how this relates to the phase switch method will be introduced. Specific implementation and computational considerations will be explained along with the validation of our implementation. Finally, results for the butane system will be presented.

5.1 Experimental data for butane

Aston and Messerly [5] found a solid-solid polymorphic phase transition at 108K for n-butane and three crystalline structures were discovered to be mechanically stable [86, 13]. All structures have two molecules in a unit cell, and belong to space group $P2_1/c$. At low temperatures, phase III is stable and phase II is metastable; above the first-order transition phase I is stable. Phase I is a disordered plastic crystal, with rotations about the long axes of the molecules. In all of the crystalline phases the molecules are in the *trans* state, where the torsion angle is 180° and the constituents are oriented in opposing directions. In phase III all of the molecules are aligned along the long axis, where as in phase I and II, they form layers at 90° to one another. The unit cells are shown in Figure 5.1.

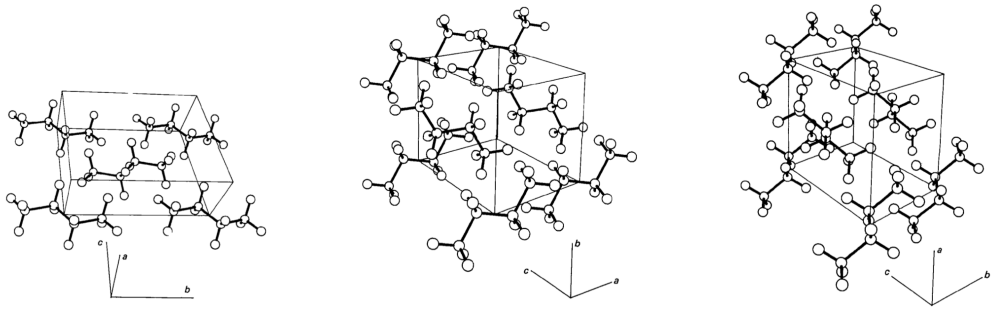

(a) (b) (c)

Figure 5.1: a) Phase III at 5K, b) Phase II at 65K, c) Phase I at 120K of butane, reproduced from [86].

The orientational disorder of phase I has been investigated, first by Hoch [49] using NMR, who suggested a model to fit the data where the molecules made 180° reorientations. However, other models that were not tested may have fitted the data equivalently. Refson and Pawley [86] further probed this orientational disorder in phase I, testing many models and found that the orientational probability was a continuous function. However, the details of this continuous function could not be narrowed down from their data. Their results were incommensurate with Hoch's

proposed model, but Hoch's data could be explained by their model. This suggests that the disorder in the high temperature butane phase is still not fully understood and hence taking this into account explicitly in any model would involve guesswork and need much further investigation. Therefore, in our work we have not explicitly included any disorder in phase I.

5.2 Hard sphere butane model

We will apply our extension of the phase switch method to a hard sphere model of butane. This still leaves us with many options that we can apply to model our system. The model needs to include enough information that it can reproduce the crystal structures of butane and treat its specific structural effects in solids.

Much work has been done on n-alkanes using freely jointed tangent sphere models [69, 30, 35, 81]. This has been extended to more geometrically realistic models of n-alkanes in the solid state [89, 90, 70]. The choices that need to be made when deciding on a model revolve around what potentials to include and which are surplus to requirements, unnecessarily increasing the complexity of the model. For Malanoski and Monson [70] the main criteria for the choice of model were based upon: (i) the repulsive forces being dominant in determining the solid structure via packing effects; and (ii) the most important contribution to the intramolecular energy involving four of more carbon atoms being described by a torsion potential.

In order to ensure simplicity, the C-C-C bond angle is set to the tetrahedral coordination value of 109.47°, and the bond lengths are 0.4σ where σ is the hard sphere diameter.

There remains one more choice to make: the form of the torsion potential. Initially three torsion potentials were suggested, the first potential (model I) was the standard hard core exclusion with no additional intramolecular interaction. The second potential (model II) involved a hard core torsion potential that does not permit *gauche* conformations ($\pm 60°$), and allows small fluctuations about the *trans* conformation (180°). The third model (model III) is a much more realistic torsion potential and involves temperature dependence, which significantly increases the complexity [78, 88].

We decided that none of these torsion potentials struck the right balance between realistic complexity and useful simplicity.

Cao and Monson [18] modified the model II version of the torsion potential to allow for *gauche* conformations. This model was shown to capture the complex physics of the rotator phase of longer n-alkanes and yet retain its athermal nature,

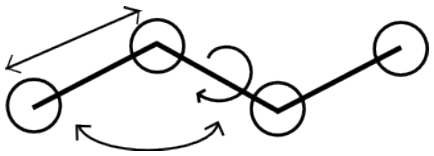

Figure 5.2: Depiction of the linked chain butane model

hence it should be sufficiently detailed for our work.

We define a torsion potential $U(\phi)$

$$U(\phi) = \begin{cases} 0 & \text{if } |\phi| < \phi_1 \text{ or } |\phi - 120^\circ| < \phi_2 \\ \infty & \text{otherwise} \end{cases} \tag{5.1}$$

where ϕ is the torsion angle, $\phi_1 = 17.4$ based upon model II's angle restriction. $\phi_2 = 10$ gives the appropriate ratio for *trans* and *gauche* populations compared with model III's Padilla-Toxvaerd torsion potential [78]. This potential is now referred to as model IV.

5.3 Phase switch MC generalised coordinates

We define a set of coordinates that describe each molecule in the system with respect to its own reference configuration. Monte Carlo moves made on the molecule can be written in terms of the reference structure plus this set of generalised coordinates. The generalised coordinates represent the collective Monte Carlo moves that have been applied to each molecule during the simulation.

They are independent of the phase and if applied to another reference state will result in the same configuration as if the original Monte Carlo moves had been directly applied to that reference state. That is, if we run a Monte Carlo simulation of phase α for some arbitrary number of cycles, we can calculate a set of generalised coordinates that describe the change from the initial configuration to the current configuration, so that if these are then applied to a completely different starting configuration or phase, we would recover the configuration that we would have gotten if the exact same Monte Carlo moves had been made to this new system instead. Having the coordinates independent of each other is important as one can reconstruct the move history associated with each coordinate without having to include information from the move history of other coordinates.

Our system has N particles in the system and $N_{\text{mol}} = N/4$ molecules. Each molecule has its own set of generalised coordinates $\{\mathbf{G}\}$, where the curly braces

denote the set across molecules.

Translations are represented by the change in fractional displacement of the first bead in each molecule.

$$\{\Delta \underline{s}\} = (\underline{\underline{h}}^{-1}\{\underline{r}_1\}^{\alpha}) - (\underline{\underline{h}}^{-1}\{\underline{r}_1^{ref}\}^{\alpha}) \tag{5.2}$$

where $\{\underline{r}_1\}^{\alpha}$ denotes the set of coordinates of the first bead in a molecule in phase α, $\{\underline{r}_1^{ref}\}^{\alpha}$ denotes the equivalent for the reference coordinates, and $\underline{\underline{h}}^{-1}$ is the inverse cell matrix of the simulation box. Fractional co-ordinates are used so that the displacement is independent of the simulation box. This is needed because the cell matrix contains the basis vectors for the coordinate system in fractional coordinates.

Rigid molecule coordinates are defined as the rotation from the reference configuration to the current configuration; we define a molecule-centred coordinate system for each molecule. The axes are defined as $\underline{a} = (\underline{e}_1, \underline{e}_2, \underline{e}_3)$ with $\underline{e}_1 = \hat{\underline{r}}_{12}$, the vector between first and second beads in a molecule. $\underline{e}_2$ is defined as the component of $\underline{r}_{23}$ vector that is perpendicular to $\underline{r}_{12}$

$$\underline{e}_2 = \underline{r}_{23} - (\underline{r}_{12} \cdot \underline{r}_{23})\hat{\underline{r}}_{23} \tag{5.3}$$

and the third axis is the cross-product of the other two axes, $\underline{e}_3 = \underline{e}_1 \times \underline{e}_2$. This gives us an orthogonal coordinate systems for each molecule in the system, $\{\underline{a}\} = \{(e1, e2, e3)\}$.

A set of quaternions $q = (q_0, q_1, q_2, q_3)$ is defined over all molecules as

$$\{\underline{a}\} = \{q\}\{\underline{a}^{ref}\}\{q^{-1}\}. \tag{5.4}$$

This defines the quaternions needed to transform each molecule from the reference coordinates to the current coordinates.

The internal representation of torsional movement,$\{\theta\}$, is defined as the change in torsion angle from the reference to the current system about the $\hat{\underline{r}}_{23}$ axis for each molecule. The angle is calculated as

$$\theta = \text{atan2}(|[\underline{b}_i \times \underline{b}_a] \times [\underline{b}_a \times \underline{b}_f], [\underline{b}_i \times \underline{b}_a] \cdot [\underline{b}_a \times \underline{b}_f]), \tag{5.5}$$

where $\underline{b}_a = \hat{\underline{r}}_{23}$ is the rotation axis, $\underline{b}_i$ is the initial torsion vector and $\underline{b}_f$ is the final torsion vector; see Figures 5.3 and 5.4.

The volume of the system, for NPT simulations, must be accounted for as

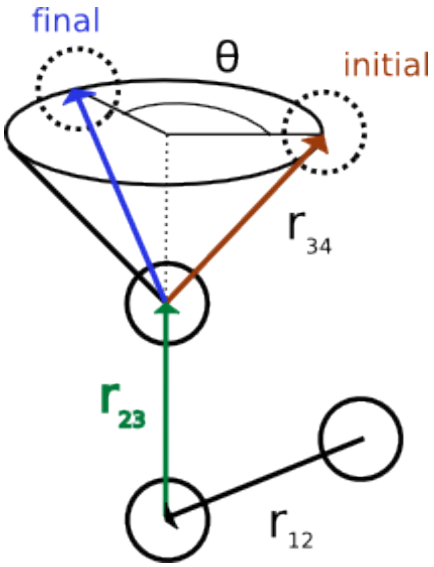

Figure 5.3: Depiction of the torsion angle in the butane model, bond length and angle are fixed so the rotation is on a circle with axis $\hat{\underline{r}}_{23}$.

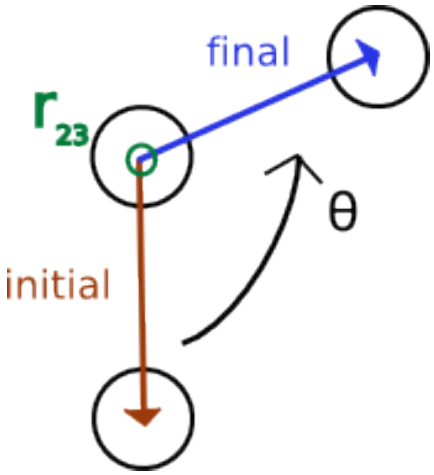

Figure 5.4: Depiction of the torsion angle in the butane model looking top-down onto the $\hat{\underline{r}}_{23}$ axis.

well. This can simply be defined as the change in cell matrix $\Delta\underline{\underline{h}}$, given by

$$\Delta\underline{\underline{h}} = \underline{\underline{h}} - \underline{\underline{h}}^{ref} \tag{5.6}$$

where $\underline{\underline{h}}$ is the current matrix and $\underline{\underline{h}}^{ref}$ is the reference matrix.

We must label the two systems we are calculating the free energy difference between, by $\alpha and \gamma$. We must also differentiate between the system in which we are currently creating the moves and calculating the probability, and the system that they are just being applied to; these will be referred to as the active and passive respectively. To symbolically denote this, a superscript + will be used for active, and a superscript $\oslash$ for passive. Therefore a vector $\underline{b}$ in the active system specifically will be denoted as $\underline{b}^{+}$ and the same vector in the passive system will be $\underline{b}^{\oslash}$.

This leaves us with a set of generalised coordinates

$$\{\mathbf{G}\} = (\{\Delta s\}, \{q\}, \{\theta\}, \{\Delta\underline{\underline{H}}\}), \tag{5.7}$$

which are independent of each other and only describe the change in configuration due to the MC moves applied.

5.3.1 Degrees of freedom

All of the degrees of freedom in the system should be accounted for in the internal coordinates. For the butane model at constant pressure, we start with $3N+6$ degrees of freedom. Each of the N particles can move in three dimensions, and the 3×3 cell matrix has 6 degrees of freedom, because some of the values are not independent. For a system at constant N and constant pressure P, this can be written as

$$3N_{\text{mol}}N_{\text{bead}} + 6, \tag{5.8}$$

where N_{mol} is the number of molecules in the system and N_{bead} is the number of beads within a molecule so that $N = N_{\text{mol}} \times N_{\text{bead}}$. For butane $N_{\text{bead}} = 4$. The numbers of degrees of freedom are given in Table 5.1.

	Degrees of Freedom
Cell box	6
Translation	$3N_{\text{mol}}$
Rotation	$3N_{\text{mol}}$
Torsion	$(N_{\text{bead}}-3)N_{\text{mol}}$
Constrained bond lengths	$-(N_{\text{bead}}-1)N_{\text{mol}}$
Constrained bond angles	$-(N_{\text{bead}}-2)N_{\text{mol}}$

Table 5.1: The numbers of degrees of freedom for each type of motion in the system.

These can all be combined to give

$$\begin{aligned} & (N_{\text{bead}}-1)N_{\text{mol}} + (N_{\text{bead}}-2)N_{\text{mol}} + \\ & (N_{\text{bead}}-3)N_{\text{mol}} + 3N_{\text{mol}} + 3N_{\text{mol}} + 6 \\ = \; & N_{\text{bead}}N_{\text{mol}} - N_{\text{mol}} + N_{\text{bead}}N_{\text{mol}} - 2N_{\text{mol}} + \\ & N_{\text{bead}}N_{\text{mol}} - 3N_{\text{mol}} + 3N_{\text{mol}} + 3N_{\text{mol}} + 6 \\ = \; & 3N_{\text{bead}}N_{\text{mol}} + 6, \end{aligned}$$

recovering the total number of degrees of freedom. This shows that our generalised coordinates account for all degrees of freedom in our model.

5.4 Phase switch move

The interphase switch move applies the set of moves that have been accepted for the active phase + to the reference configuration of the passive phase ⊘. Therefore the acceptance criterion for the constant N, V ensemble is a standard Metropolis acceptance probability

$$P_{+\to\oslash} = \min(1, \exp[-\beta(E(\underline{r})_{\oslash} - E(\underline{r})_{+})]), \tag{5.9}$$

and it is only dependent on the energy change between the passive system (⊘) and the active system (+). Since in the hard sphere system the energy of all allowed states is zero, β is arbitrary and can be set to one for convenience. This also means that if there are no overlaps in the passive system, its energy is zero, and then the interphase switch move will always be accepted since $\exp[0-0] = 1$. Therefore the acceptance probability does not need to be explicitly calculated if both systems are in allowed states.

If we are in the isothermal-isobaric ensemble we have to take into account the volume change that would occur from phase switching to a crystal structure of a different volume. This is just the standard volume move acceptance probability

$$P_{+\to\oslash} = \min(1, \exp[-\beta\{E(\underline{r})_{\oslash} - E(\underline{r})_{+} \ + P(V_{\oslash} - V_{+})\} - N\ln(V_{\oslash}/V_{+})]), \quad (5.10)$$

where $V_{\oslash}$ is the volume of the passive system and P is the external pressure. Again, since the energies of the two systems can only be zero for allowed states, we can remove the energy calculation and simplify the computation needed.

We can alter the order parameter to include the volume change term in the acceptance criterion for the isothermal-isobaric ensemble as suggested for the hard sphere system in equation (4.17). Since the perfect fcc and hcp crystals have the same volume this does not cause an issue. However, if the two phases under investigation have a large difference in volume this could cause problems with the order parameter. Therefore McNeil-Watson et al. [74] suggested using the change in volume from a reference state for each phase instead of the absolute volume, such that the order parameter is

$$\mathcal{M}(\mu) = \mu(\alpha) - \mu(\gamma) + P(\mathcal{V}_{\alpha} - \mathcal{V}_{\gamma}), \quad (5.11)$$

with $\mathcal{V}_{\alpha} = V_{\alpha} - V_{\alpha}^{\text{ref}}$ and $\mu(\alpha)$ being the number of overlaps in the α system.

5.5 Implementation for flexible molecular hard spheres

The Ponders code is a Monte Carlo hard sphere phase switch code working in three dimensions. It was written as a C front-end over a Fortran MC engine. The two phases are simulated concurrently and each move accepted in the active is immediately applied to the passive. The MC moves available are:

Translation of a molecule:

For a randomly chosen chain, each component of the fractional coordinate of the first bead in the chain is changed by an amount randomly chosen uniformly from $-1 \to 1$. This fractional displacement vector is then scaled by $s_{\max}$, a specified extrema. This change is then applied to all beads in the chosen chain.

Rigid rotation of a molecule:

For a randomly chosen molecule a random three dimensional axis of rotation and angle of rotation, between specified extrema $\pm\phi_{\max}$ are generated. The entire molecule is rotated about the first bead by the chosen axis and angle

using quaternions.

Volume move, i.e. expansion/contraction of the simulation box:
Implements isotropic or anisotropic changes in the size of the simulation box. The fractional position of the first bead of each molecule is constant throughout the move. The relative position of all beads in a change to the first bead is conserved. The change in simulation box is chosen by uniform scaling (isotropic) or by perturbing a sub-diagonal element of the volume matrix (anisotropic). Due to the re-scaling of all particles a complete recalculation of the order parameter is needed

Internal rotation of a torsion bond:
For a randomly chosen molecule, a dihedral angle is chosen at random (for butane there is only one dihedral to choose) and altered by a random angle between $\pm\theta_{max}$. The angle is chosen by generating a random rotation and choosing equally between each torsion well (equation 5.1).

Configuration-bias (cbmc) move, complete regrowth of a molecule segment:
For a randomly chosen molecule, a randomly chosen subsection of the molecule is regrown. A set number of attempted segments of molecule are regrown, their Rosenbluth factors found and used to randomly select a segment according to the appropriate weight [96].

Rigid molecule moves are made using the first bead of the molecule rather than the centre of mass since internal movement changes the centre of mass.

Due to the nature of the MC moves bond lengths and bond angles can never be broken or changed from those specified in the model. However, when applying torsion or configurational bias moves from the active to the passive, angles that are not allowed by the potential can occur. These internal violations are included in the overlap order parameter as internal overlaps; that is the bead overlaps with another bead in the molecule. Each torsion angle violation is only ever counted as one overlap.

Implementing the phase switch method via concurrent updates of both systems can lead to a deviation between the two boxes due to floating-point errors. This deviation between the systems causes the equilibrium overlap value to drift; see Figure 5.5. In order to rectify this we must synchronise the two systems periodically, as first discussed in section 4.4.3. This involves a complete re-calculation of the generalised coordinates that have been applied to the active system from the

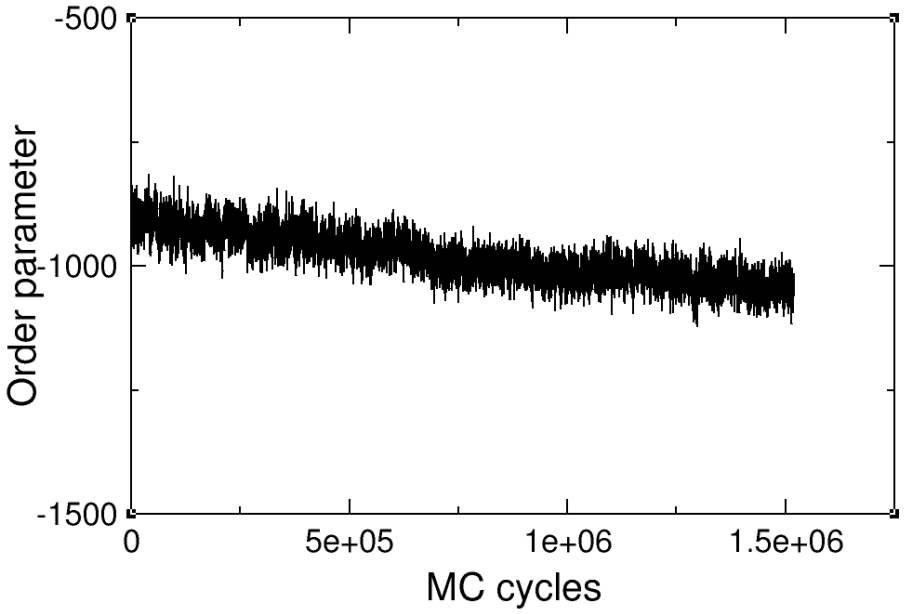

Figure 5.5: The equilibrium order parameter value drifts when no synchronisation is applied, with $N = 768$ beads at a pressure of $P\sigma^3/k_{\mathrm{B}}T = 50$.

reference. The generalised coordinates are then applied to the passive reference system and the resulting configuration is taken as the updated current configuration of the passive system.

When applying the rigid rotation we want this to be the same in both systems relative to their reference configurations. In order to achieve this we calculate the quaternion to rotate between the reference states, $\{\underline{r}_\alpha^{ref}\} \leftrightarrow \{\underline{r}_\gamma^{ref}\}$. This is then combined with the generalised coordinate quaternion, which gives us the combined rotation from reference state of system i to the current state of system j (where $i, j = \alpha, \gamma$ (Equation 5.12). If we just applied the generalised coordinate quaternion we would be applying the exact same rotation to both systems, regardless of how differently they are oriented in space. By including the quaternion to rotate between the two systems we can take this into account. If our systems are very similar in orientation then this step is not necessary, however, it makes for a more generalisable method to include it.

$$q = q(r_i^{ref} \rightarrow r_i) \cdot q(r_i^{ref} \rightarrow r_j^{ref}) \tag{5.12}$$

When the synchronisation procedure is applied periodically the system reaches equilibrium in the order parameter space as shown in Figure 5.6.

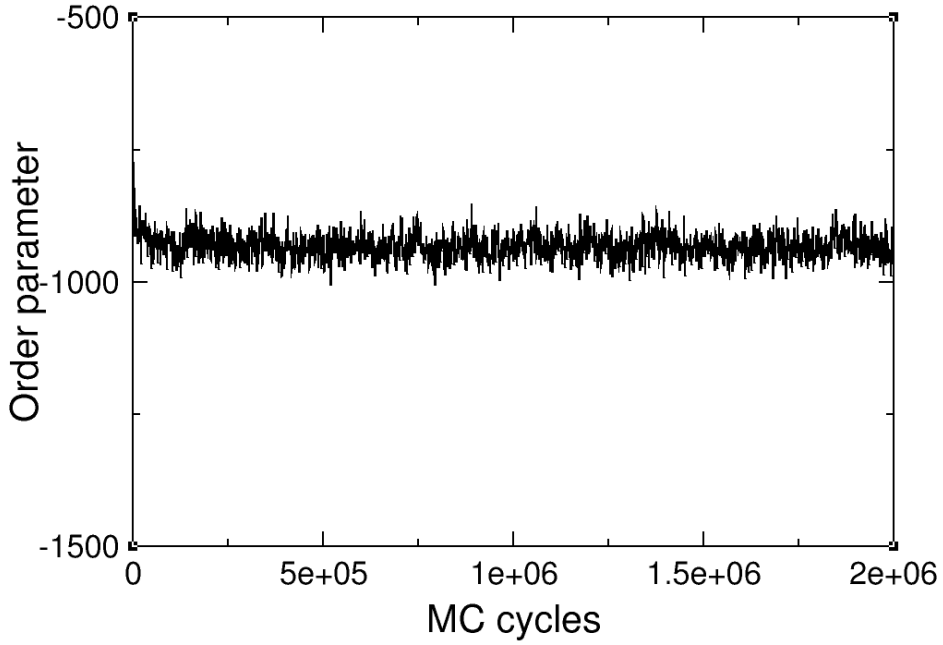

Figure 5.6: The equilibrium order parameter value is no longer drifts when synchronisation is applied, for a system with $N = 768$ beads at a pressure of $P\sigma^3/k_{\mathrm{B}}T = 50$.

5.5.1 Application of MC moves to passive system

In our implementation of phase switch Monte Carlo, we concurrently simulate both systems of interest. Moves are made and accepted based on the active system and then the resultant move is applied to the passive system. Care needs to be taken in how this is achieved to ensure the generalised coordinates remain the same in both systems.

Translation: The same fractional displacement of the first bead is applied to the equivalent molecule in the passive system. The fractional displacement is calculated in the active and then transformed in the passive system to a cartesian displacement and then applied to all particles in the molecule. This preserves all bond length and angle constraints, and keeps both the orientation (q) and internal torsion (θ) constant.

Rotations: The same rotation quaternion plus the relative rotation between the molecules, is applied to the equivalent molecule in the passive system. This preserves the relative fractional position of the first bead (δs), the internal torsion angle (θ) and all bond/angle constraints.

Torsion: The same angle of rotation about a bond in the equivalent molecule is applied to the passive system. A new quaternion is calculated using the bond in the passive system as the axis of rotation. This preserves the relative fractional position of the first bead (δs), and keeps rigid orientation (q) constant.

5.6 Parallelising Ponders

The Ponders MC code has been parallelised via a multiple walkers approach using MPI (message passing interface). This means that for each processor the same simulation is initialised, each with a different seed for the random number generator. The only collective information is the weighting array and histogram of visited overlaps. The communication cost is reasonably low since these do not need to be updated every step, only every hundreds of cycles. We need to communicate reasonably often because otherwise we will be biasing the simulation based upon out of date histograms. Care must be taken to not double count previous values and only distribute the data that has been updated since the last communication between processors. This means that the weighting function will be smoother and more accurate as the data from every simulation is being fed into one single function, as shown in Figure 5.7.

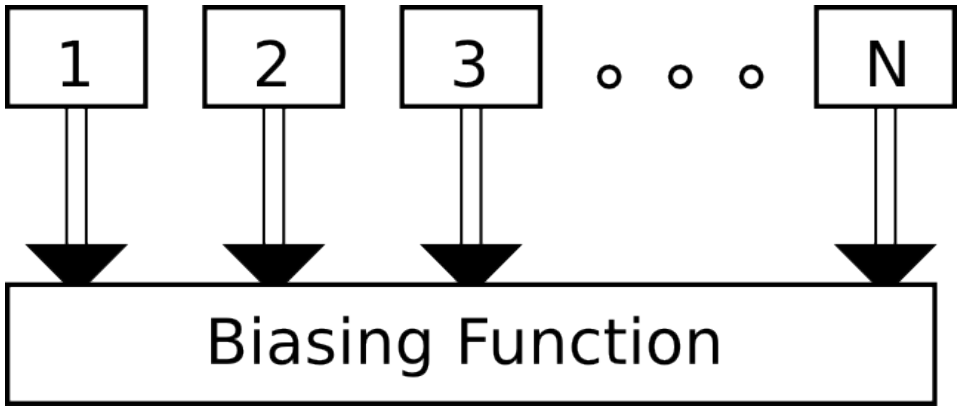

Figure 5.7: All of the N processors feed into the same biasing function.

As a result we can only check the flatness of the histogram for the multicanonical biasing after every communication. If we checked at any other time, each processor would have a slightly different histogram and they would not all necessarily be flat. This approach is used due to the nature of Monte Carlo simulations

and the inherent difficulty parallising them. Care was taken to ensure the ability to still run in serial, so harness routines have been employed that may be compiled for serial or parallel runs.

5.6.1 Speed comparison

Our code Ponders, is build upon a Fortran MC engine so we calculated the overhead associated with the phase switch front end, as shown in Figure 5.8.

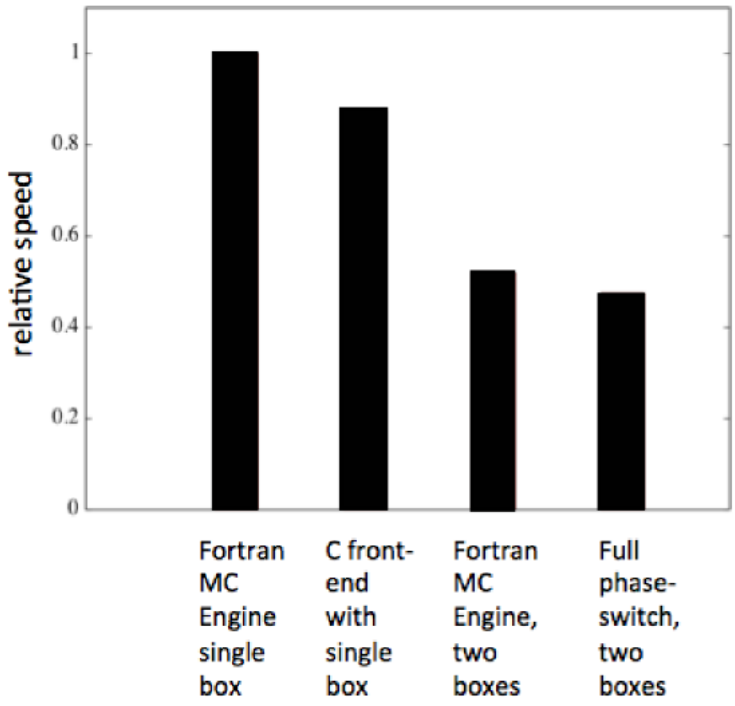

Figure 5.8: Relative speed of our phase switch MC implementation compared with its Fortran MC engine without the phase switch overhead.

This shows that the main cost in our implementation is the need to simulate two systems/boxes at once; the phase switch overhead is minimal in comparison. The overhead cost has a few contributing factors, the main factor being the need to count overlaps for the order parameter value. Normally for hard sphere MC once an overlap is found in an energy calculation then the calculation can just be stopped as the move will not be accepted. However, overlaps in the passive system need to be counted, which means that all pairs of atoms need to be checked for overlaps, and this is slower. Another additional phase switch overhead is the synchronisation between boxes, as this is never done for standard, single box MC simulations and it

involves recalculation of coordinates for all particles in the system. However, this is only done every 100-1000 MC cycles, and so it will not contribute too much to the overhead. Similarly the communication cost will be included in the overhead, but is only run every 100 MC cycles at most, and only two arrays are communicated between processors. The extra calculation of what to apply to the passive system will also add to the overhead, however, this will not be much greater computationally than the standard calculation of a MC move. The second largest contribution to the phase switch overhead comes from volume moves. When applying a volume move to the system a complete recalculation of the order parameter is necessary, as well as scaling all particles with the volume change. This makes volume moves more expensive, however we would need to check the system for overlaps after a volume move anyway so the added cost is not huge.

In general, including phase switch MC does add extra computational cost to the simulation, and this comes mainly from the need to simulate two systems simultaneously. The advantage of having no extra computation to calculate the order parameter balances this out.

The speedup of a parallel program using p processors is given by

$$S_p = \frac{T_1}{T_p} \tag{5.13}$$

where T_1 is the execution time for the serial program and T_p is the execution time of the parallel program with p processors. The ideal speedup is a linear speedup with $S_p = p$. In general, efficient programming gives and efficiency $E_p = S_p/p > 0.75$.

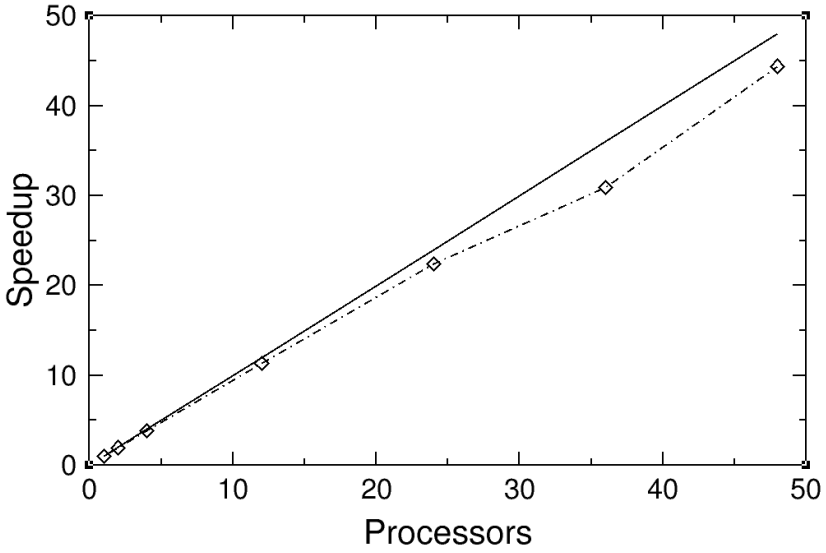

Figure 5.9: The speedup of Ponders (dashed line) against perfect speedup (solid line) for phases I and III, in systems of $N = 768$ beads and a flatness criterion of 90%.

It can be seen in Figure 5.9 that our speedup from using parallel processing is excellent, however, this is to be expected as our approach is based upon having separate simulations on each processor. Therefore, this metric does not give us any new information.

Another metric to measure the parallelisation of our code is to look at the convergence of the biasing function with time as a function of number of processors. This is a measure that is more relevant to our goal which is to converge the biasing function as quickly as possible. We will be looking at the reduction in the increment factor, that is the amount by which the biasing function is incremented. If this is small then we know that the biasing function is well converged, therefore, the faster this reduces, the quicker our biasing function has converged.

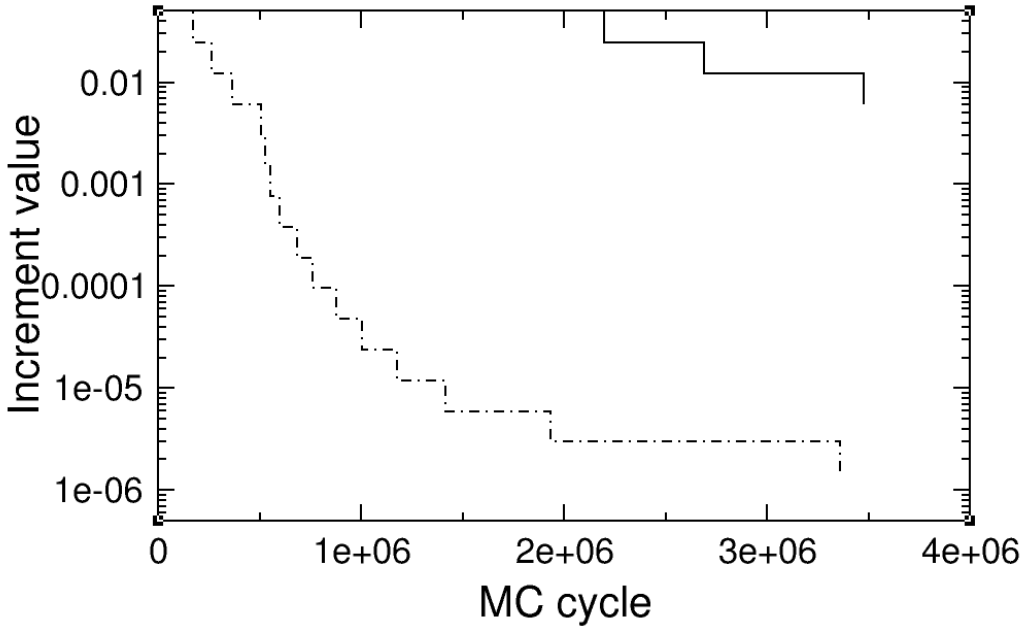

Figure 5.10: $\ln(f)$ for a flatness criterion of 90%, and with $N = 768$: solid black line is for a single processor; dashed line is with four 12-core nodes.

It can be seen that a single processor is extremely slow in reducing the increment factor. In figure 5.11 we have plotted the average time to reduce the increment factor three times, as a function of the number of processors.

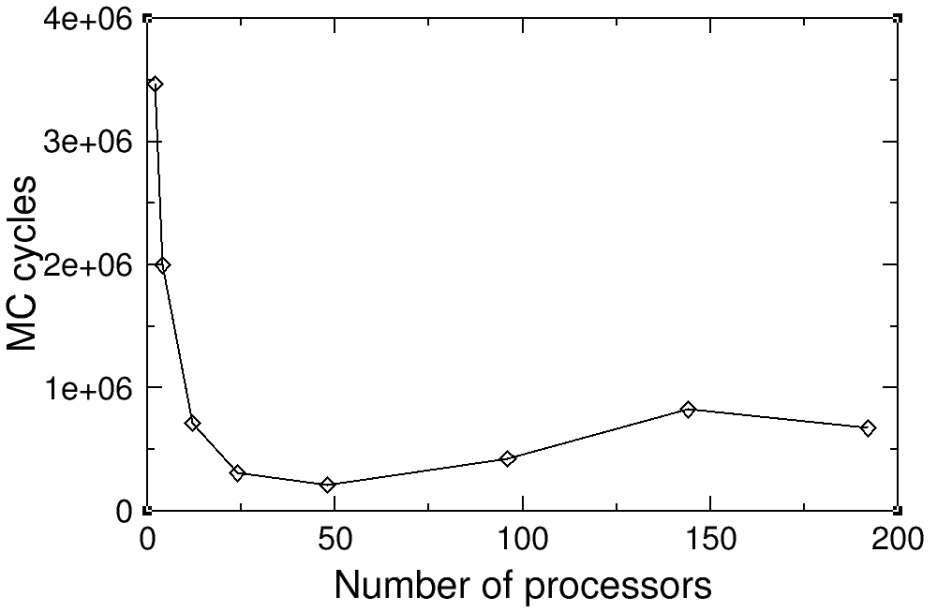

Figure 5.11: Average time in MC cycles taken to reduce $\ln(f)$ three times with flatness criterion of 90%, and with $N = 768$ particles.

In Figure 5.12 we have plotted the final increment value reached after simulating for 24 hours.

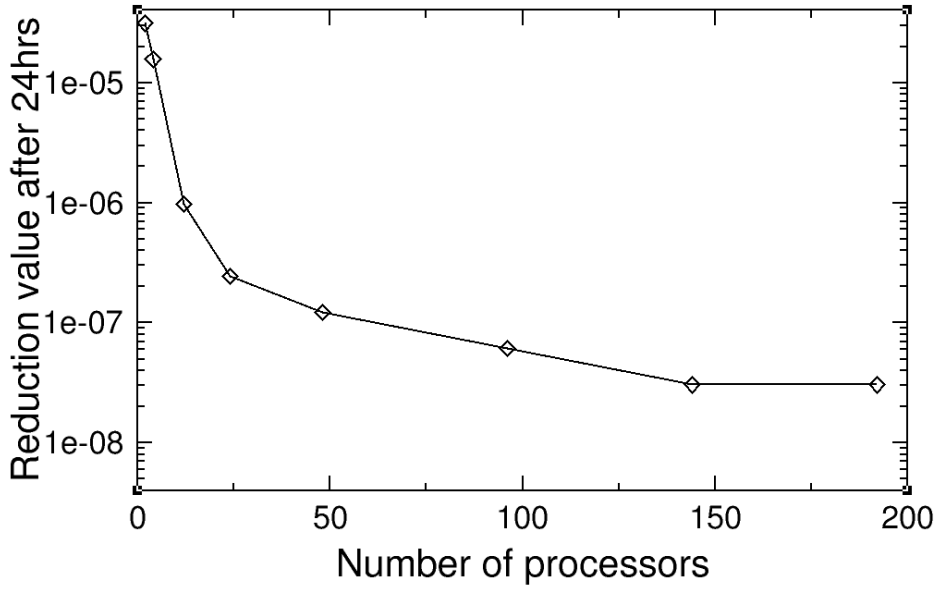

Figure 5.12: The final $\ln(f)$ value reached after 24 hours of simulation with flatness criterion of 90%, and with $N = 768$ particles.

It can be seen that there is no large improvement in the speed of converging the biasing function by having more than 48 processors; less than 24 is much slower. Below 50 processors performs better for small reductions in $\ln(f)$ and is not much slower than large numbers of processors for longer simulations. This shows that 24 processors strikes a nice balance between speed and efficiency for the biasing function.

5.7 Computational considerations

5.7.1 MC move attempt ratios

When running a Monte Carlo simulation we must decide with what probability we will attempt each move type. In order to be efficient we should spend an equal amount of time in each type of move per MC cycle. This means that if a move is much more expensive than others we should attempt it much more infrequently [39, p.119–122]

$$P_{\text{attempt}} = \frac{T_{\text{move}}}{T_{\text{total}}}, \tag{5.14}$$

where T_{move} is the time spent in a single type of move and T_{total} is the total simulation time. That is, the attempt probability of each move type is dependent on the ratio of their computational expense to the total expense of all the move types.

For the single particle hard sphere system we only use volume and translation moves. When we make a volume move, we are moving all N molecules in the system, whereas in a translation move we are only moving a single particle. So we can simply say that we will attempt volume moves N times less frequently. In practice we attempt volume moves with a probability of $\frac{1}{N}$ and translation moves the rest of the time.

When we include more move types we need to change this acceptance to take them into account. Logically rotation moves are as costly as translation because we are rotating a single molecule. Torsion moves are only rotating a single particle so they should be less expensive and so should be attempted more often. Simulations were run consisting of only one of each of the move types and their average speeds are compared in Table 5.2. This gives us a basis for comparison between the moves. We compared the average speed per cycle for each move with similar acceptance ratios of 30 %.

It can be see that torsion moves are significantly faster than all other moves, and hence we should increase their relative frequency; we will use the probabilities from Table 5.2. Translation and rotation moves are relatively similar in compu-

MC move type	MC cycles per second	Ratio of total MC/s	Ratio, no CBMC
Torsion	337 ± 5	0.41	0.43
Rotation	200 ± 16	0.24	0.25
Translation	230 ± 31	0.28	0.3
CBMC	41 ± 2	0.05	0
Volume	3 ± 1	0.0037	0.004

Table 5.2: Table showing the number of MC cycles per second for each move type and the percentage of the total number of MC cycles per second.

tational effort and so we will leave them at the same ratio. CBMC moves are exceedingly slow compared to all other single molecule moves. Therefore, we should either completely exclude them as they are sampling the same degrees of freedom as torsion moves, or reduce their attempt probability significantly. Since their contribution to the total time is very large and because it is not necessary to include CBMC moves when simulating butane as they will provide less benefit, we decided to just remove them from our move set entirely. Volume moves are about as much computational effort as was already assumed and we will stick with a $\frac{1}{N_{\text{mol}}}$ probability of attempting them.

5.7.2 Creation of crystal inputs

Experimental data for the crystal structure of the three phases of butane exist [86]. However, we need to adapt these for use with our hard sphere model to ensure the bond lengths and angles are commensurate with the constraints we impose. After that we still need to remove all overlaps between molecules in our system. This was done by expanding the system until all overlaps are removed and then equilibrating for 10^6 MC cycles. We chose to use the same number of molecules in the x, y and z directions for each phase and to number them equivalently. This ensures a reasonable mapping between the two systems during the phase switch method.

In order to produce the inputs, we equilibrated the systems to a constant pressure and then ran the equilibrated system for another 10^6 MC cycles; we output the density and coordinates of the system frequently. From these data we calculated the average system size for that phase and pressure, and chose the outputted coordinates with a size closest to this average value. For constant density crystal inputs these average systems from constant pressure simulations were scaled isotropically to produce the correct density. Care was taken to only increase the volume of the systems so as not to introduce any overlaps.

Due to the triclinic cell vectors and the anisotropic volume moves in our simulations, we also have to be aware of how the system shape will affect finite size errors. If the cell vectors scale anisotropically with pressure, then using configurations at different pressures to get a constant density configuration will give us different free energy differences.

We investigated how the cells change with pressure and density; constant pressure simulations were run and the average cell vectors and their associated error were calculated. Each element of the cell vectors has been calculated for a range of pressures and the average density of the system was also computed. The cell vectors were converted into lattice parameters, a, b, c (see Figure 5.13) with angles between the crystallographic axes defined by:

$$\alpha = \text{the angle between } b \text{ and } c,$$
$$\beta = \text{the angle between } a \text{ and } c,$$
$$\gamma = \text{the angle between } a \text{ and } b$$

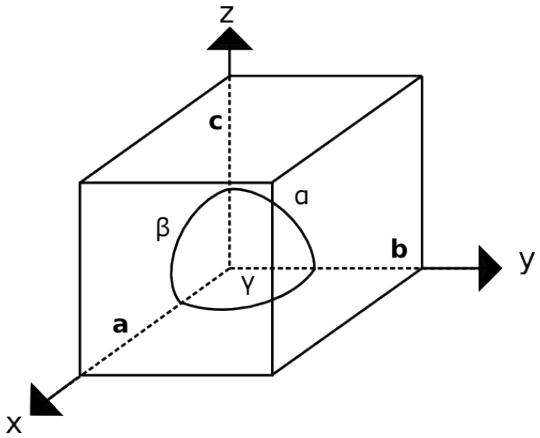

Figure 5.13: Depiction of the lattice parameters in three dimensions.

We computed the percentage change in the lattice parameters with respect to pressure for both phases. All systems were fully equilibrated and then the cell parameters were averaged for at least 5×10^6 MC cycles with a system size of 192 chains for all simulations. The cell parameters were output every 500 MC cycles to allow the system to equilibrate; on average 500 volume moves are made between each cell reading.

For phase I, Figure 5.14 shows that the change similarly with pressure; a and b are very close but c scales slightly anisotropically in comparison. However,

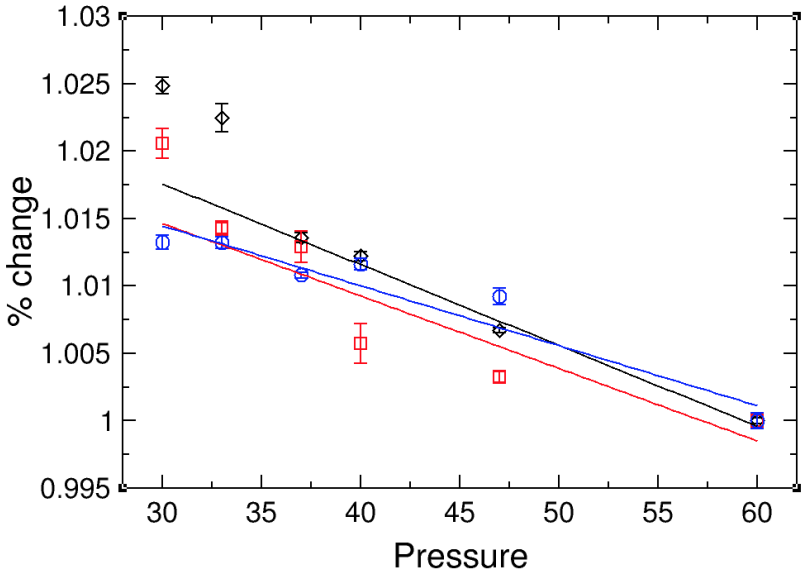

Figure 5.14: Percentage change in a (black diamonds), b (red squares) and c (blue circles) lattice parameters for phase I, at pressures, $P\sigma^3/k_{\mathrm{B}}T$.

considering the spread of the data points and the error in the points, there is still good agreement between all three parameters which suggests that phase I can be said to scale isotropically with pressure.

The change in the lattice vectors for phase III are shown in Figure 5.15: a and c change by very similar amounts, as the gradients of the regression lines are extremely close, whereas b has a noticeably different gradient. This means that there is anisotropy in the scaling of the lattice vectors for phase III. There is a lot more anisotropy than in phase I. However, it is still relatively minor over the pressure range investigated, the difference being only around 0.015%.

If the angles between the axes change, this also tells us about anisotropy in the system. Figure 5.16 shows the three angles in our lattice parameters as a function of pressure for phase I.

The percentage changes in the angles between the lattice vectors is very small, meaning that there is not much anisotropic fluctuation in the shapes of the cells as the pressure changes. The regression lines were calculated using weighted least squares and the gradients are of the order of 10^{-5}.

For phase III the percentage changes in the angles, as shown in Figure 5.17. These angles are also reasonably constant with the change in pressure, with the gradients being of the same order as those for phase I.

This validates our choice of anisotropic volume moves for this system. It

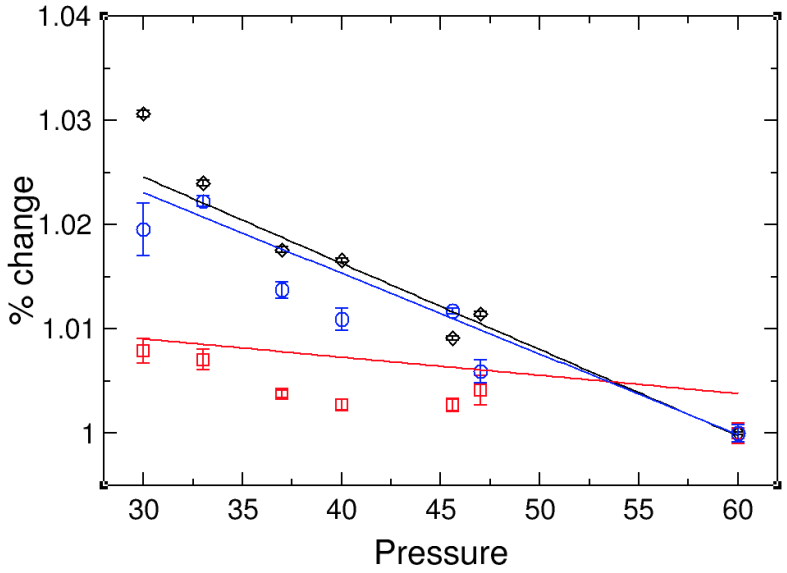

Figure 5.15: Percentage change in a (black diamonds), b (red squared) and c (blue circles) lattice parameters for phase III, at pressures, $P\sigma^3/k_{\mathrm{B}}T$.

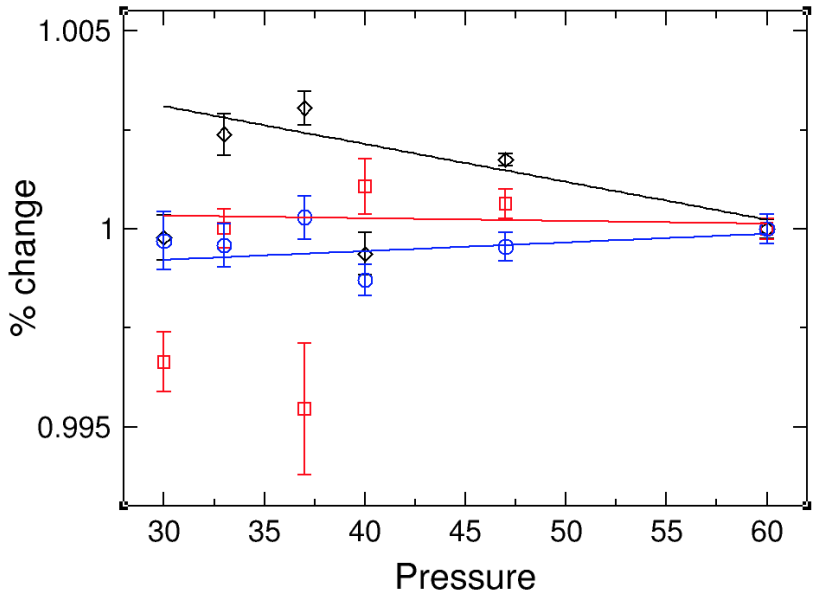

Figure 5.16: Percentage change in α (black diamonds), β (red squared) and γ (blue circles) for phase I, at pressures, $P\sigma^3/k_{\mathrm{B}}T$.

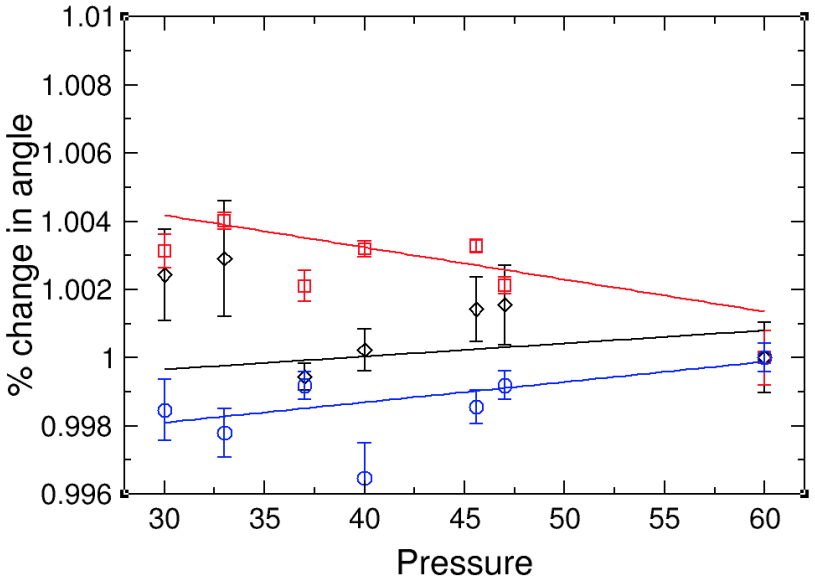

Figure 5.17: Percentage change in α (black diamonds), β (red squares) and γ (blue circles) for phase III, at pressures, $P\sigma^3/k_{\mathrm{B}}T$.

also tells us that we can take an equilibrated configuration from any pressure and scale it to produce a good initial crystal for phase I. However, for phase III we need to equilibrate at a pressure that gives us a density close to the one we want and then scale it. This will minimise any finite size effects due to shape. When our simulations systems are large enough, the effect of slight deviations in shape on the free energy difference will reduce to zero. However, at smaller system sizes this will play an important role and needs to be acknowledged and accounted for.

5.7.3 Biasing

We have discussed some computational considerations of our biasing method in section 4.3. When we are running simulations in parallel we are putting a contribution of $N_{processor} \times \ln(f)$ per MC cycle into the biasing function due to the extra number of processors updating the same weighting function. Therefore, to get the same rate of convergence we should divide our starting value of the increment factor by the number of processors used. This will ensure that we are not building up the weighting function too quickly or reducing the increment value too fast. It is important because if the histogram is built up too fast and the increment value reduces too quickly, we may get stuck with an incorrect biasing function which will take a long time to correct when our increment is small.

We also need to decide how to best discretise our order parameter space. We have already discussed non-uniform width bins in section 4.3.1, however we also need to decide on the optimal number of bins for the width of the order parameter space. If we have too few bins, then there will be large areas of our biasing function that are flat because the bins are so wide. This will slow down the convergence of our weighting function because the system may get stuck in each bin for a significant period of time. On the other hand, if we have a single bin for each overlap in the system, there will be a lot of noise in our biasing function and this will converge slower as the increment factor decreases and to a size on the order of noise. Therefore, we need a compromise between the two; a large enough number of bins so that the system can easily traverse between them, while having few enough bins to reduce the noise. In order to tell what width bins our system can easily traverse we can look at an equilibrium run with our biasing, and calculate the average order parameter change for a small number of MC cycles; this will show us how far our system will ordinarily travel.

We also need to decide how converged we want our weighting functions to be before we run with fixed weights. A balance needs to be struck between wanting a very small increment factor and how long we want to have to run our simulations for. For the butane system we chose to run our fixed weight simulations after the increment factor had reduced below 1×10^{-7}. This was chosen as it could be achieved in less than a week of simulation and has allowed for over twenty Wang-Landau reductions. Also from visual inspection, the weighting functions are no longer changing noticeably.

5.7.4 Gibbs free energy difference

Our work on calculating the Gibbs free energy difference for butane will be discussed in this section. Phase I and phase III have different volumes when simulated at the same pressure, which causes a problem for the hard sphere system. The acceptance criterion for an interphase switch move at constant pressure (equation 4.26,5.10) includes an energy and a volume term. For hard sphere systems the energy term can only be zero or infinity.

In case of difference cell shapes, a synchronised change in simulation cell vectors leads to different changes in volume of the two simulation boxes, and may result in initially similar volumes diverging as one samples the currently active crystal. Identifying (and biasing to sample) gateway states purely by means of equation 4.16 will hence fail, as the set of states visited at $\mathcal{M} = 0$ becomes dominated by those possessing volumes for which equation 4.26 is negligible.

In the case of hard particles as studied here, including volume into the order parameter would result in sufficiently large and enthalpically favourable volume differences offsetting a non-zero number of overlaps in the passive phase, leading to non-physical sampling upon accepting a switch. Similar arguments preclude the use of separate branches for the weight function depending on which phase is currently active, as suggested for soft crystals of substantially differing volume by Jackson et al. [56]. As our interest in extending PSMC is motivated primarily by soft coarse-grained models of polymorphic molecular solids [47], we do not pursue alternative solutions to this issue here.

5.8 Validation for butane system

It is necessary to validate our implementation of the butane model and our MC sampling against previous work and check that our implementation conserves the crystal structures of the two phases.

Figure 5.18 shows four snapshots of our simulation at different times. It can be seen that overlaps only exist in one system at a time and switch between the two systems, oscillating in number. Both phases remain representative of their crystal structures (excluding overlaps) throughout the simulation. This shows that our implementation of the MC moves onto the passive system do not push them into defective areas of configuration space.

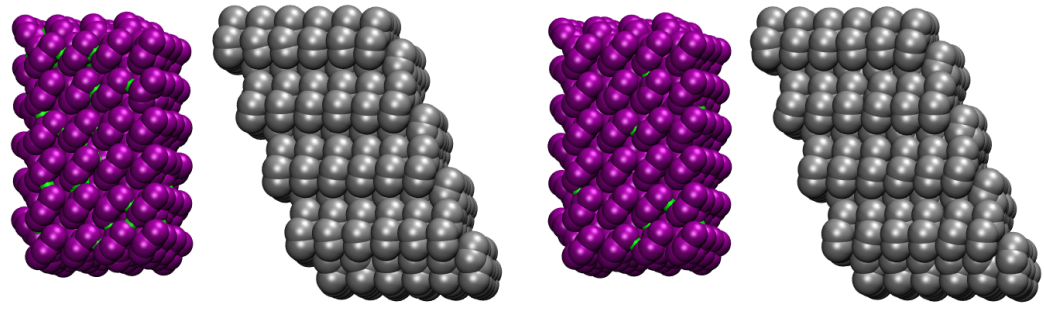

(a) phase I is passive (left)

(b) phase I is passive (left)

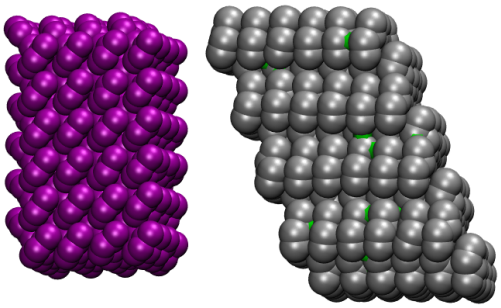

(c) phase III is passive (right)

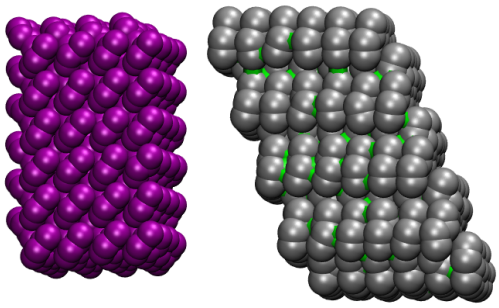

(d) phase III is passive (right)

Figure 5.18: Snapshots of phase switch Monte Carlo on $N = 192$ hard sphere butane molecules at $P\sigma^3/k_{\mathrm{B}}T = 50$. Phase I is shown in purple and phase III is shown in grey, and overlaps between molecules are shown as green bonds.

We can validate our implementation of the butane hard sphere model by looking at previous work on this model. Malanoski and Monson studied the fluid-solid coexistence of hard sphere models of n-alkanes [70]. They calculated the equation of state pressure vs density curves of a closed packed structure of n-butane which we will use to validate our model and Monte Carlo sampling. In our simulations we use model IV, while Malanoski and Monson used model II. However, model IV is just a small extension from model II so we should be able to reasonable verify our data with theirs. Figure 5.19 shows the results for the pressure-density curves of the solid phases of n-butane for 192 chain systems. The error in the density calculations is of the order of 0.001, which is less than 1% of the result.

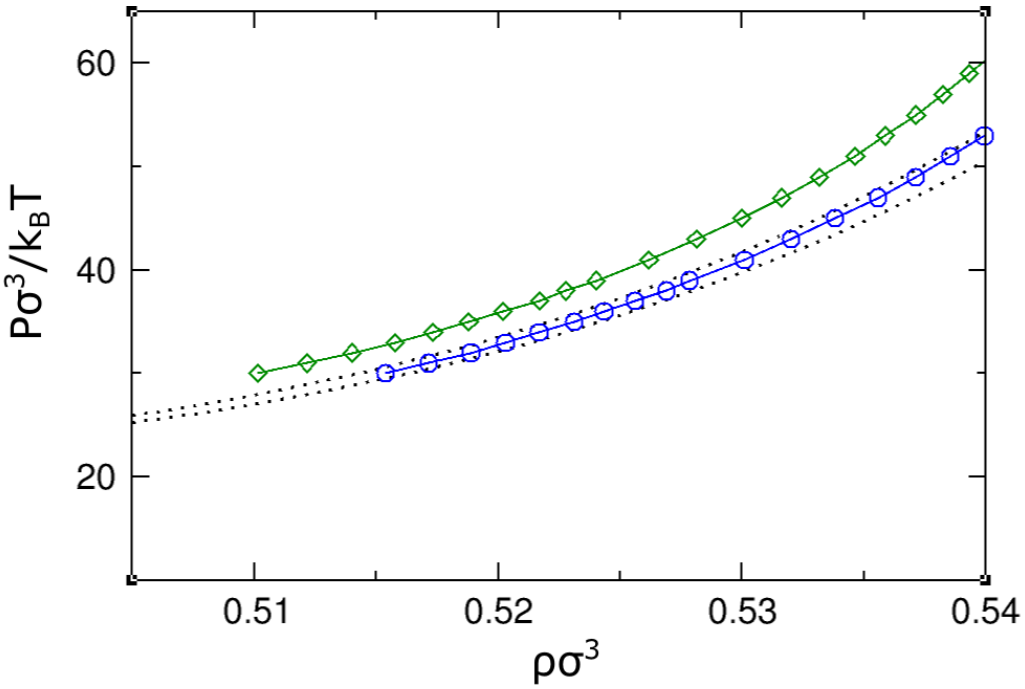

Figure 5.19: Pressure ($P\sigma^3/kT$) vs density ($\rho\sigma^3$) for model IV of *n*-butane from our Ponders code. The green line with diamonds is for phase I, the blue line with circles is for phase III, and the black dashed lines denote the error range for the close-packed crystalline phase of model II of *n*-butane from Malanoski and Monson [70]. The error in the density from our simulations is smaller than the size of the points.

In the work of Malanoski and Monson, the variables are scaled by a factor d^3. This is the diameter of a sphere that has the same volume as the chain. The volume of the chain was calculated using the work of Lustig [67] to give us a volume of $V_m = 1.4051\sigma^3$ which results in a value of $d^3 = 2.68\sigma^3$ for this model. Vega et al. [109] calculated only a 1% change in the chain volume for different configurations of short chains. For model II this volume is independent of conformation.

It can be seen in Figure 5.19 that our pressure-density curve for phase III agrees very well with the work of Malanoski and Monson. This means that we can be confident in our Monte Carlo sampling and implementation of the butane model. Since phase III is purely in the *trans* conformation, and the extension from model II to model IV is only to further include the *gauche* torsion conformation, we can assume that this inclusion would not affect the behaviour of phase III; hence our validation using this data is justifiable.

In their work, Malanoski and Monson calculated the Helmholtz free energy

between phase I and phase III at $\rho\sigma^3 = 0.5$. They found that phase I has a slightly lower Helmholtz free energy by $0.4N_{\mathrm{mol}}k_{\mathrm{B}}T$. From this result they suggested that phase III is not thermodynamically stable in this model. They do not quote the uncertainty in their calculations of the Helmholtz free energy. However the difference between values calculated using the Einstein crystal method and via integration of the equation of state, for model II butane, was of the order of $\pm 0.3N_{\mathrm{mol}}k_{\mathrm{B}}T$. Therefore their calculated free energy difference is inconclusive. Since they used the equation of state to calculate free energy differences their use of a close-packed crystal phase will have had a large effect. In Figure 5.19 the curves for each of the structures are noticeably different, hence at the same density, they will be at different pressures. They also found that if they used a reference state with a very small change in the unit cell this had a noticeable affect on the free energy calculated [71]. Since we are not using thermodynamic integration there should not be the same issue with our method.

We ran our own phase switch calculations at constant density for comparison with the results of Malanoski and Monson. Figure 5.20 shows the difference in Helmholtz free energy per chain for 120, 192 and 250 chains. Our results are negative which means that phase I is the most stable, since $\Delta F_{1,3} = F_I - F_{III} < 0$ because $F_I < F_{III}$. This is consistent with the calculations of Malanoski and Monson. Our potential is a slight variation of theirs which did not include the *gauche* conformation of butane chains, but is included in our model. Our calculated value of the free energy difference is lower than theirs, however, the error on their result is very large and our value is well within the error in their work. The simulations were run with fixed bias functions that had been reduced to $\ln(f) = 6\times10^{-9}$ for 120 and 192 chains and $\ln(f) = 7 \times 10^{-9}$ from 250 chain system. For 120 chains, the order parameter range $(-550, 500)$ was split into 401 bins, for 192 chains an order parameter range of $(-1000, 850)$ was split into 601 bins, and the 250 chain order parameter range of $(-1100, 1000)$ was split into 641 bins.

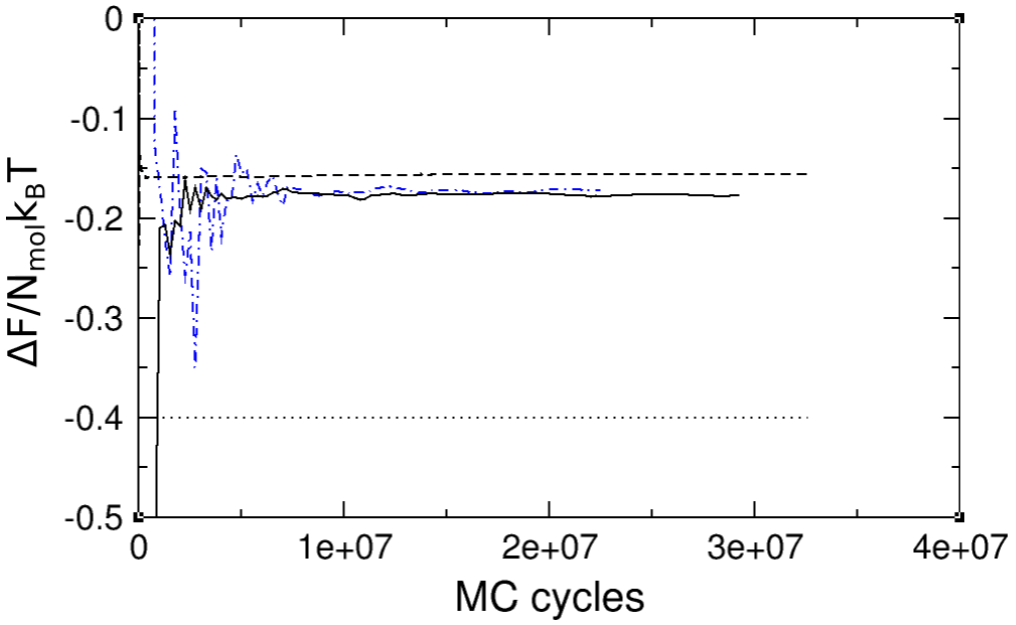

Figure 5.20: Helmholtz free energy per chain as a function of MC cycles at a constant density of $\tilde{\rho} = 0.5$ for phase I - phase III, with 120 chains (dashed black line), 192 chains (blue dashed and dotted line), 250 chains (solid black line) and the result of Malanoski and Monson (dotted black line).

Our calculated value for the Helmholtz free energy at a constant density of $\rho\sigma^3 = 0.5$ is -0.174 ± 0.001 $N_{\text{mol}}k_{\text{B}}T$, favouring phase I. Table 5.3 gives the full comparison between our values and the previous work including the uncertainties. From these results we can see that 192 chain system size is representative of the thermodynamic limit and we know the associated uncertainty. Therefore, for all further work we will use 192 chains systems or larger. The initial configurations for these simulations were scaled isotropically from the average value of constant pressure simulations at $P\sigma/k_{\text{B}}T = 30$.

N_{mol}	$\Delta F N_{\text{mol}} k_{\text{B}}T$	Reference
250	-0.4 ± 0.3	[70]
250	-0.174 ± 0.001	CW
192	-0.171 ± 0.004	CW
120	-0.154 ± 0.003	CW

Table 5.3: The Helmholtz free energy difference for a density of $\rho = 0.5$: CW denotes current work.

5.9 Simulation details

Our simulations were run on between 12 and 48 processors with an initial biasing increment of $f = 1.0005$. The biasing function was updated until f had reduced at least ten times.

5.10 Results for butane system

5.10.1 Helmholtz free energy difference

First it is necessary to check that our simulations cover the full order parameter landscape. Figure 5.21 shows 12 walkers for a simulation with a fixed biasing function. It can be seen that the walkers are visiting the entire order parameter space well.

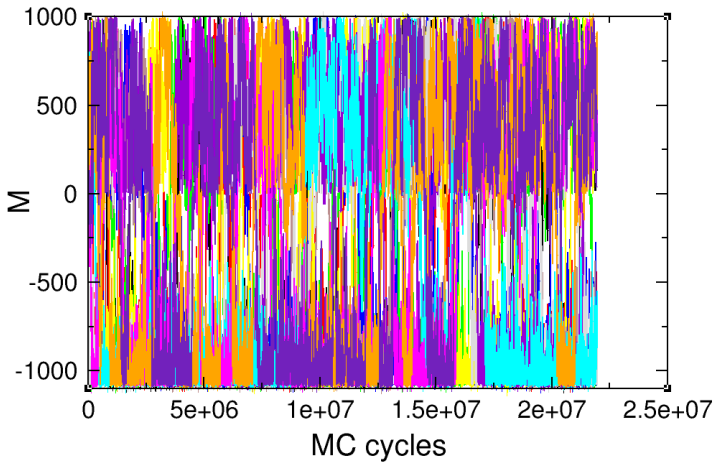

Figure 5.21: Order parameter from 12 walkers during a fixed biasing function run at a density of $\rho = 0.5$ for 250 chains of butane between order parameter values $1000, -1100$.

Next we checked that the simulations were switching phase often. Figure 5.22 shows the number of switches for a fixed bias simulation at $\rho\sigma^3 = 0.5$ for 250 chains of butane. The number of switches is increasing for all walkers at a reasonable rate. This means that both sides of our biasing function are well equilibrated with each other and the biasing function is converged sufficiently for us to traverse the full order parameter space. The biasing function was converged to an increment value of $\ln(f) = 3.0 \times 10^{-8}$.

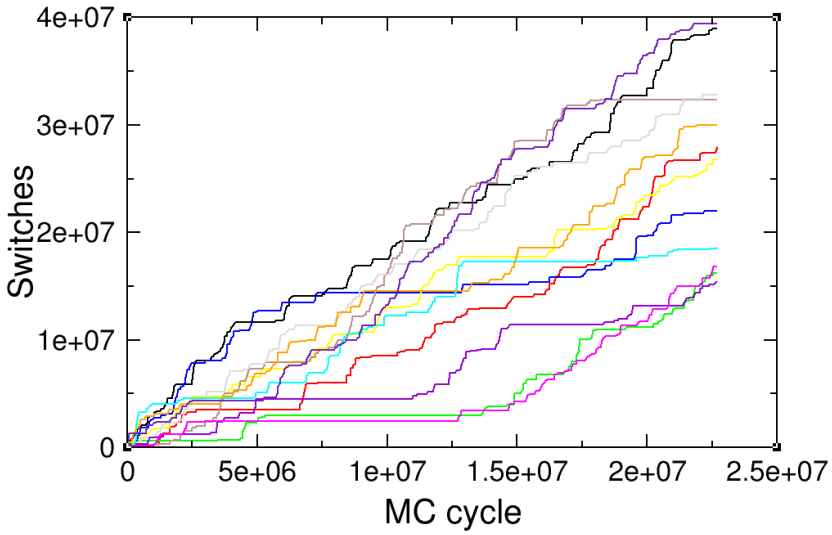

Figure 5.22: Switches between phases I and III from 12 walkers during a fixed biasing function run at a density of $\rho\sigma^3 = 0.5$ for 250 chains of butane.

Even though the individual processors do not always switch often, the combined number of switches across all processors as shown in Figure 5.23 is linear and shows that both sides of our order parameter distribution are well equilibrated with each other.

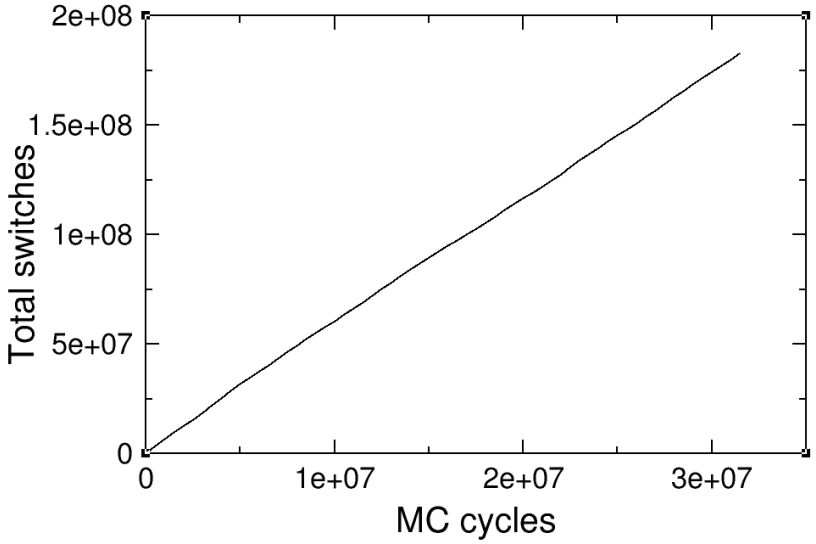

Figure 5.23: Total switches between phases I and III from 12 walkers during a fixed biasing function run at a density of $\rho\sigma^3 = 0.5$ for 250 chains of butane.

We then ran simulations at a range of densities with 192 chains to calculate

the Helmholtz free energy difference as a function of density. The initial configurations for each density were scaled isotropically from average configurations simulated at a pressure of $P\sigma^3/k_{\mathrm{B}}T = 75$.

At a density of $\rho\sigma^3 = 0.5$ we have shown that phase I is the most stable, which also agrees with the literature. We investigated higher densities to check for a phase transition. We ran simulations for increasing density with an interval of 0.01 up to $\rho\sigma^3 = 0.54$. For all simulations the order parameter space was split into 601 bins, ensuring that the middle, gateway bin was solely for zero overlaps. For all densities we limited the order parameter to lie between ± 1000 overlaps.

At $\rho\sigma^3 = 0.51$ the bias and probability distribution function calculated are shown in Figure 5.24. The pdf favours negative order parameter values which means that phase I is stable at this density. Figure 5.27 shows the convergence of the Helmholtz free energy difference as a function of MC cycles when running with fixed bias function. The average Helmholtz free energy difference is $\Delta F/N_{\mathrm{mol}}k_{\mathrm{B}}T = -0.0837 \pm 0.0015$; this is significantly lower than the value at $\rho\sigma^3 = 0.5$. This suggest that a phase transition might occur in this system.

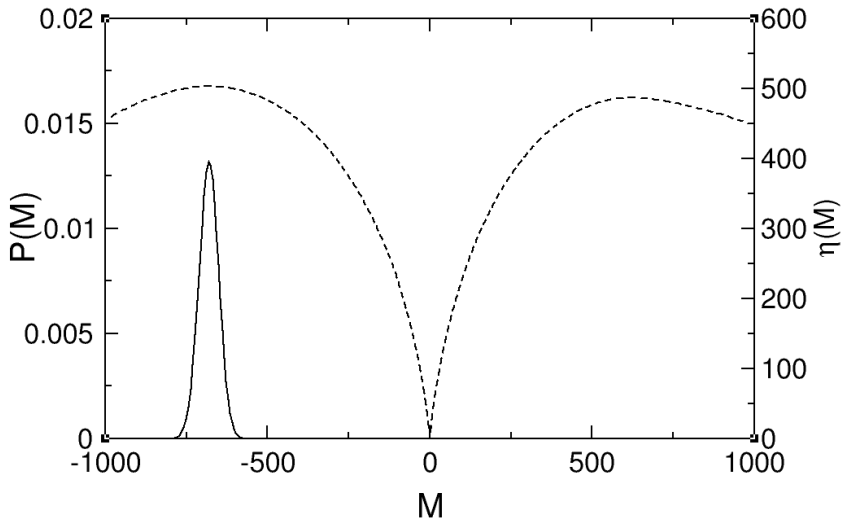

Figure 5.24: Biasing function (right hand side, dashed line) and probability distribution function (left hand side, solid line) from a density of $\rho = \sigma^3 0.51$ for 192 chains of butane, phase I vs phase III.

Another simulation was run at a density of $\rho = \sigma^3 0.52$; the bias and probability distribution functions are shown in Figure 5.25. It can be seen that the peak in the probability has changed sign in order parameter value. The left hand peak of the pdf is also of the same order of magnitude. This means that a phase transi-

tion has occurred and phase III is now stable. The density is also very close to the transition point due to the visible double peaked nature of the pdf.

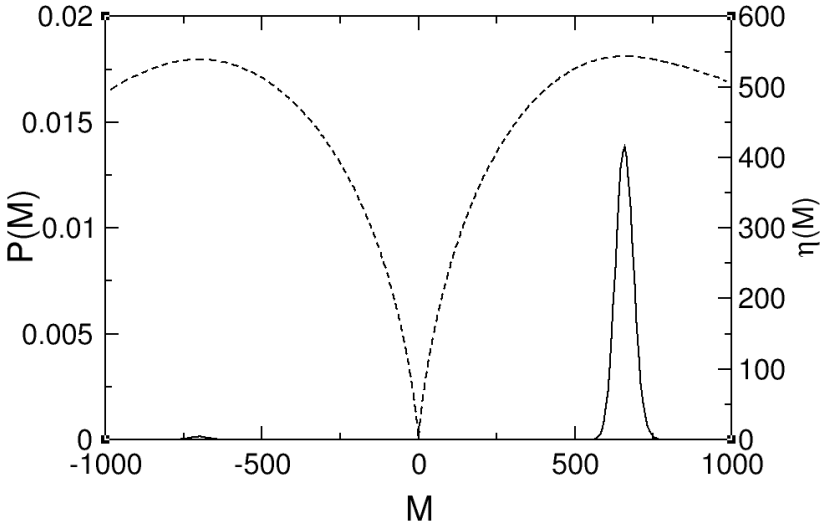

Figure 5.25: Biasing function (right hand side, dashed line) and probability distribution function (left hand side, solid line) from a density of $\rho\sigma^3 = 0.52$ for 192 chains of butane, phase I vs phase III.

The average value of the Helmholtz free energy difference between phase I and phase III is $\Delta F/N_{\mathrm{mol}}k_{\mathrm{B}}T = 0.0228 \pm 0.002$.

In order to pinpoint the density of the phase transition we ran at a new estimate of $\rho\sigma^3 = 0.518$. We initialised our configurations by scaling isotropically from samples equilibrated at a pressure of $P\sigma^3/k_{\mathrm{B}}T = 37$. Figure 5.26 shows the bias function and probability distribution for 192 chains. The probability distribution is clearly double peaked with the right hand side only slightly larger. This shows that we are very close to the phase transition.

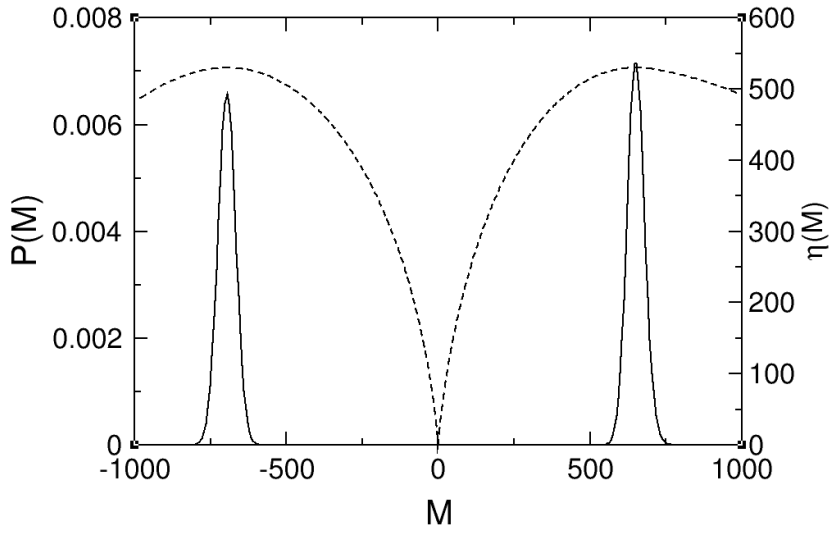

Figure 5.26: Biasing function (right hand side, dashed line) and probability distribution function (left hand side, solid line) at a density of $\rho = 0.518$ for 192 chains of butane, phase I vs phase III.

The final calculated value is $\Delta F/N_{\mathrm{mol}}k_{\mathrm{B}}T = 0.001 \pm 0.001 N_{\mathrm{mol}}k_{\mathrm{B}}T$. The finite size error for 192 chain systems we calculated is ± 0.004. This means that our final result is on the order of our finite size error which has now become the dominant error.

Figure 5.27 shows the convergence of the Helmholtz free energy differences for a range of densities.

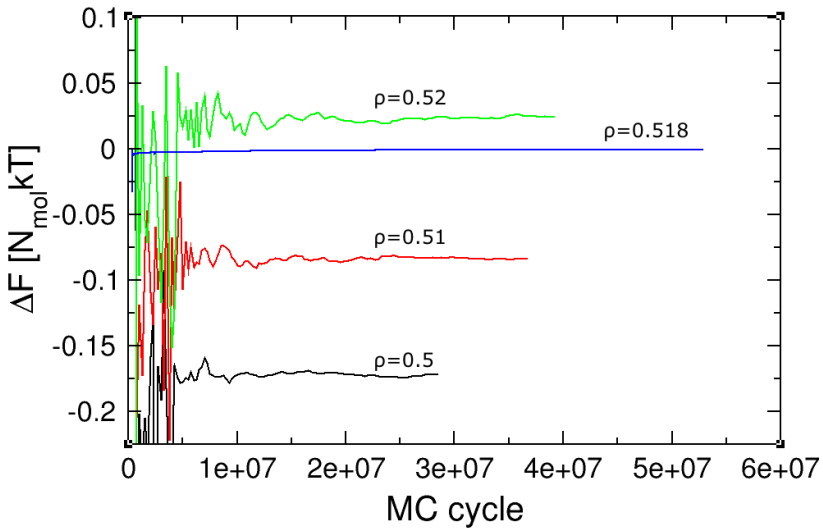

Figure 5.27: Convergence of Helmholtz free energy difference for 192 chains of butane, phase III - phase I.

$\rho\sigma^3$	$\Delta F_{1,3}/N_{\mathrm{mol}}k_{\mathrm{B}}T$	Reference
0.5	-0.4 ± 0.3	[70]
0.5	-0.165 ± 0.001	CW
0.51	-0.058 ± 0.004	CW
0.518	0.001 ± 0.001	CW
0.52	0.027 ± 0.002	CW

Table 5.4: The Helmholtz free energy difference for different densities. CW denotes current work.

From these calculated values we can plot the Helmholtz free energy difference as a function of density and calculate the exact transition density, as shown in Figure 5.28.

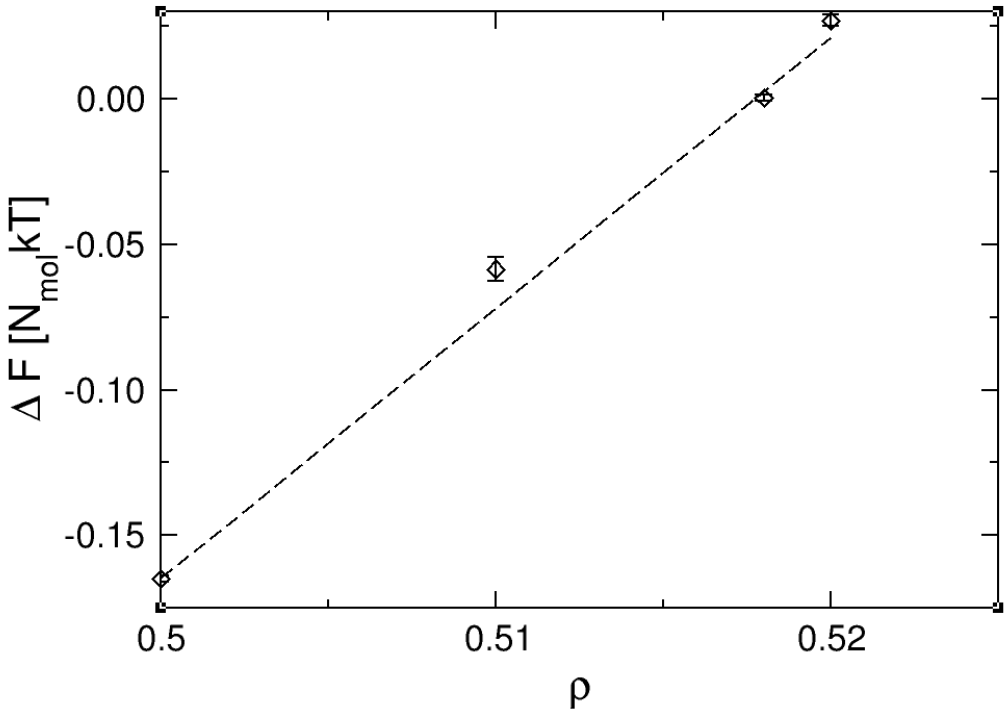

Figure 5.28: Helmholtz free energy as a function of density for 192 chains of butane, linear fit to the data is the dashed black line.

We calculated a linear regression fit to the data reported in Table 5.4, using the weighted least squares method to take into account the error in each data point. This is shown with the data in Figure 5.28, and it can be seen that the regression fits very well to our data. The Chi-squared value was calculated to be $\chi^2 = 18.91$ which corresponds to a probability (p-value) 0.001; this is considered to be very statistically significant.

From this regression line we can calculate the density for which the free energy difference is zero. The resulting density transition was calculated to be $\rho\sigma^3 = 0.518 \pm 0.001$. The error in this result comes from the finite size error taken into account in the free energy values, arising from both system size and shape. Also taken into account is the error in our regression calculation. This error is much smaller than from finite size effects.

Different configurations and cell dimensions were used for calculations at $\rho\sigma^3 = 0.5$. The difference between the resulting free energies is larger than the statistical uncertainty, but it does not significantly alter our calculation of the transition density. The calculated slope of the fit in Figure 5.28 does not change significantly when either result is used. Therefore we can be confident that our calculated density

of transition takes into account finite size effects in shape as well.

We investigated the variation in cell parameters between the two different configurations used for each phase at $\rho\sigma^3 = 0.5$. The configurations of phase I are within one standard deviation of each other, whereas the configurations used for phase III are within two standard deviations of each other. This implies that the variation in cell parameters for phase III is more likely due to the difference in preparation, in that they were scaled from different equilibrium pressure simulations. The resulting free energy differences calculated will have been affected by these differences.

It is clear that the anisotropy in phase III with pressure has led to cell variations caused by the scaling of the system to a constant density from different starting pressures. Phase I was shown to scale reasonably isotropically and does not have the same variation in cell parameters.

The free energy difference reduces if we isotropically scale from a sample equilibrated at a higher pressure. This can help us understand the phase transition which occurs as the density increased. If the cell of phase III become more anisotropic with increasing density and this anisotropy lowers the free energy difference between phase I and III, then it is likely to be an important factor in the phase transition.

If the cell parameters scale isotropically, then the entropy is only affected by the reduced volume available. However, if the cell parameters scale anisotropically, then entropy will be affected by the same reduction in volume and also by the change in shape of the cell.

If we were only simulating with isotropic volume moves, we may not even have captured this transition, or its position may have been drastically different.

Using our pressure-density curve (Figure 5.19) we can calculate the associated pressure change corresponding to the error in our transition density for both phases. The error in our calculated transition density is of equivalent size to the error in calculating the density at a given pressure. The associated pressure for a density of $\rho\sigma^3 = 0.518$ for phase I is $P\sigma^3/k_{\mathrm{B}}T = 35$ and for phase III is $P\sigma^3/k_{\mathrm{B}}T = 32$. The difference in pressure between the two phases at the transition density is $\Delta P\sigma^3/k_{\mathrm{B}}T = 3$.

This is a previously unknown first-order phase transition in the hard sphere model of butane. It was previously thought that the hard sphere model was not complex enough for a transition to occur in this model.

Looking at the pressure-density curve for the two phases at the same density (Figure 5.19), phase III has a lower pressure. Phase III is a more efficiently packed

crystal structure than phase I as it has all the chains aligned in a single direction. Therefore, at the same density (and volume) there will be more available rearrangement of the chains in phase III and hence higher entropy. However, phase I is a more disordered crystal and it is the interplay between these two effects that results in a phase transition in density in this system. As the density increases, the entropy in phase III surpasses the entropy in phase I and there is a phase transition from low density phase I to high density phase III.

In order to calculate the first-order phase transition in butane we accurately calculated Helmholtz free energy differences. Previous work on this system is not accurate enough to locate the transition.

Each simulation began with converging an accurate biasing function, and it was then run with this fixed biasing function. It was necessary to reduce the biasing increment factor below a value of $\ln(f) < 5 \times 10^{-8}$ before we could stop converging the biasing function. The CPU time taken to reduce the increment factor for butane was around 40 CPU days, However, due to the parallel nature of our simulations for 48 processor running simultaneously this only took 19 hours; this shows the advantage of our parallel scheme. Once we finished converging our biasing function we ran simulations with a fixed biasing function, and these simulations were generally run for around 50 hours on 48 processors. This length of run led to an error of the order of $3 \times 10^{-5} N_{\mathrm{mol}} k_{\mathrm{B}} T$. We ran at four different densities which involved a total of 12 days of running time. If we take into account the CPUs from all of the processors this gives us a CPU time of around 500 days, which is equivalent to the time taken to run thermodynamic integration on a system of atomic hard spheres by Wilms et al. [117]. The system we are simulating is more complex and when we take into account the parallelism in our simulations then this is significantly less process time - 12 days compared to 500. Considering our system is considerably more complex, phase switch MC is still much more efficient for equivalent or better accuracy than thermodynamic integration.

Malanoski and Monson calculated the Helmholtz free energy difference between phase I and phase III at $\rho\sigma^3 = 0.5$, the error in their result was $\pm 0.3 N_{\mathrm{mol}} k_{\mathrm{B}} T$. It is clear that with an error this large, any calculation of a phase transition would have very large errors. From our calculations, the change in free energy difference between $\rho\sigma^3 = 0.5$ and $\rho\sigma^3 = 0.52$ is only $0.2 N_{\mathrm{mol}} k_{\mathrm{B}} T$. All of our results would be within the error in a calculation using thermodynamic integration.

Chapter 6

Crystalline cholesterol literature review

This literature review will discuss the existing research on the simulation of crystalline cholesterol, primarily focussing on work relating to the anhydrous crystals. Membrane simulations and the vast expanse of medical literature are outside the scope of this review.

Cholesterol is an organic molecule that has many important roles in the properties of biological membranes and their dynamics. It cannot be replaced by other sterols in mammalian cells [121] and is crucial to cellular viability and proliferation [37]. Cholesterol molecules have a unique structure with a rigid multi-ring architecture that has chiral methyls on one side of the molecule, giving it a directionality and a flexible tail. The hydrophilic alcohol group drives orientation in bilayers [11] and forms structural hydrogen bonds in the crystal phases.

Cholesterol has also been shown to crystallise in the human body and has been found experimentally in gallstones and atherosclerosis. An experimentally determined solid-solid phase transition occurs at 37°C, determined via differential thermal analysis (DTA) [62]. There is a slight spread of transition temperatures ($\pm$5K) calculated using many different experimental methods, however, the consensus is that the transition is biologically relevant [102, 93, 106, 62, 43, 59].

Hsu and Nordman [51] determined the crystal structure of the high temperature phase and found it to be larger and unusually less symmetric than the low temperature crystal [51, 52]. At room temperature there are eight molecules in the unit cell but above the transition there are sixteen unique molecules in the unit cell.

Experimentally, cholesterol's crystal structures have been calculated from X-ray data. However, many of the atoms have very high thermal indicies which leads

to an ill-defined structure. X-ray data can be used to differentiate the monohydrate from anhydrous structures, but it is very difficult to use such data to look at the two anhydrous polymorphs. NMR spectra have been measured and assigned for the carbon atoms of cholesterol as well [101, 57, 4]. However, due to the extremely large unit cell O(1000) atoms, and the pseudosymmetry, the spectra are very complex. *Ab initio* calculations have been used to assign the carbon peaks for cholesterol monohydrate (ChM) and the low temperature anhydrous phase (ChAl) [101]. The high temperature anhydrous phase (ChAh) remains unassigned due to its increased size and complexity.

All crystalline forms of cholesterol contain a repeating pseudo bilayer structure with approximately 34Å between repeats. This means that the X-ray diffraction peak will be the same for all crystal structures and cannot be used to distinguish between crystalline forms [6]. Loomis et al. [66] observed definite structural changes associated with the transition from X-ray diffraction patterns of the two phases, however, the differences are very minor. Overall, it can be very difficult to experimentally differentiate between the three phases (two anhydrous and one hydarated).

Experimental work has investigated the polymorphic phase transition. van Putte et al. [106] and Poyry et al. [83] implicated the aliphatic side chain as the major contributors in the phase transition; the energy change and volume contraction from a rotation isomerism in this side chain is comparable to the enthalpy change observed in the cholesterol phase transition [106, 83].

In the presence of water, a hydrated crystal structure is formed [23]. However, it has been shown that, given enough time, this undergones a transition to an anhydrous structure [66]. In bile, cholesterol monohydrate has has been shown to be the major ingredient, however, anhydrous forms have been indicated in early nucleation and growth [45, 3, 100, 61]. This shows us that knowledge of early nucleation may be extremely important for further work.

Currently computer simulation studies are focussed on the role of cholesterol in bilayers, but force fields fitted to work in membrane environments are not guaranteed to accurately reproduce the structure and thermodynamics of crystalline phases. The force field determines many properties of the system that should be taken into account, for example the melting temperature and hence the whole phase-diagram. It is necessary to understand how force fields are created, what they are designed to be used for, and under what conditions they can be utilised.

The polymorphic transition is not very well studied via molecular simulation and it is not even known if it exists within current cholesterol force fields.

6.1 Cholesterol force fields

We are specifically interested in force fields that can deal with crystalline cholesterol. The crystal structure of ChAl was derived from X-ray data and has an issue with high thermal factors for a large number of atoms. This means that those atoms have a reasonably high mobility and any coordinate position should be thought of as having a large error bar. This makes reproducing the exact structure with simulation methods difficult. However, if these atoms are removed from the calculation of a fit, then a closer test can be attained.

Most force fields are all-atom descriptions of cholesterol. This is obviously the simplest mapping and since there is no loss of information. However, as mentioned previously, cholesterol crystals have very large unit cells so this might not always be the most viable description.

Liang et al. [64] compared the CFF93 [72, 53] and CVFF [48, 65] force fields for their ability to reproduce experimental crystal structures of cholesterol. They derived missing parameters for the force field CFF93 as well. The two were compared against the cholesterol acetate structure and the low temperature cholesterol crystal structure [95, 94]. Energy minimisation of the crystal structures and MD simulations were employed to test the force fields. CVFF was found to over estimate cell volumes for both crystals; since the computed cell volumes were at 0K they really should be smaller than those obtained from simulations at finite temperature. The MD simulations were run in the NVT ensemble at a temperature of 298K. Since a constant volume ensemble was chosen, we cannot see how the cell volume during MD differs from the energy minimisation result. This also may have had an effect on the structural comparison of the MD data with experiment as a fixed volume will not allow the molecules to change positions as much. Liang et al. concluded that the CFF93 force field for cholesterol is accurate, and that MD simulations rather than just energy minimisations are necessary to reproduce experimental crystal structures accurately.

CVFF is a force field originally derived for peptides, proteins and hydrogen-bonded crystals. It wasn't explicitly fitted for sterols, but was derived from a wide variety of experimental data for numerous molecules via the consistent force field (CFF) method.

CFF93 was also based upon the consistent force field method using hydrocarbons and alkyl functional groups for training. Again it was not tested against cholesterol or parametrised for it originally.

The OPLS all atom [58] force field (OPLS-AA) is popular for simulation of

biomolecules, and has been adapted from the AMBER all-atom force field [113]. It was fitted using *ab initio* data from over 50 organic molecules and ions, but not sterols. It was calculated from pure organic liquids as well and not from or for crystal structures, however it has been tested on some. This force field has been further optimised for long alkane chains [97], primarily to improve its use in the study of lipid membranes. So far it has not been tested for the stability of crystalline cholesterol phases.

Frincu et al. [40] tested the CVFF and CFF based force fields, and they noted very minor differences between the two. In their work they looked at cholesterol crystalline growth on a calcium carbonate substrate. Arterial plaque has a calcified outer layer for which calcite is a good proxy model. Initially they only used geometrical matching to determine the faces of cholesterol crystals which best matched onto calcium carbonate. They found that cholesterol monohydrate was a very good match, as was a face of the low temperature anhydrous phase. They later tested the monohydrate experimentally [41] and confirmed the preference. They simulated this computationally but did not look into the anhydrous epitaxial growth in detail. They investigated the epitaxial growth because cholesterol monohydrate is known to be deposited in the body [23], however, it has been shown that anhydrous cholesterol may be a precursor and aid nucleation [61]. This growth was not investigated thoroughly by Frincu et al. and only the growth on the faces suggested by the geometrical optimisation were looked into. It has been generally agreed upon that anhydrous cholesterol acts as a substrate for the monohydrate phase to form in the body which will supersede the anhydrous. However, the initial growth of the anhydrous phase is not well understood or discussed.

Cournia et al. [21, 22] parametrised an all-atom force field based upon the existing CHARMM27 potential [15] specifically for cholesterol. They used quantum chemistry calculations to fit their force field parameters and tested it via molecular dynamics simulation of the low temperature anhydrous crystal structure and reproduced its structure well. The cell volumes from energy minimisation were slightly larger than experiment, whereas they are expected to be smaller at 0K. The MD simulation data are very close to the experimental cell data. These MD simulations were done in an NPT ensemble at 298K, the same as the experimental data. This force field has not been used in many simulations of crystalline cholesterol and is mostly used for bilayers and membranes.

Cromie et al. [24, 25] created their own all-atom force field for cholesterol based upon the Amber potential and using density functional (DFT) results for parametrisation. The Amber potential has a simpler form than CHARMM but the

same Lennard-Jones parameters were used in both force fields. Cournia et al. [22] made a detailed comparison between the two. Both anhydrous phases and the monohydrate phase of cholesterol were tested, and the volumes of their cells compared well with experimental data. Using their force field they looked at the structure of cholesterol nano-particles under a range of conditions: in vacuum, water and carbon dioxide. They calculated low energy structures and found similar properties to the crystal phases. However, more work still needs to be done to study the actual nucleation of small cholesterol crystals.

Hadley and McCabe [46] parametrised a coarse-grain force field for cholesterol specifically fitted for the room temperature anhydrous phase. The other phase is mentioned but no clear comparison of their results with experimental data is given. No clear transition temperature is given either. They fitted their coarse-grain force field to the atomistic CHARMM potential of Cournia et al.; fitting methods were discussed in section 2.1.2. They used the centre of mass position of groups of atomistic particles for the coarse-grain bead coordinates and a modified Boltzmann inversion method for the non-bonded potentials; see section 2.1.2. The modification included a damping factor when modifying the potential which minimises the oscillation issues with calculating potentials for crystals. Two levels of coarse-graining were implemented, where the carbon ring-sheet beads can be individually parametrised or consist of a single bead type. Their estimation of the melting temperature of their model was 519K, which is much higher than the experimental value of 422K.

There are other coarse-grained force fields for cholesterol, however most are based upon simulations in lipid membranes and bilayers and have not included crystalline cholesterol in their fitting set [77].

Even though all of these force fields have reproduced one or more of the crystal phases of cholesterol, very little, if any, mention of the polymorphism and phase transition is made. Therefore, further investigation into polymorphic phase transitions in force fields is needed. This transition is especially important when thinking about the nucleation of cholesterol, which is one of the important areas of study at the moment. Since there is a lot of debate experimentally about which phases of cholesterol are present in the body, this is a very important avenue of research that could be greatly helped by simulation work.

Jayalakshmi et al. [57] used NMR to characterise the cholesterol polymorphs in cancerous and benign gallstones and found that the type of disease correlated very well with the polymorph present; they found that cancerous gallstones had a prevalence of anhydrous cholesterol whereas benign ones were mainly comprised of monohydrate. Their sample sizes were not very large, with less than 30 samples of

all types, therefore more investigation needs to be carried out. They also did not specify which anhydrous phase of cholesterol was found in the cancerous gallstones.

6.2 Cholesterol crystalline bilayer domains

There has been a lot of recent work focussed on crystalline domains of cholesterol in bilayers. Initially experiments on thin films using differential scanning calorimetry (DSC) showed peaks for the polymorphic phase transition at 36°C which suggested that anhydrous cholesterol forms inside bilayers at high cholesterol concentration.

Since the bilayers are so thin, most standard solid-state techniques cannot be used to investigate the structure of these cholesterol domains. Bragg peaks can only be observed by X-ray scatteriong from 3D crystals [6, 33]. The rigidity of the structure is also very difficult to investigate due to the small size of the domains.

Ziblat et al. [123] showed using X-ray diffraction that pure cholesterol domains form in bilayers at concentrations relevant to cell plasma membrane composition. Ziblat et al. did not discuss which structure of cholesterol was formed and their experiments were performed at 7°C, which suggests that either the low temperature anhydrous structure or the monohydrate is formed. Whether this result is still relevant at biological temperatures is also not discussed.

Plesnar et al. [80] performed a computer simulation comparison between pure cholesterol domains, standard bilayers with cholesterol and lipids, and the low temperature anhydrous cholesterol crystal structure. No actual data from crystal simulations was given. Plesnar et al. found that the pure cholesterol bilayer was highly mobile compared to the crystal phase, and only slightly less mobile than the standard mixed bilayer. These simulations were performed at a much more relevant temperature of 310K. They used the low temperature anhydrous crystal but did not mention the possibility of a phase transition, which occurs experimentally at 308K.

The pure cholesterol bilayer was shown to be stable when hydrated for the length of their simulations, over 200ns. However, it was not stable within the mixed bilayer, as it is experimentally. Neither the formation of this pure cholesterol domain nor its stability were investigated. It was concluded that the diffusion of the cholesterol domains are closer to the mixed bilayer than the anhydrous crystal. They used the OPLS-AA force field, which was parametrised for liquid organic molecules and does not necessarily accurately reproduce the crystal phases. Therefore the high mobility found in these bilayer regions may be partially due to this.

Other experimental work has shown anhydrous and monohydrate structures of organised cholesterol in bilayers.

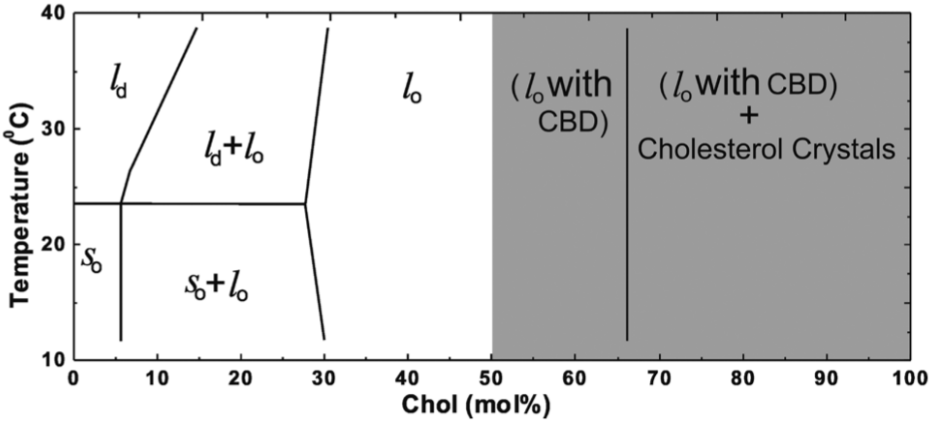

Figure 6.1: Extended phase diagram of cholesterol concentration in phospholipid bilayers reproduced from [68] showing the formation of cholesterol bilayer domains (CBD) at 50 mol% and crystalline cholesterol at 66 mol%, l_d signifies liquid disordered phase, l_o liquid ordered phase and s_o solid ordered phase of the bilayer.

Mainali et al. [68] showed using EPR and DSC that cholesterol bilayer domains preceded the formation of cholesterol crystals in phospholipid membranes.

They extended the phase diagram for cholesterol to much higher concentrations (Figure 6.1) and found that cholesterol bilayers are the precursor to crystalline formation. They suggested that previous thin film techniques were flawed becuase the anhydrous state was formed upon creation rather than during the experiment. These studies located a polymorphic phase transition peak in DSC. However, using a rapid technique to create the thin film bilayers, DSC no longer shows the polymorphic peak, just the monohydrate dehydration at 86°C. This suggest that monohydrate cholesterol crystals are formed from bilayers.

This still does not explain how anhydrous cholesterol is formed within the body and whether the polymorphic phase transition is important to biological function.

6.3 Summary

In other areas of the body, anhydrous cholesterol has been linked to the early nucleation and growth of crystals in bile [45, 3, 100, 61]. There has also been a lot of debate about which structure of cholesterol is formed in gallstone cancer.

In summary, it is clear from this review that the polymorphic phase transition in cholesterol has not been widely simulated and it is unclear whether it is correctly reproduced in current force fields. The nucleation of cholesterol is highly important

biologically and the crystals have been found in many different situations. This all supports the need for work into the nucleation of the two phases and therefore the ability of force fields to locate the transition accurately in the phase diagram.

Chapter 7

Extending phase switch Monte Carlo to soft fully-flexible molecules

This chapter will discuss the existing extension of the phase-switch Monte Carlo method to soft potentials [74, 34]. Then our extension to fully flexible soft molecules will be introduced. The motivation behind the model chosen to test this extension will be given along with our validation and finally the results.

7.1 Soft potentials

Phase-switch Monte Carlo was extended to continuous potentials by Errington [34] specifically for the Lennard Jones case. However, this extension is applicable to all soft potentials.

Since the energy function of the system is no longer discrete and we can distinguish between energies, an 'overlap' order parameter no longer makes sense. Hence, a new order parameter needs to be devised that describes a suitable path between the equilibrium and the gateway states. In the discrete hard sphere system, the gateway state only existed at zero order parameter, as this was the only energetically allowed value for both systems. When this is extended to soft potentials we no longer have a single order parameter value but a range of values with varying probabilities.

The probability of an interphase switch move occurring from phase α to

phase γ at constant volume V is

$$P_{\alpha\to\gamma} = \min(1, \exp[-\beta(E(\underline{r})_\gamma - E(\underline{r})_\alpha)]), \tag{7.1}$$

where $E(\underline{r})_\gamma$ is the energy of the system in phase γ. Since this probability of acceptance depends upon the energy difference between the two systems, the gateway states will be the states at which this energy difference is minimised and hence the probability of acceptance is maximised.

Therefore, an obvious order parameter is just the difference in energy of the two systems, for constant volume simulations. This has the advantage that changes to the order parameter from each Monte Carlo move can be made without complete recalculation. However, if the two systems have very different starting energies, this order parameter will be very hard to minimise enough for an interphase switch to occur. McNeil-Watson et al. [74] suggested using

$$\Delta E_{\alpha\gamma} = (E_\alpha - E_\alpha^{\text{ref}}) - (E_\gamma - E_\gamma^{\text{ref}}), \tag{7.2}$$

where E_γ^{ref} is the reference energy for phase γ. This reference energy is the energy of a representative microstate of phase γ and for our purposes is taken as the equilibrated initial configuration for a simulation. Since $\Delta E_{\alpha\gamma}$ measures the change in the energy of each system with respect to a representative energy value for that system, we have effectively equalled the playing field as we are now only calculating relative changes in each. As the order parameter value approaches zero, the probability of an interphase switch increases.

This definition of the order parameter still has some potential issues with strongly repulsive potentials because these would cause very large variations in the energy and hence in the order parameter value. To balance this out we modulate $\Delta E_{\alpha\gamma}$ by a monotomic function f such that

$$\mathcal{M} = f[\Delta E_{\alpha\gamma}] \tag{7.3}$$

In the work of Errington the square root function was used whereas McNeil-Watson et al. use a logarithm in their work. One may also include a factor of β in the order parameter to closer resemble the acceptance probability if desired.

The problem with applying this monatomic function, especially in the form of a logarithm, is that it adds much more computational complexity to the calculation of the order parameter at each Monte Carlo step. Instead of just addition and subtraction we now have to completely recalculate a logarithm. Since computational

calculation of logarithms is generally based on Taylor expansions and look-up tables, this will be a relatively costly process compared with simple addition, which will need to be done anyway. Therefore what we gain in simplicity we may lose by extending the computation time.

For constant pressure simulations the order parameter should measure the change in the enthalpy $\mathcal{H}_\alpha = E_\alpha + pV_\alpha$ between the two systems. Similarly to the energy, we can also shift the volume of the two systems by a representative volume V_α^{ref}. McNeil-Watson et al. use volume scaling incorporated into the interphase switch move to alleviate issues with different density systems. The order parameter used in this work is

$$\mathcal{M} = \text{sgn}(\Delta H_{\alpha\gamma}) \ln[1 + |\Delta H_{\alpha\gamma}|] \tag{7.4}$$

where $\text{sgn}(\Delta H_{\alpha\gamma})$ gives us the sign of $\Delta H_{\alpha\gamma}$. We need to shift the value inside the logarithm so that it is centred on one rather than zero since $\ln(1) = 0$.

7.2 Full flexibility

7.2.1 Monte Carlo moves

In our Monte Carlo simulations, we will be using anisotropic volume scaling, rigid translation, rigid rotation, bond-stretch and bond angle moves along with single particle moves. The rigid translation and rotation moves are describe in section 5.5. We first label the molecular system under investigation and define the first three beads in the molecule as ones that are bonded and form an angle centred around the second bead; all molecules in both systems must be labeled consistently. These MC moves do not depend upon the specific model or topography of the system.

Single particle moves A single particle in a molecule is chosen at random and a randomly chosen displacement, within the fixed extremum $\pm\Delta\underline{r}_{\max}$, is applied. We could make only these single particle moves in our simulation and would be able to sample all configurations, however, the sampling would be very slow with a long correlation length. This is why it is useful to include concerted motion of the molecules to speed up sampling.

Bond-stretch moves The bond is chosen at random, $\underline{b}_i = \underline{r}_i - \underline{r}_{i+1}$ between the first two bonds in the molecule only. It is then scaled to a magnitude, b_{move} chosen to randomly lie between $\pm b_{\max}$.

$$\underline{b}_i^{\text{new}} = \hat{\underline{b}}_i * b_{\text{move}} \tag{7.5}$$

where $\hat{\underline{b}}_i$ is the unit vector of the bond between particles i and $i+1$. This new bond length is then added onto the current bond and also applied to all other particles of higher index in the molecule. That is, all other bond lengths remain constant when the move is made.

Bond angle moves The only angle change is for the angle enclosing the first three beads in the molecule. An angle of rotation θ_{move} is chosen randomly between $\pm\theta_{\text{max}}$. The rotation is in the plane of the bonds defining the angle and hence the axis of rotation is the cross product of these two bonds $\underline{a} = \hat{\underline{b}}_i \times \hat{\underline{b}}_{i+1}$. This angle and axis can be transformed into a quaternion using Equation (A.12), ensuring that all vectors are normalised. This quaternion is then conjugated with the cartesian position of the third bead in the molecule, that is the last particle defining the angle, so only that particle is moved.

7.2.2 Generalised coordinates

We need to define a new set of generalised coordinates for fully-flexible systems. The coordinates will be used in the same way as in section 5.5, for synchronisation between the two systems.

Since we are dealing with a system with no constraints we have $3N_{\text{mol}}N_{\text{bead}}+6$ degrees of freedom for constant NPT simulations. As in section 5.3, we define a set of coordinates that are independent of the cartesian coordinate system and describe any combination of Monte Carlo moves applied to an arbitrary reference system. These generalised coordinates should be independent of each other. In order to calculate each coordinate change from the reference to the current system, the previous difference is applied to the reference system to remove all degrees of freedom after they have been calculated.

All the degrees of freedom for our system are represented in the generalised coordinates. The change in fractional displacement of the first particle in the molecule $\{\Delta\underline{s}\}$, was described in Equation (5.2). This is basically the difference, in fractional units between the current and the reference system. The reference system is usually defined as the initial configuration of the Monte Carlo simulation. This configuration should be well equilibrated and representative of the system under the chosen conditions.

It is simple to apply the fractional displacement to each entire molecule as a rigid translation. We can just shift each molecule so that the position of the first bead of each molecule in the reference system is the same as the position of the first bead of the equivalent molecule in the current system.

Rigid molecule rotation is defined by a quaternion, $\{q\}$ in Equation (5.4) (described in Appendix A) such that the the quaternion transforms from the molecule-centred reference axes $\{\underline{A}\}$ to the current molecule-centred axes $\{\underline{a}\}$.

To calculate this quaternion we use Equation (A.10) to get the rotation of the first bond from the reference to the current system. (The first bond can be any bond in the molecule as long as it is consistently defined.) This quaternion is then applied to the whole molecule. When applying the quaternion, using Equation (A.7), we must shift the entire molecule by the position of the first bead beforehand, as quaternion rotation is about the origin. We then need to find the rotation of the third bead about the axis of the first bond. This can similarly be applied to the entire molecule, from particle three upwards as particles one and two will be invariant to the rotation as they are on the axis of rotation.

The two quaternions can be combined via Equation (A.8) to give us the quaternion describing the full rigid rotation of the molecule from the reference configuration to the current configuration.

In order to calculate these values, we have used the first three particles in the molecule. However, we have only accounted for 6 degrees relating to these three particles in each molecule. This means that there are 3 degrees of freedom unaccounted for relating to these three particles, since they should have $3 \times 3 = 9$ degrees of freedom in total.

The quaternion rotation described above is invariant to the bond length between the particles and to the bond angle in the plane described by the bonds between the three particles. Hence, these naturally should be included in our coordinate scheme. There are only two bond lengths and one angle each accounting for one degree of freedom.

The change in bond length is described by

$$\{\Delta|\underline{b}|\} = |\underline{b}_{1,2}| - |\underline{b}^{\mathrm{ref}}_{1,2}|, \tag{7.6}$$

where $\underline{b}_{i,j} = \underline{r}_i - \underline{r}_j$ with i, j being the particle index in the molecule, $i, j = 1, ..., N_{\mathrm{mol}}$. $\underline{b}^{\mathrm{ref}}$ is the bond length in the reference system.

The bond angle, in the plane of the bonds is defined as

$$\Delta\theta = \theta - \theta^{\mathrm{ref}}, \tag{7.7}$$

where

$$\theta = \arccos(\|\underline{b}_1\| \cdot \|\underline{b}_2\|). \tag{7.8}$$

The axis of this rotation is perpendicular to both $\underline{b}_1$ and $\underline{b}_2$.

We now have three degrees of freedom left for each of the other particles in the molecule equal to $3N_{\text{mol}} - 9$. Since there are no constraints on the position of these particles we can just represent their positions as a relative change from their reference positions

$$\Delta\underline{r}_k = \underline{r}_k - \underline{r}_k^{\text{ref}} \tag{7.9}$$

where k is the index of the particle in the molecule with $k = 3, ..., N_{\text{bead}}$. However, in order for this to be independent of the other generalised coordinates, both $\underline{r}_k$ and $\underline{r}_k^{\text{ref}}$ are evaluated in a coordinate system centred on the first bead which rotates with the molecule.

Since the generalised coordinates represent all the Monte Carlo moves that have been applied to the reference configuration to produce the current configuration, our choice of coordinates is based upon which moves we can make in our simulations. These generalised coordinates are also independent of the model being used, provided it has no constraints.

7.3 Cholesterol Model

The model we are using is the coarse-grain representation of cholesterol by Hadley and McCabe [47]. They used radial distribution function (RDF) data from atomistic simulations using the CHARMM potential [15] to optimise the non-bonded force field; see section 2.1.2.

The atomistic to coarse-grain (CG) mapping uses the centre of mass of groups of atoms as the position of a CG bead. The rigid multi-ring structure was retained and represented by 5 beads; the flexible tail is modelled by two beads and the methyls are also included as single beads. These methyls are thought to be important in the stability of the structure and phase transition of the solid phases [47]. Figure 7.1 shows the mapping between atoms and CG beads.

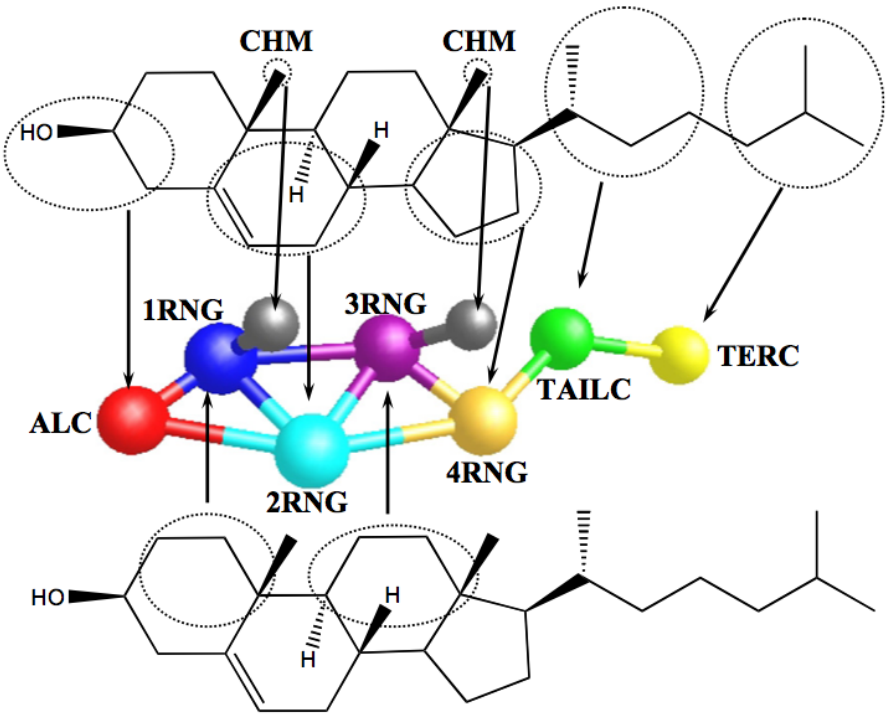

Figure 7.1: Mapping between the CG beads and atomistic cholesterol, reproduced from [47].

Hadley and McCabe estimated the melting temperature of their model is 519K from the change in slope of the self-diffusion constant. The experimental value is 422K but this is explained by the effect of periodic boundary conditions. The model has a cutoff of 12 Angstroms, which is large compared to the unit cell of cholesterol; we exclude 1-4 interactions.

The solid structures of anhydrous cholesterol used are from Shieh et al. [95] and Hsu et al. [52]. These structures were converted into coarse-grain configurations by taking the centre of mass of the atom groups as the CG bead coordinate. These configurations were then relaxed to their equilibrium structures. All simulations are run at atmospheric pressure and at biologically relevant temperatures. The two anhydrous phases are mechanically stable in this model, as investigated by Hadley and McCabe.

If one of these two phases were not stable with respect with the other, we would find that the phase switch simulations would have zero free energy difference since we would be calculating the free energy difference of the same phase with itself.

The van der Waals potentials in the model were tabulated with an inter-grid

spacing of 0.01 Angstroms.

7.3.1 Potentials

It is clearly shown in Figure 7.2 that the 15 potentials in the CG cholesterol model are not smooth functions. Molecular dynamics accurately calculates ensemble averages given that integration is valid. Therefore, if the integration cannot be trusted, the results cannot either for MD. When integrating the equations of motion the energy should not vary greatly over a single timestep. Since the troughs in the potentials are narrow and the diffusion of a particle is also small MD may not easily escape the wells in the potential. Especially because the forces will be very strong from such sharply oscillating functions.

The sharp troughs in many of the potentials will trap the molecular dynamics simulations, whereas for a Monte Carlo simulation we are sampling randomly the potential rather than integrating along it and therefore, since the troughs are only narrow, we will sample them infrequently. This implies that we can simulate via Monte Carlo on this potential without having the same issues as MD with sharp oscillations but there may still be sampling issues due to the potential. However, it was still fitted with the molecular dynamics and will not necessarily represent the desired behaviour. Nevertheless, we will continue to benchmark this model with a view to doing further work on refining or refitting the potential, and ensuring that the polymorphic phase transition can be captured by the model.

7.3.2 Model validation

We ran molecular dynamics simulations in DL_POLY [104, 99] (which was also used by Hadley and McCabe) with the tabulated potential files given to us by the authors to compare with their results.

To test the force field we ran simulations in the NVE ensemble with a timestep of 0.01fs, this timestep is 100 times smaller than the suggested timestep from the paper.

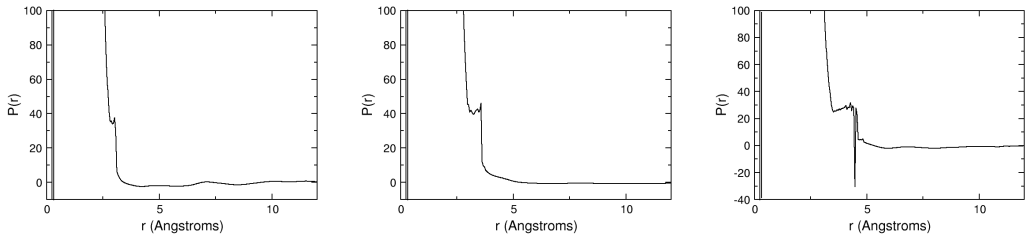

(a) ALC-ALC (b) ALC-RNG (c) ALC-TAILC

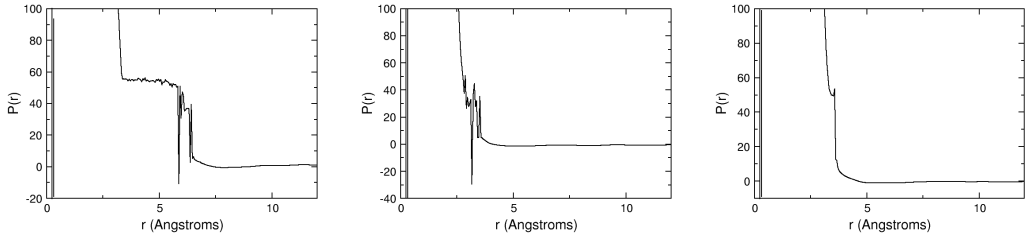

(d) ALC-TERC (e) ALC-CHM (f) RNG-RNG

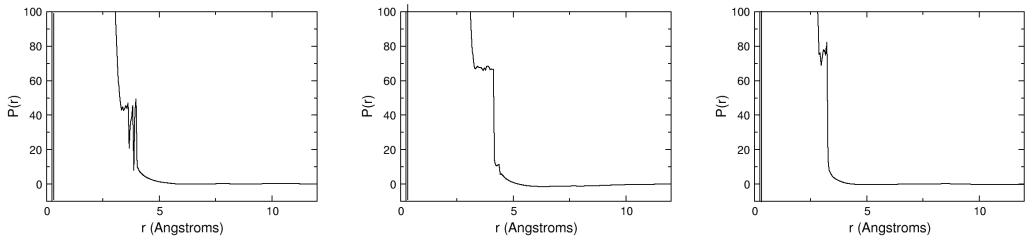

(g) RNG-TERC (h) RNG-TERC (i) RNG-CHM

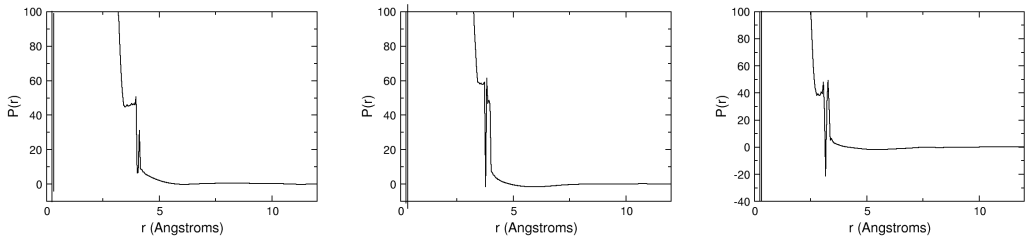

(j) TAILC-TAILC (k) TAILC-TERC (l) TAILC-CHM

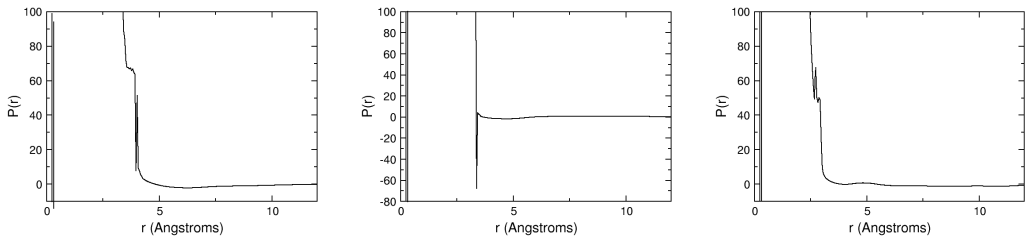

(m) TERC-TERC (n) TERC-CHM (o) CHM-CHM

Figure 7.2: Tabulated non-bonded potentials from Hadley and McCabe [47] for all interactions between coarse-grain beads with a homogenous ring bead RNG=1RNG,2RNG,3RGN,4RNG.

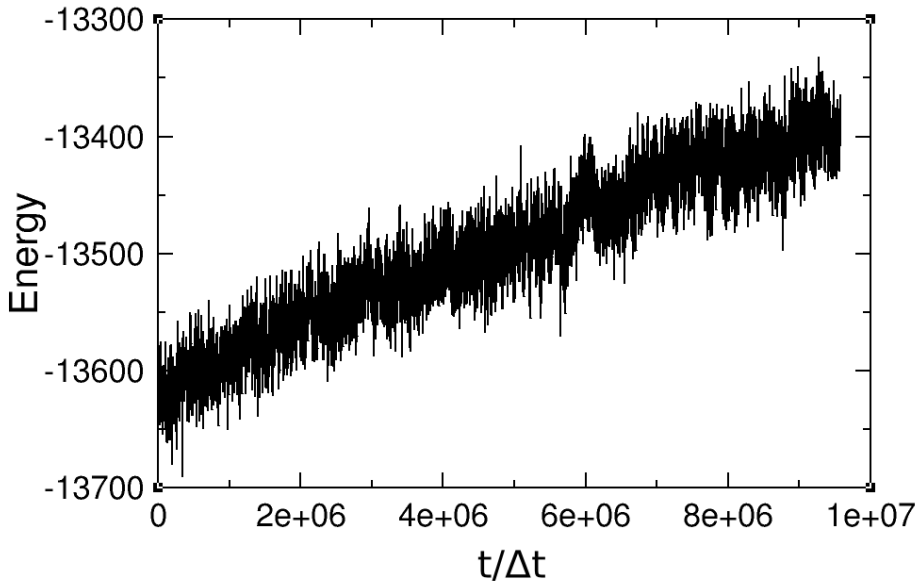

Figure 7.3: The total energy that should be conserved in a NVE MD simulation for a timestep of $\Delta t = 0.1fs$ for the coarse-grain cholesterol model of Hadley and McCabe [47]

The total energy is shown as a function of time in Figure 7.3. It is clear that the energy is not conserved in this simulation. This means that the MD trajectory is incorrect. Hadley and McCabe do not plot the conservation of the energy in their paper, therefore we must conclude that MD simulations with this force field cannot be used and we cannot validate our MC implementation against them effectively.

Even though the MD simulations do not conserve energy, we can still use the force field for MC because no forces are used in MC. Due to the extremely rough nature of the van der Waal potentials shown in section 7.3.1 the forces are very sharp, which has a strong effect on MD simulations but not on MC.

Therefore in order to check the force field implementation within our MC simulations we must use other comparisons.

7.4 Computational details

We will discuss the computational details of our implementation of phase switch Monte Carlo. The code Phlex was written in Fortran95 and MPI, completely from scratch by the author. It implements the phase-switch Monte Carlo method for soft, crystalline, flexible molecular polymorphs. A multi-canonical biasing scheme is used and can be run in serial or parallel across multiple walkers. It implements a

checkpointing of current data into binary files for each processor to enable restarting of the simulation. Tabulated potentials are read in from a file for van der Waals energy calculation. Input data are read in from a file so that simulations can be run under different conditions without needing to recompile the code.

7.4.1 Units

The units chosen for the Phlex code are the ones used internally in DL_POLY. This is so that we can easily compare between the two and so that our values will be of reasonable orders of magnitude. The internal molecular units are:

- unit of length, l_o is 1×10^{-10} metres
- unit of energy, E_o is $1.6605402 \times 10^{-23}$ Joules (10Jmol^{-1})
- unit of pressure, $P_o = E_o l_o^{-3}$ is 1.6605402×10^7 Pascals
- Boltzmann constant k_B is 0.831451115
- unit of temperature, T_o is 1 Kelvin

The force field is given in energy units of kcal/mol and we can easily transform to our internal units using $1\text{kcal/mol} = 418.4E_o$. Care needs to be taken to transform the non-bonded and bonded potentials.

7.4.2 Periodic boundary conditions

Since the model has a large cutoff for the non-bonded potential, we must ensure that all periodic images are taken into account in the energy calculations. The fastest and simplest method to calculate the energy between two atoms is to use the minimum image convention. The closest image is found and used to get the energy; this will not be sufficient if more than one image is within the potential cutoff. Therefore, we calculate how many images of our system are needed at the beginning of the simulation and we then store all the image vectors for the cell vectors. This speeds up the calculation because we just need to retrieve these vectors and loop through them while summing the energy contributions. We need to recalculate these vectors after every volume move but this will not significantly impact the computation time.

7.4.3 Energy calculations

Non-bonded energy

The van der Waals potentials are read in from a tabulated potential file; the grid spacing and number of entries can be varied.

When calculating the energy contributions we must not double count pairs of atoms i, j and j, i. For whole system energy calculations we only calculate the energies of the upper diagonal elements of our $N \times N$ matrix of particle interactions; this is an $IN^2/2$ order calculation, where I is the number of images we need to loop over.

In order to speed up our calculation of the change in energy due to a MC move, we do not need to recalculate the energy of the whole system. For all moves except volume, we only modify one molecule so only the energy associated with those interactions will change. Therefore, we can loop over all particles in all images with each of the atoms in the molecule that moved, making sure we include the interactions with its own image. When we are in the original box we need to take into account the exclusions of the bonded particles. Since we are only calculating the change on a single molecule we will not double count the energy. We are now only doing a calculation of order INN_{bead}, where N_{bead} is the number of particles in a molecule.

For single particle moves, we can calculate even less and only look at the single particle that was moved with respect to all other particles in every image, so our calculation is now of order IN.

In order to recreate the model created as used in DL_POLY by Hadley and McCabe, we ensured that our energy calculations from the tabular potential were equivalent. This involved recreating the three-point interpolation utilised in DL_POLY. Since a tabulated potential is discrete, an interpolation is used to give a better estimate of energies.

Bonded energy

The bonding topology of the molecules is hard-wired into the code and since the topology will never change this can been used to optimise the code.

To easily calculate the bonded energy, we organise the data into arrays of structs holding all the information for each type of bond. Since the bonding information is the same for all molecules we need to only store that information once and then use it to calculate the energies associated with each particular molecule.

We also store all of the bonds, angles and torsions that each particle is part

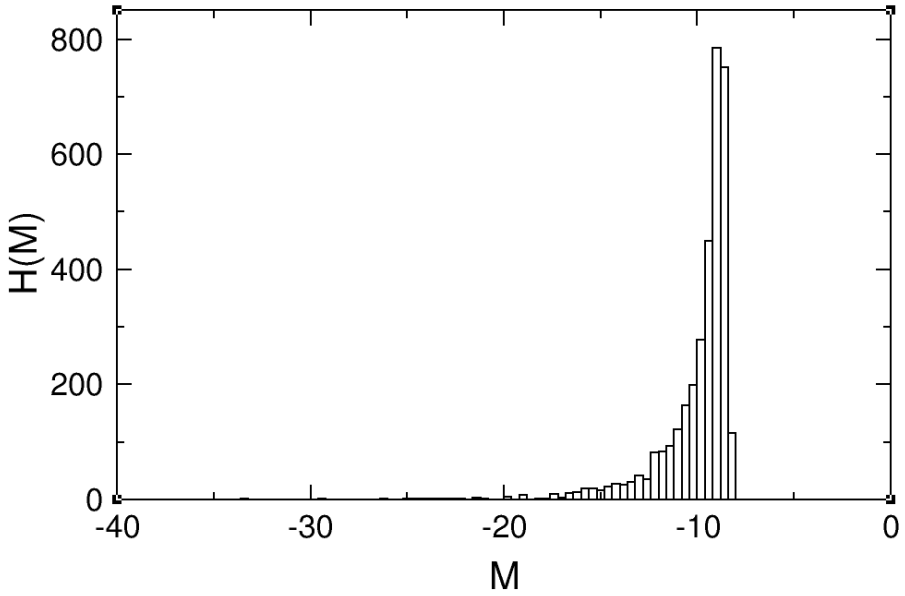

Figure 7.4: The quasi-stationary distribution function of the order parameter without inter-phase switches of biasing at $T = 294$K for 16 molecules.

of so that we can loop over only the bonds that have changed for single particle moves.

7.4.4 Biasing function

Uniform width bins were used for the biasing function. This is because the form of the function is not known before we run the simulations, therefore, the non-uniform scheme used for butane (section 4.3.1) will not necessarily be useful.

We ran simulations without any biasing function or inter-phase switches to find the form of the probability distribution, and calculate the desired width of the order parameter space, Figure 7.4.

It can be seen that the distribution function has a very long tail and so the width of our order parameter space needs to be large; this is validation of our choice of order parameter. If our simulations cut off the distribution function too early we can fit an exponential function to estimate the area under the rest of the curve.

7.4.5 Speed comparison

Since our cutoff is very large, linked cells will not be a very efficient algorithm until very large numbers of molecules are simulated; our system size would have to be greater than four times the linked cell cutoff, which must be greater than

our potential cutoff. This means the cell lengths would have to be greater than 48 Angstroms Since the length of the unit cell is around 10 Angstroms we would need about 64 unit cells and over 1,000 molecules. Verlet lists might be useful since the neighbours should not change greatly when we simulate crystals.

7.5 Histogram reweighting

The aim of our work is to look for solid-solid phase transition in the coarse-grain cholesterol model; currently there are none known. We have a method that will give us a free energy difference between the two phases for a certain pressure and temperature. Therefore we can just run lots of simulations at a range of pressures and temperatures and calculate bounds within which the transition lies. We then can run another range of simulations within this new interval and so on and so forth until we reach our desired accuracy. This application of the phase switch method is very wasteful of computing resources and produces lots of un-needed data and will be quite slow as a lot of levels of full simulations will need to be run before a reasonable result is acquired.

Another way to find the transition pressure and temperature is to run a single simulation (or a few spread across an interval). From the data accumulated we use histogram reweighting to estimate the state point that would correspond to a probability distribution with equal weighting on each side; this represents a zero free energy difference. We then run a new simulation at this calculated pressure and temperature, initialising it with the estimate of the biasing function we have from histogram reweighting. Depending on how accurately we want the result we can reweight again and run a new simulation, further refining our result. This has the advantage of efficiently using computing resources.

Histogram reweighting utilises the idea that histograms of observables obtained at one state point can analysed to provide an estimate of the histogram at other state points.

For a standard ensemble average

$$\langle A \rangle_T = \frac{\int A e^{[-\beta_T E]}}{\int e^{[-\beta_T E]}}, \tag{7.10}$$

given that $\beta_T = \beta_o + \Delta\beta$ we can rearrange to remove β_T.

$$\langle A \rangle_T = \frac{\int A e^{[-(\beta_o + \Delta\beta)E]}}{\int e^{[-(\beta_o + \Delta\beta)E]}} \tag{7.11}$$

$$= \frac{\int A e^{[-\Delta\beta E]} e^{[-\beta_o E]}}{\int e^{[-\Delta\beta E]} e^{[-\beta_o E]}} \tag{7.12}$$

$$= \frac{\langle A e^{-\Delta\beta E} \rangle_o}{\langle e^{-\Delta\beta E} \rangle_o}. \tag{7.13}$$

This shows that the ensemble average of A at temperature T can be written in terms of ensemble averages at temperature o. For histogram reweighting we use the same theory on the probability distribution to get

$$p(E|N, V, \beta_1) = \frac{Z_1}{Z_0} e^{-(\beta_1 \mathcal{H} - \beta_0 \mathcal{H})} p(E|N, V\beta_0), \tag{7.14}$$

The resulting histogram is only an estimate for the new state point due to the finite length of a simulation and hence not all states will be visited; it will be poorly sampled if the relevant states have low probability at the original state point. Therefore, in practice, one should only extrapolate close by to the original values. This is because the reweighting technique modifies the relative statistical weights of the configurations. Configurations that have a very low statistical weight in the original data may contribute significantly at the reweighted state point. Due to their low Boltzmann weight in the original system, the sampling of these configurations will be disproportionately low and magnify the error in these samples. This leads to a reweighted histogram that is not smooth, with many 'jagged' regions at the edges. In order for the reweighted histogram to be at all relevant, one must ensure that the probability distributions will overlap significantly.

7.5.1 Implementation of histogram reweighting

A very detailed description of the implementation of histogram reweighting was described by Wilding [115]. We followed their methodology and will describe the relevant details and the application to a constant NPT ensemble.

We run a simulation with a fixed weighting function with the modified acceptance criterion (equation 4.20). The probability distributions we seek to obtain are the order parameter, energy and the volume of the active system. We could bin these into an array and build up statistics during a simulation but our choice of bin-width might not be satisfactory and we would have to repeat the entire simulation. Therefore, it is suggested that the data analysis be separate to the simulation by

recording the raw data and post-processing it in a specific analysis program. This gives us the most flexibility but it is necessary to output a lot of data from the simulation to use in the post-processing.

The data is written out to a file at regularly spaced intervals during the simulation; obviously, the smaller this interval is, the more data we accumulate. However, we do not need the interval to be smaller than the correlation length of the data since we need to take into account the statistical error.

The post-processing program will read in this data, unfold the bias, print out the current probability distribution function and then reweight to the desired pressure and temperature.

In order to remove the bias we assign each entry, j, in the data list a weight

$$w_j = \exp[-(\beta_1 - \beta_0)\{E_j + (P_1 - P_0)V_j\} + \eta(\mathcal{M})], \tag{7.15}$$

where β_1 and P_1 are the parameters we wish to extrapolate to.

The set of weights $w_1, , , w_j, , , w_M$ then construct the reweighted histogram for an observable O

$$H(O|N, \beta_1, P_1) = \sum_{j=1}^{M} w_j \delta(O - O_j). \tag{7.16}$$

When normalised, this histogram gives a discrete estimate of the probability distribution function at $\beta_1,\ P_1$. This probability distribution can be transformed into the biasing function

$$\eta(\mathcal{M}) = \ln(H). \tag{7.17}$$

We can then run a simulation with this new biasing function at the reweighted parameters to ensure full sampling of all important states and for added accuracy or if further extrapolation is needed.

We are concurrently simulating two phases, but the Markov chain is only ever following one phase at a time, the active phase. Therefore it is the active data that can be reweighted.

So to use histogram reweighting, we simply print out the data we need at a frequent interval; in this case the volume and energy of the active phase and the order parameter value. We then write a post-processing analysis program that reads this data in line by line, to save on memory. For each line of data we calculate the weight it would have at the new parameters and remove the biasing. If we are dealing with very large numbers we can shift this by a constant value so that exponential doesn't overrun. We then calculate which bin in our histogram this weight should

be added to by looking at the order parameter value we read in. We loop over all data samples and build up the unbiased histogram at the new parameters.

When using histogram reweighting with our implementation of phase switch Monte Carlo we have two systems rather than just one. Care needs to be taken to only use data from the active system in the reweighting. Therefore when data is printed out it should only be for the active system regardless of which phase it derives from.

When used with phase switch Monte Carlo we are often interested in calculating the phase transition parameters. We get a bimodal probability distribution function and if the areas of the two sides of this function are equal then we have found the point of transition. Therefore, when reweighting to find a transition our program should direct a search in parameter space to give us an equal-weighted probability distribution function (pdf). This can be enacted using an iterative approach, homing in on zero area difference between the two peaks.

In this iterative approach we start by calculating the pdf for the current parameter, P_o and T_o and from there we get the initial difference in areas of the two sides of the pdf $\Delta A = A_\alpha - A_\gamma$. Next we increase the parameters by Δ, a value chosen so that is falls well within the extrapolation range of the reweighting but not so small as to make a negligible difference. We then reweight to these new parameters $P = P_0 + \Delta P$, $T = T_o + \Delta T$, and calculate the new difference in areas. If ΔA is closer to zero then we increment the reweighting parameters again by Δ, if it is further away we change the sign of Δ and double its value. If ΔA changes sign then we change the sign of Δ and halve its value. The idea is to keep changing sign and reducing Δ until we converge on $\Delta A = 0$ to within a certain given tolerance. This will give us a good estimate of the transition parameters. We can then run another full simulation at the new parameters, after checking that the new weighting function is reasonable. If it has extrapolated too far we must run a simulation at intermediate parameters towards the transition and repeat the process.

7.6 Validation

In order to validate our Monte Carlo implementation of the model we need to compare our energies with the energies computed in the molecular dynamics code. Table 7.1 shows the bonded and non-bonded energies from our Monte Carlo calculations in Phlex and those calculated using DL_POLY [99] (the MD package for which the model was written).

Code	E_{bond}	E_{angle}	$E_{torsion}$	E_{VdW}
DL_POLY	233.0446	387.2063	379.6345	−15364.75
Phlex	233.044589	387.206326	379.634461	−15364.747581

Table 7.1: Bonded and non-bonded energies (kcal/mol) for a single configuration of cholesterol.

It can be seen that the calculated energy values are identical to within the precision. We compared the energies for a range of different configurations and number of particles, and the differences were all of the same order as in Table 7.1.

Now that we are confident in the calculation of the energies in our code, we tested the sampling by running equilibrated samples to check that the energies converged. We ran in the NPT ensemble at atmospheric pressure with a temperature of 274K.

The energy of the system is plotted as a function of MC cycle in Figure 7.5. It can be see that the energy is equilibrated and there is no drift.

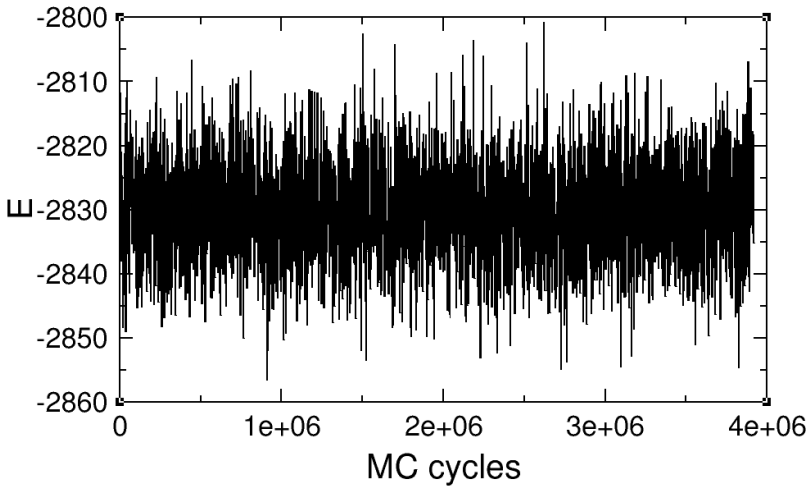

Figure 7.5: Energy in kcal/mol for the low temperature phase of CG cholesterol with 16 molecules and at 274K.

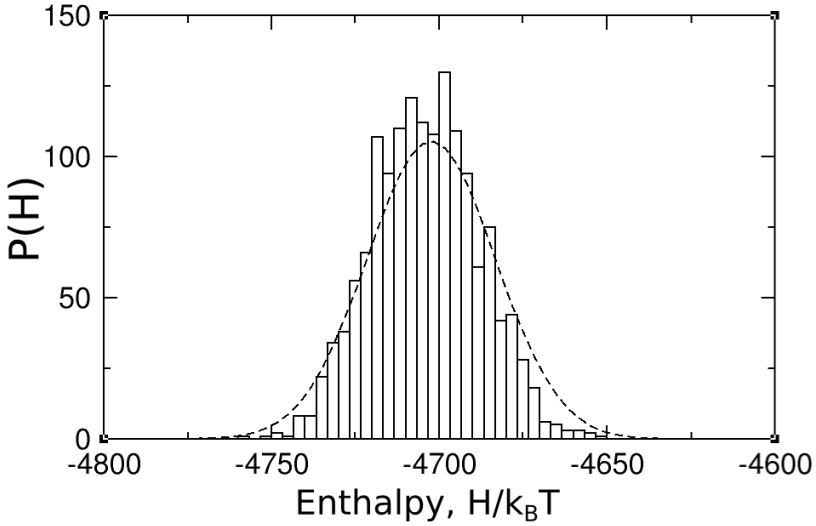

Figure 7.6: Distribution of enthalpy, dashed line is gaussian fitted to distribution for low temperature phase of CG cholesterol with 16 molecule and at 274K.

We checked that the distribution of the enthalpy at a constant temperature was gaussian, Figure 7.6. We binned the distribution using a bin size of 8 and then fitted a gaussian to this data. The fit was very close and we are confident in the result.

Next we tested the self-consistency of our work by calculating the heat capacity at constant pressure, C_P by two different methods in units of $JK^{-1}\text{mol}^{-1}$. We used the results in section 2.3.2. For the low temperature phase we calculated the gradient of the enthalpy in units of $k_\text{B}T$ at constant pressure, using equation 2.38 we calculated $C_P = 1.527JK^{-1}\text{mol}^{-1}$. We then calculated the mean squared fluctuations in the enthalpy for the low temperature phase at $T = 294\text{K}$ using equation 2.37 we found the heat capacity at constant pressure to be $C_P = 1.52JK^{-1}\text{mol}^{-1}$. This is very good agreement and shows that our sampling is self-consistent and we can reliably trust this work.

7.7 Phase switch simulation details

All simulations were carried out at a constant pressure of 1 atmosphere with anisotropic volume moves. 16 molecules were used, which is the size of the high temperature unit cell; the low temperature unit cell was doubled along the x-axis. Initially we ran at a range of temperatures between 0°C and 100°C, as these are biologically relevant. We investigated higher temperatures to check for a possible transition.

The order parameter used will be $\mathcal{M} = m_{\text{lowT}} - m_{\text{highT}}$, where

$$m_\alpha = E_\alpha - E_\alpha^{ref} + V_\alpha - V_\alpha^{ref}, \tag{7.18}$$

is the order parameter for a phase α. When the low temperature phase is active, it will have low energy and so m_{highT} will be dominant and so the order parameter will have a negative value. This means that negative order parameter values favour the low temperature phase and positive values favour the high temperature phase. Hence if the low temperature phase is more stable, $G_{\text{lowT}} < G_{\text{highT}}$ and we are calculating

$$\Delta G_{\text{l,h}} = G_{\text{lowT}} - G_{\text{highT}}. \tag{7.19}$$

All simulations were run in parallel on three or four 12-core processors, with communication every 100 MC cycles. Our biasing factor was initialised to $f = 1.0005$ and reduced at least 5 times during the creation of the biasing function. The order parameter (Equation 7.4) was confined depending upon the temperature with the maximum width being $\mathcal{M} = \pm 35.0$ to ensure the long tail was covered; the range was split up into 600 equal width bins.

7.8 Results

Figure 7.7 shows the variation in enthalpy of the two phases of CG cholesterol with temperature between 0°C and 100°C. This is the Gibbs free energy excluding the entropy term.

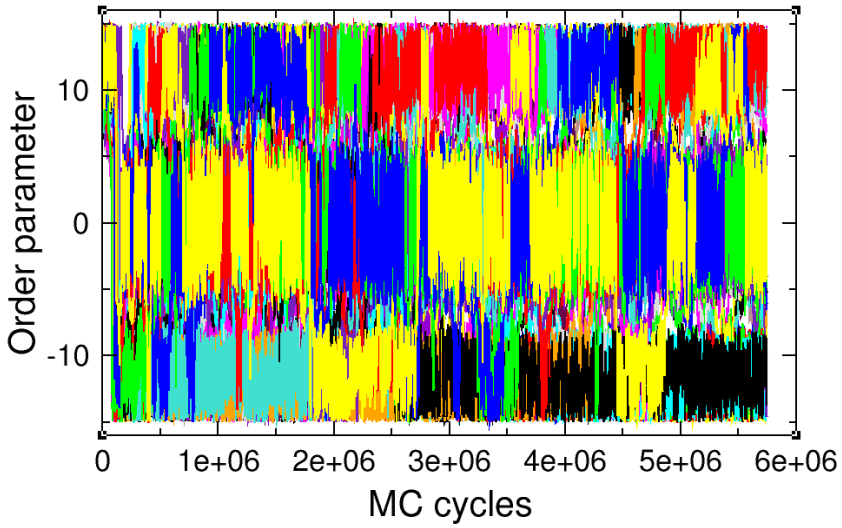

Figure 7.8: 36 walkers fully cover the order parameter space during a simulation at $T = 384$K, colours depict the path of different walkers.

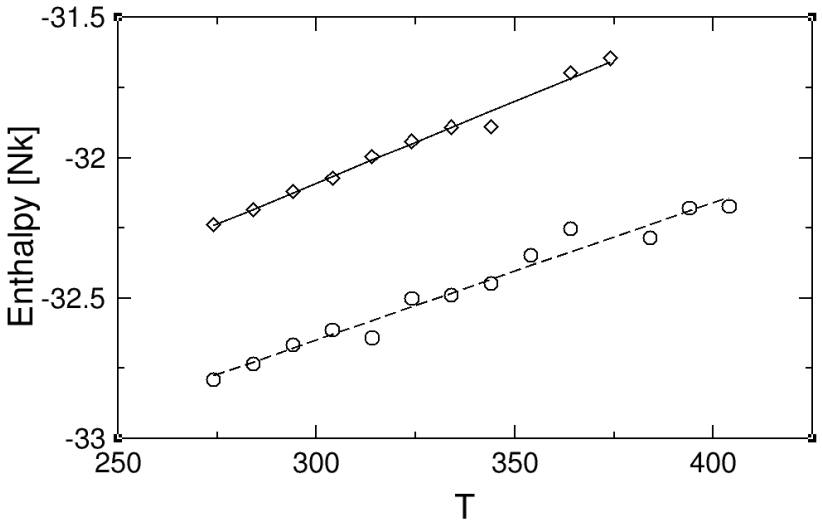

Figure 7.7: $H = E + PV$ per bead for the low temperature phase (dashed line is regression fit to circles) and the high temperature phase (solid line and diamonds) of CG cholesterol 16 molecule crystals. The statistical error in the results is smaller than the symbol size.

From figure 7.7 we can see that the enthalpies per bead, in the two crystals are very similar. The low temperature phase is lower in enthalpy for all biologically relevant temperatures. Therefore, entropy must had a strong effect for a phase transition to occur in the model. This confirms our need for a highly accurate free energy method.

To test our simulations, we checked that we were covering all of the order parameter space, as shown in Figure 7.8. As can be seen, all of the walkers cover the entire order parameter space; there is rougher coverage around $\mathcal{M} = \pm 6$, but this is where the biasing function varies the most. In the hard sphere butane system, we used non-uniform width bins to alleviate the issue of steep biasing function. It would be much more complicated for this system because the steep areas are not centred around zero and have a more complex geometry. Therefore we have just used uniform width bins for the biasing function and made sure that there is enough coverage of the steep areas without increasing the number of bins by too much.

We also checked that the simulations are switching between phases consistently through out the simulations, as shown in Figure 7.9.

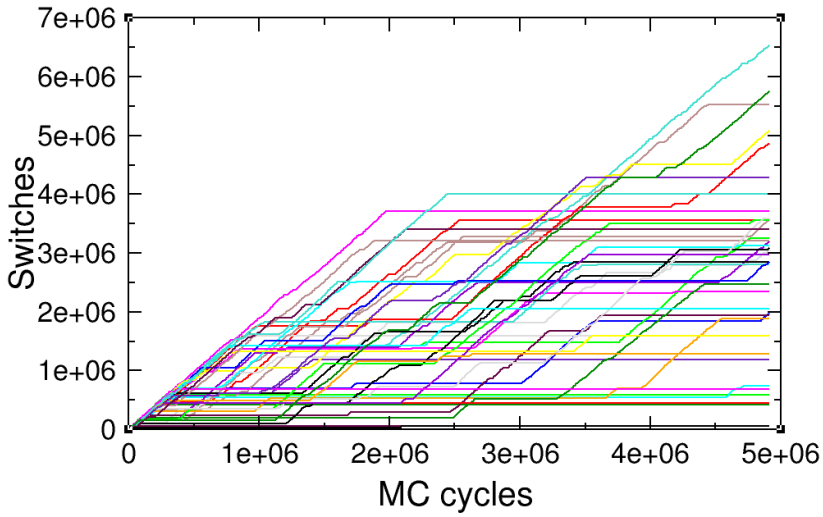

Figure 7.9: The number of switches between phases at $T = 384$K for 48 walkers.

The number of switches does not increase at a constant rate for all processors, however, there are a large number of switches for a significant number of walkers. We calculated the total number of switches for all the processors (Figure 7.10) and it is clear that the number of switches always increases at a reasonably constant rate. Since we are only interested in the combined biasing function of all the processors it should not matter if the switch rates of all the processors are not the same.

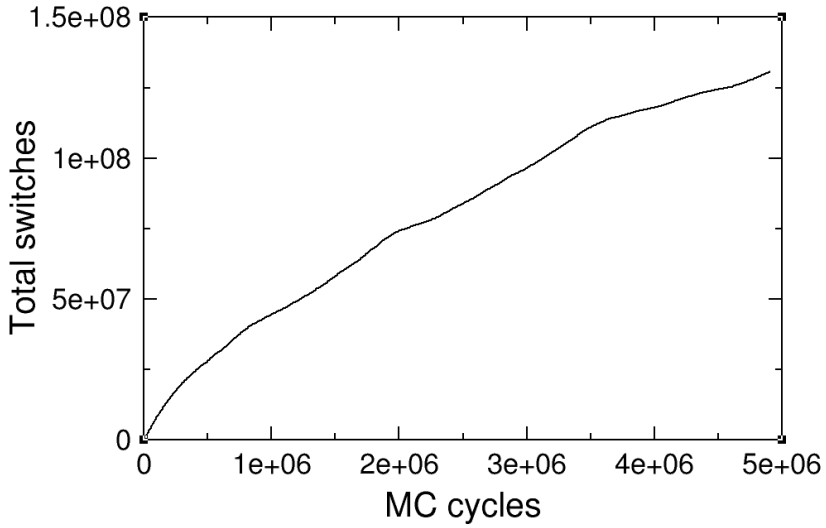

Figure 7.10: The total number of switches between phases at $T = 384$K for 48 walkers.

We ran phase switch calculations at a range of temperatures spanning the biologically relevant range.

The converged biasing function at $T = 274$K is shown in Figure 7.11. The increment factor was reduced seven times to a value of $\ln(f) = 3.8 \times 10^{-7}$. The left side of the function is strongly favoured which means that the low temperature phase is more stable.

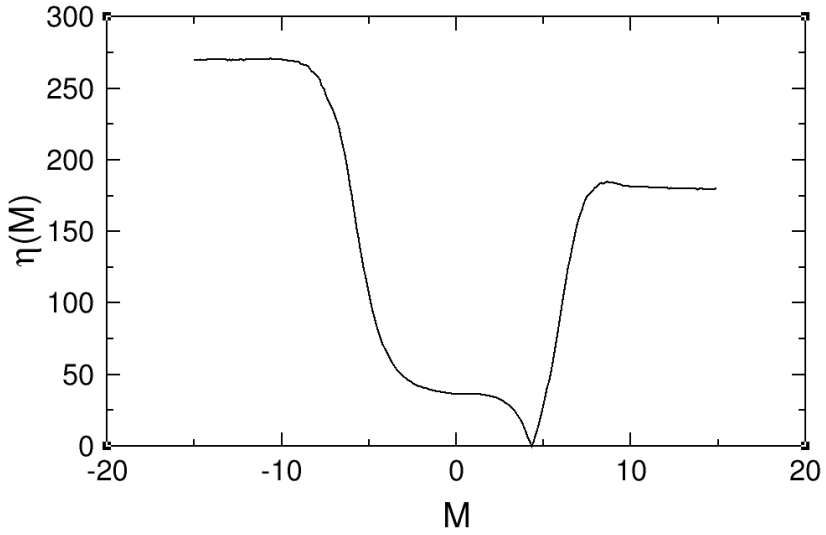

Figure 7.11: Converged bias function at 274K using 36-walkers.

We next ran a simulation at $T = 384$K, just outside the biologically relevant

range. We extended our order parameter range to $M = \pm 30$ so the probability distribution goes fully to zero. The biasing function for $T = 384$K, shown in Figure 7.12, has been converged nine times to a value of $\ln(f) = 9.6 \times 10^{-}7$. At this temperature the low temperature phase is still favoured. This shows that there is no transition between these two temperatures as the probability distribution has not changed sign.

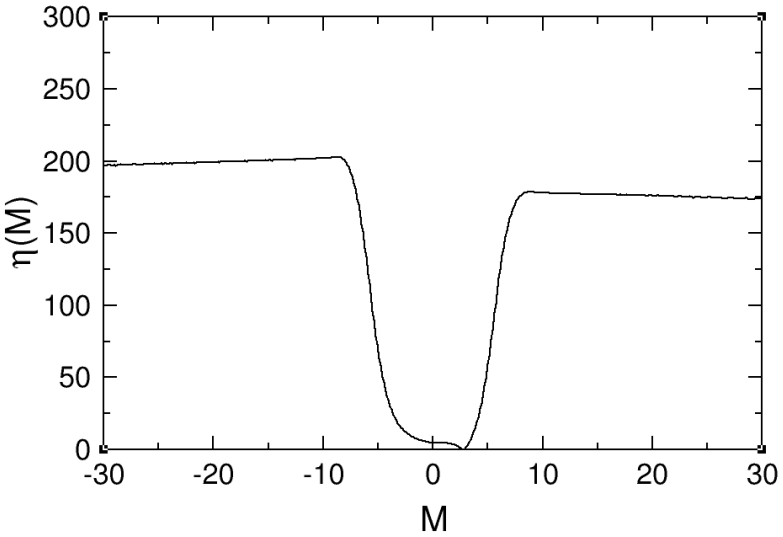

Figure 7.12: Converged bias function at 384K using 48 walkers.

The height difference between the two sides of the bias function has reduced significantly from 274K, which suggests that a transition might occur at higher temperatures.

We ran with this fixed bias function to calculate the Gibbs free energy difference between the two phases at $T = 384$K. Figure 7.13 shows the convergence of the free energy difference as a function of MC cycles. The converged value was calculated to be $\Delta G_{l,h}/Nk_{\mathrm{B}}T = -0.1657 \pm 0.0003$.

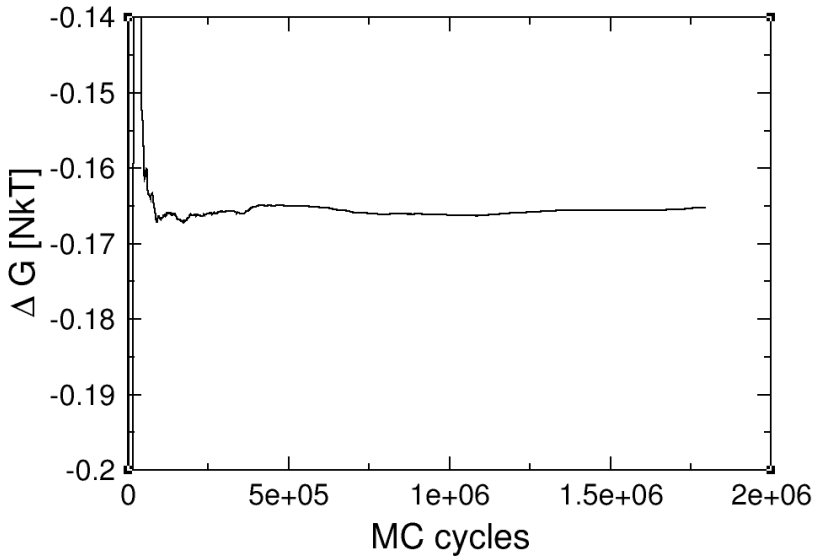

Figure 7.13: Convergence of $\Delta G_{l,h}/Nk_{\mathrm{B}}T$ at 384K using 48 walkers.

The unbiased probability distribution at $T = 384$K, is shown in Figure 7.14 has a one-sided peak favouring negative order parameter values. There is a small peak for positive values, however it is significantly smaller and hence cannot be seen on the same scale.

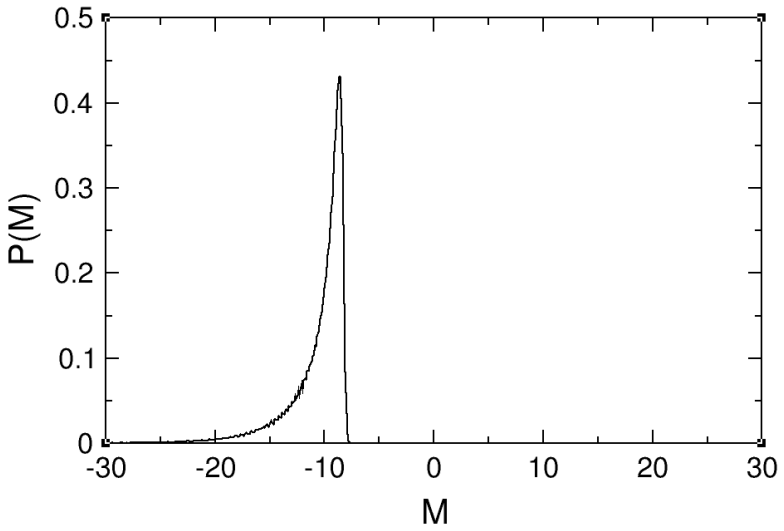

Figure 7.14: Unbiased probability distribution from fixed bias simulation at 384K using 48 walkers.

This shows that there is not a phase transition in this model at biologically relevant temperatures.

We simulated at a slightly higher temperature of $T = 404$K, for which the

bias function is shown in Figure 7.15. The increment factor was reduced to $\ln(f) = 3 \times 10^{-6}$, we then ran with this fixed bias function, and calculated the Gibbs free energy difference 7.16, using Equation (4.13).

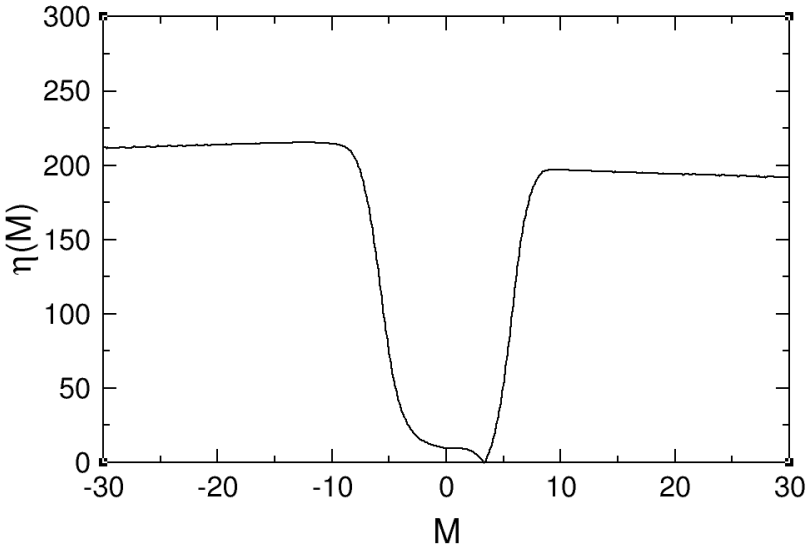

Figure 7.15: Biasing function at $T = 404$K using 48 walkers.

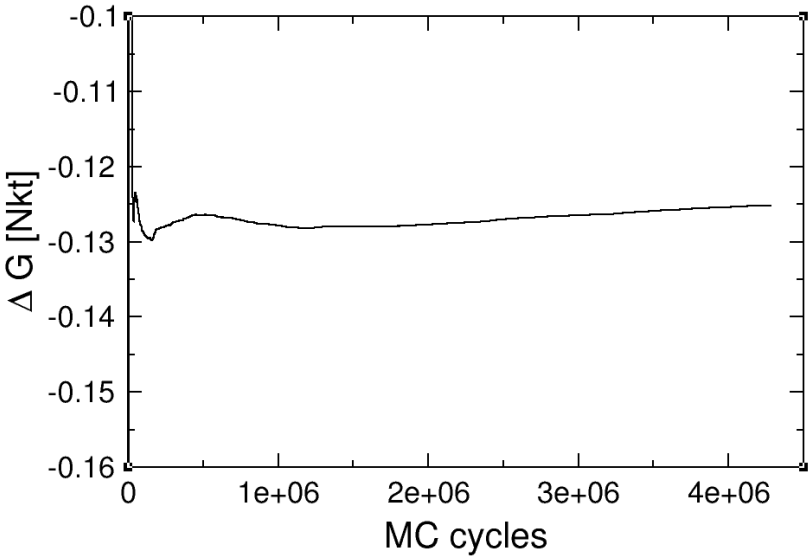

Figure 7.16: Convergence of $\Delta G_{l,h}/Nk_{\mathrm{B}}T$ at 404K using 48 walkers.

The unbiased probability distribution for $T = 404$K still is dominated by a peak for negative order parameter values, as shown in Figure 7.17. The final value for the Gibbs free energy difference is $\Delta G_{l,h}/Nk_{\mathrm{B}}T = -0.1260 \pm 0.001$.

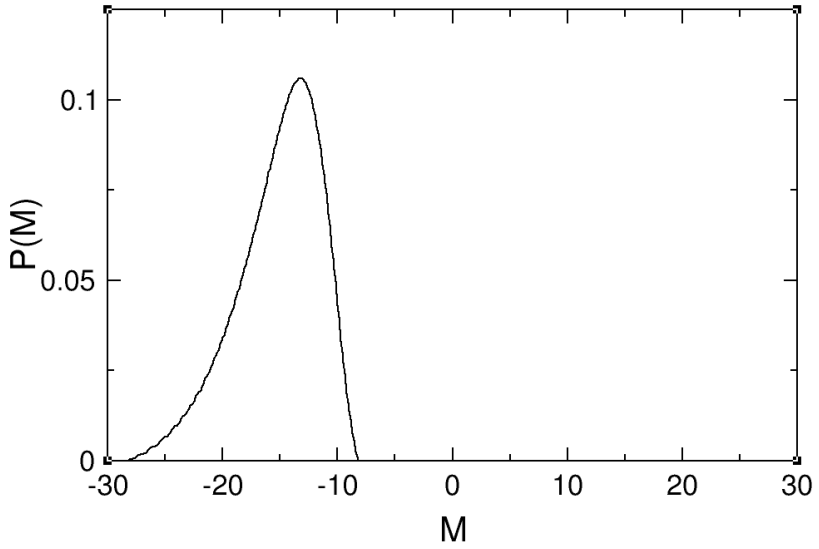

Figure 7.17: Unbiased probability distribution from fixed bias simulation at 404K using 48 walkers.

We used data from both $T = 384$K and $T = 404$K to check our implementation of histogram reweighting.

Using the data at $T = 384$K we calculated a Gibbs free energy difference of $\Delta G_{l,h}/Nk_{\mathrm{B}}T = -0.1251$ at $T = 404$K which is within the error range of our phase switch MC calculation. Conversely, using the data calculated at $T = 404$K and reweighting to $T = 384$K gives us a Gibbs free energy difference of $\Delta G_{l,h} = -0.1655$ which again is within our calculated error of the phase switch MC calculations. This shows that we can accurately calculate Gibbs free energy differences over an interval of at least ± 20K.

Histogram reweighting was used to calculated the free energy difference for a range of temperatures and a phase transition in temperature was discovered, as shown in Figure 7.18. There seems to be some disparity between the histogram reweighting results and phase switch MC calculations. Our two estimates of the transition temperature are $T = 478$K and $T = 490$K. The histogram reweighting data seem viable up to around $T = 420$K, after which it starts to diverge. This will be due to the temperature we are trying to reweight to being too far from where the data was calculated, as discussed in section 7.5.

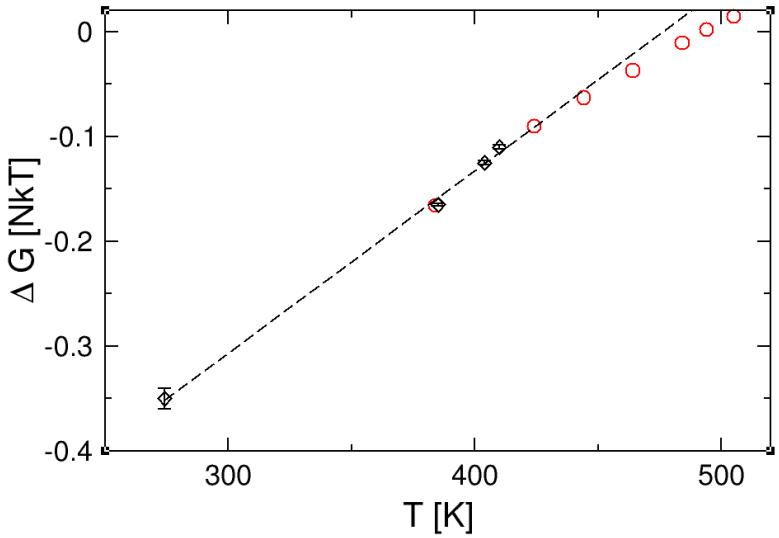

Figure 7.18: Gibbs free energy as it varies with temperature. Black diamond points with error bars denote phase switch MC results dashed black line is the linear fit to data, red circles are calculated using histogram reweighting from $T = 404$K data.

We need to investigate this further with another simulation at a closer temperature. A temperature of $T = 478$K was decided upon as it is the apparent transition temperature from the fit to the phase switch MC data. We converged the biasing function until the increment factor reached $\ln(f) = 7.8 \times 10^{-7}$, Figure 7.19.

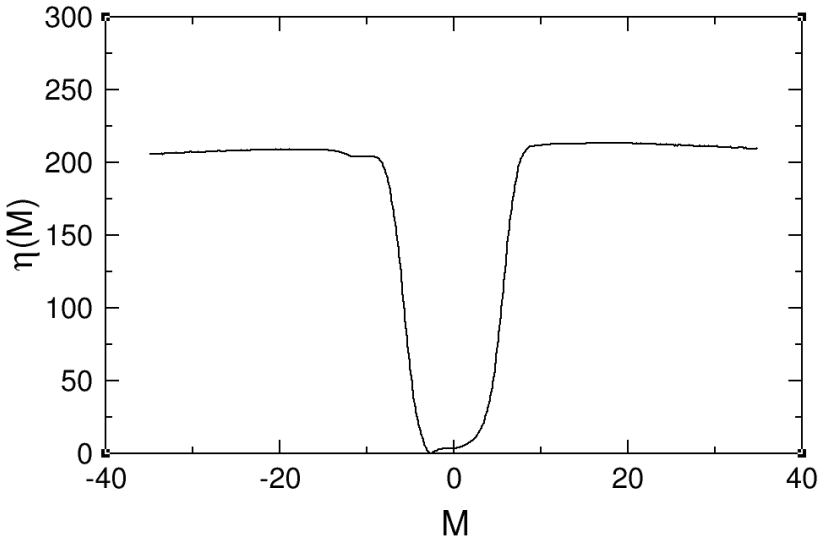

Figure 7.19: Biasing function for $T = 478$K using 48 walkers.

Figure 7.20 shows the normalised probability distribution at $T = 478$K. It can be seen that the distribution is double peaked and hence very close to the phase

transition temperature.

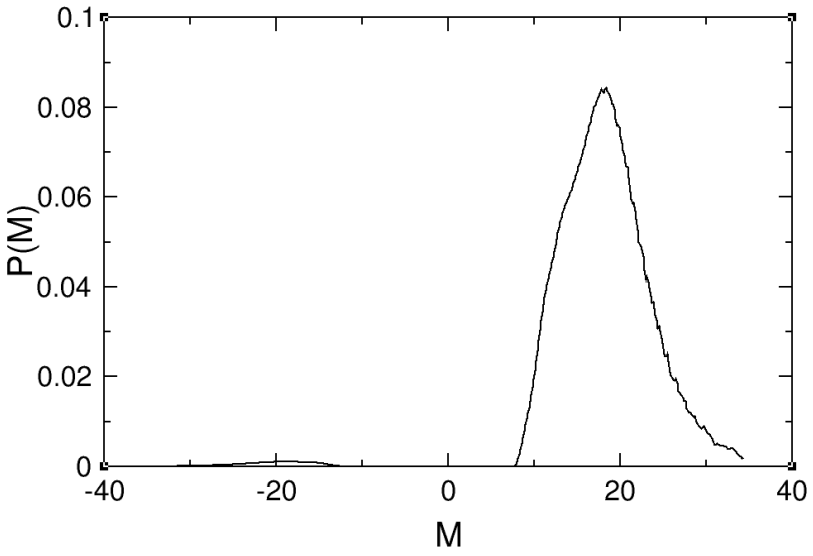

Figure 7.20: Probability distribution function for $T = 478$K averaged over 10 bins.

The convergence of the Gibbs free energy difference with MC cycle is shown in Figure 7.21.

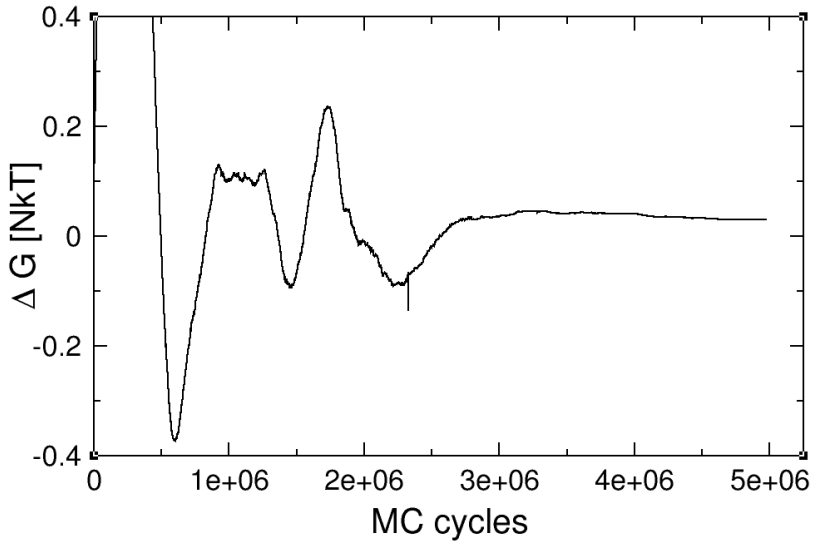

Figure 7.21: Convergence of $\Delta G_{l,h}/Nk_{\mathrm{B}}T$ at $T = 478$K run with fixed biasing function

At a temperature of $T = 478$K we calculated the Gibbs free energy difference to be $\Delta G_{l,h}/Nk_{\mathrm{B}}T = 0.037 \pm 0.005$. A very small second peak at negative order parameter values can be seen in the probability distribution.

Table 7.2 shows all of our Gibbs free energy differences calculated using phase switch MC for the coarse-grain model of cholesterol.

Temperature	$\Delta G_{l,h}/Nk_{\mathrm{B}}T$
274	-0.35 ± 0.01
384	-0.1657 ± 0.0003
404	-0.1260 ± 0.001
410	-0.110 ± 0.002
478	0.037 ± 0.005

Table 7.2: The Gibbs free energy difference between cholesterol polymorphs at different temperatures from phase switch MC simulations.

To closer locate the phase transition in temperature we ran histogram reweighting using the data from the simulation at $T = 478$K to converge on the temperature for which the Gibbs free energy difference is zero. We calculated the transition temperature to be $T = 470 \pm 1$K The probability distribution functions for temperatures of 470K and 470.5K are shown in Figure 7.22. The calculated Gibbs free energy difference at $T = 470$K is $\Delta G_{l,h}/Nk_{\mathrm{B}}T = -1.3 \times 10^{-3}$ and at $T = 470.5$K it is $\Delta G_{l,h}/Nk_{\mathrm{B}}T = 5.8 \times 10^{-4}$.

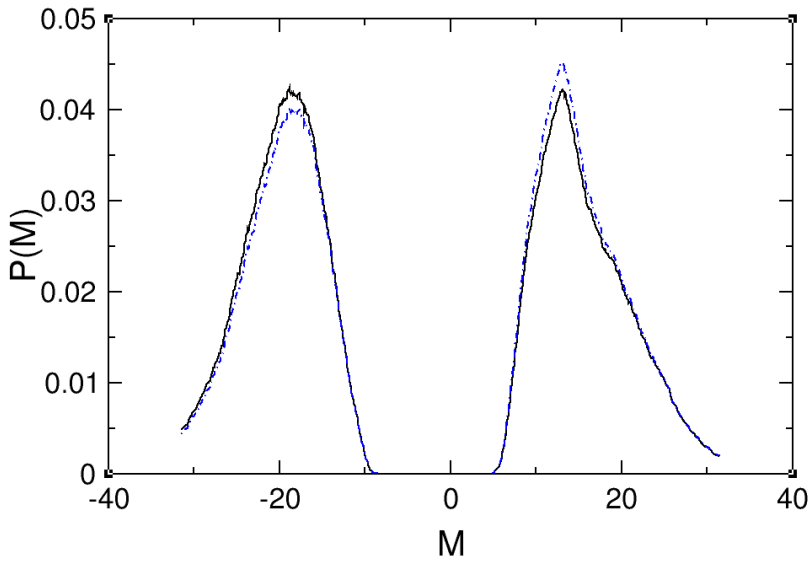

Figure 7.22: Probability distribution function for $T = 470$K (black solid line) and $T = 470.5$K, (blue dashed line), for order parameter range $\mathcal{M} = \pm 35$ reweighted from $T = 478$K.

In Figure 7.22 the probability distribution functions do not go fully to zero

because of the averaging used to smooth out the graph. The full distribution function goes to zero on both sizes. Even if we miss some of the tail of the distribution, the change in free energy difference would be minimal and the change in transition temperature would be smaller that our error.

We also calculated the trend with pressure at $T = 470$K Figure 7.23. It shows that higher pressures favour more negative free energy differences (highT phase). This also has a smaller effect than changes in temperature.

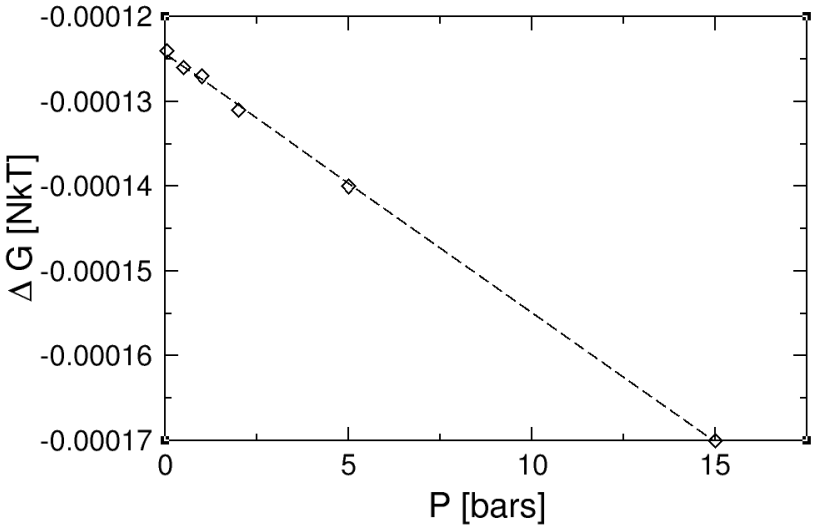

Figure 7.23: Gibbs free energy difference,$\Delta G_{l,h}/Nk_{\mathrm{B}}T$, reweighted from $T = 478$K to $T = 470$K for a range of pressures, diamond points with linear fit shown as dashed black line.

We have shown that the coarse-grain potential of Hadley and McCabe has a phase transition between the two solid anhydrous polymorphs. The direction of the transition in the model is the same as for cholesterol. However, the transition temperature in the model of $T = 470$K is well above biologically relevant temperatures and the experimental melting temperature of $T = 422$K However, the melting temperature of the model is also higher than it should be by around 100K

The model shows great promise and, to our knowledge, is the first force field of cholesterol with a known and located polymorphic solid phase transition. However, more work could be done to modify the model and make it more suitable for further use.

In section 3.1.2 we saw that the average error in the calculation for a free energy difference using thermodynamic integration is $1 \times 10^{-3} Nk_{\mathrm{B}}T$, where the absolute free energy is around $5Nk_{\mathrm{B}}T$. If we used TI to try and calculate the phase

transition for cholesterol, our accuracy would not be enough to differentiate between a wide range of temperatures. At a temperature of 478K our free energy is already down to the order of the error in TI calculations. This suggests that the error on the transition temperature would be around ±8K if we used thermodynamic integration for this calculation. This is a much greater error than using phase switch Monte Carlo and really highlights the need for accurate methods of free energy calculation.

When the systems of interest get larger and more complex, the more likely it is to have a large absolute free energy. This means that the error from using TI is likely to be even greater that $10^{-3}Nk_{\mathrm{B}}T$ as we would have to take the difference between much larger numbers and so in order to get the same degree of accuracy the initial calculations of the absolute free energy would have to be even more accurate. Phase switch MC has no such problem since it only deals with relative free energies.

The error in our calculations has two main sources, the statistical error in the results and finite size error. The statistical error is controlled by calculating the correlation length of our data and only sampling that often when averaging our results. The finite size error in this work is unknown because we only simulated one system size. This is due to the large size of the unit cell of cholesterol and the length of the cutoff. The large cutoff makes speeding up the simulations difficult as we need to include a lot of particles in the energy calculations. However, the advantage of the large unit cell is that the system is likely to be large enough for finite size effects to have minimal effect.

We can compare this biasing function and normalised probability distributions with those generated from the butane model (section 5.10.1). The two probability distribution functions have a significantly different form, the butane model has a much narrower and symmetric peak compared to the sharp peak and long tail of the cholesterol model. This is probably due to the difference between hard spheres and soft potentials; there is a higher possibility for the passive system to have very high energy in a soft model. The minimum of the biasing function is at zero for hard spheres, as we would expect the gateway order parameter to be the hardest to reach. For the cholesterol biasing function, the minimum is at positive order parameter values for $T = 384$K and $T = 404$K and is fairly constant across to negative order parameter values where it sharply rises followed by slow straight descent. The minimum is not a zero due to the volume and energy differences between the two systems and the need to account for this in the order parameter. The sign of the order parameter value corresponding to the minimum of the bias function changes sign after the phase transition, as can be seen from Figures 7.19 and 7.15).

An interesting artefact of our simulations is the need to increase the width of

the order parameter range sampled as we get closer to the transition. At $T = 274$K the quasi-stationary distribution (Figure 7.4) goes to zero by $\mathcal{M} = \pm 15$, whereas at $T = 478$K a range of $\mathcal{M} = \pm 35$ or greater is necessary. This suggests that as we get closer to the transition, the systems explore a much wider tract of order parameter space. This can also help to explain why histogram reweighting for $T = 404$K did not predict the correct transition temperature. The larger order parameter states will not have been sampled enough from a lower temperature and hence do not contribute enough weight to the reweighted histogram. This explains why histogram reweighting overestimated the transition temperature as large, positive order parameter states would not have been sample enough. Since our final use of histogram reweighting, was to narrow down the transition temperature from $T = 478$K only reweighted by 8K, the probability distributions overlap almost completely and hence our resulting transition temperature is reliable and another simulation at the transition temperature is unnecessary.

Chapter 8

Conclusion

The aim of this thesis has been to address the need for more accurate free energy calculations between crystal polymorphs of flexible molecular systems. We demonstrated that existing methods are limited in their accuracy by the need to calculate absolute free energies and take the difference. Inclusion of the ability to treat flexible molecules is needed to open up phase switch Monte Carlo to a much wider array of systems and applications.

Chapter 4 shows that our alternative 'logical' implementation of phase switch MC is equivalent to the existing 'geometric' approach. We reproduce all key results in the literature to within the stated errors for both Helmholtz and Gibbs free energy differences. There was one discrepancy between our work and that in Bruce et al. [17] for a system size of $N = 216$ at a constant pressure. However, our results for larger systems at the same pressure agreed well with the work of Bruce et al. [17]. This suggests that the discrepancy may be due to a typographical error in their results table. The methodology used in this thesis does not use the optimal mapping as used by Bruce et al. [16], and will be significantly less efficient but this allows us to generalise to a much wider set of systems.

We extended this work on hard sphere crystals to investigate the role of anisotropic volume moves. Our calculated Gibbs free energy difference showed no significant variation from that calculated with isotropic volume moves. We also investigated the inherent uncertainty in the method by comparing two fcc crystals with different labelling. We showed that the result converges to zero quickly and the variation from zero is much smaller than the uncertainty of our previous calculations between fcc and hcp.

In chapter 5 our extension of phase switch MC to hard-sphere models with internal flexibility, bond, and angle constraints was introduced. We tested it upon

a linked chain model of butane, where our work was validated against previous calculations in the literature. We also found a previously unreported phase transition in density between phase I and phase III. The importance of anisotropic volume moves was highlighted for this system.

We have shown that for hard sphere systems the calculation of Gibbs free energy difference between polymorphs with different cell dimensions is difficult. Further work needs to be done, for example splitting the weighting function either into completely separate functions or splitting the $\mathcal{M} = 0$ bin by volume differences. However, this is a small subset of possible uses and does not affect soft potentials.

The hard sphere linked chain model does not include the rotational disorder in the high temperature phase (phase I) that exists in butane. Therefore, we cannot extrapolate our result from the linked chain model to the behaviour of butane, see section 5.1. Inclusion of this rotational disorder would increase the entropy of phase I and hence increase the density at which the phase transition occurs. However, it might also remove the transition completely.

The uncertainty in our calculated transition density comes partially from the extrapolation from points of known free energy, which can be reduced by increasing the accuracy of our simulations by running them for longer. However, a reasonable compromise has been reached between length of simulation and accuracy. The uncertainty is also becuase it is a first order transition. Another contribution to the uncertainty in our simulations is from the fixed length of our runs. This gives us a fixed convergence of the biasing function; from the literature discussion of similar methods we could do further work on adapting our reduction in increment factor. However, since we can accurately calculate free energy differences of order $10^{-5} k_{\mathrm{B}} T$ per molecule this is not necessary. The error from finite size effects was investigated and it was concluded that we had used a system large enough and with a known uncertainty. The statistical uncertainty in our results was accounted for by calculating the correlation length and averaging over samples taken at that interval.

We implemented a framework to further extend this method to any fully flexible molecular system with a soft potential in chapter 7.

Another objective of this work was to investigate cholesterol force fields for solid-solid polymorphism. In chapter 7 our fully flexible phase switch MC code, Phlex, was used to study a coarse-grain model of cholesterol that had been shown to include both solid anhydrous phases. Since the two phases are very similar in structure, we used the phase switch method as a high degree of accuracy was likely to be necessary. We also used MC because the CG potential is extremely sharp and jagged and the forces used in MD may cause problems during thermodynamic

integration. Using the MC method and histogram reweighting, we located a phase transition between the two phases at $T = 470 \pm 1$K.

Taken into account in this transition temperature is the statistical error in the data, by calculating the correlation length and only sampling that often when averaging the data. However, the finite size effects are unknown, but due to the large size of the unit cell of cholesterol, they are unlikely to have a great effect.

No other force fields, to our knowledge, have been investigated in regards to this solid-solid phase transition in anhydrous cholesterol. Very few have even been probed as to whether the crystals structures are mechanically stable during simulations. There is a broad field of study into crystallisation and cholesterol's role in the body that needs this knowledge and we have shown that a CG force field can reproduce that behaviour. The transition point is too high by over 100K, however, so is the melting temperature of the model. This suggests that the model can be used to effectively study the role of cholesterol crystallisation in biological processes with some adjustments. In order to study crystalline cholesterol in bilayers some more work needs to be done with this model to characterise its behaviour in bilayers first. There is also no knowledge of whether this model can be used to study the monohydrate crystalline form.

Inclusion of parallelism into the phase switch MC method makes it very computationally competitive. The length of our simulations would be prohibitive without the parallel walkers scheme to concurrently update a single biasing function; this inclusion reduces the time cost at the expense of extra processing power. The number of CPUs necessary to speed up the computation is not excessive and is easily obtained with today's wide availability of processing. Since we are basically simulating completely separate systems on each CPU, the scaling is extremely close to perfect and any number of processors may be used.

When trying to calculate a free energy difference far from a phase transition, phase switch MC will not work very well. It will establish which phase is stable but may not sample the transition accurately. Therefore, it should be used alongside thermodynamic integration when closer calculation of a transition is necessary. It may be especially useful when phase transitions need to be pinpointed for further use in studying crystallisation and nucleation. Definitive and accurate knowledge of the phase diagram of models is necessary for investigation into crystal growth behaviour.

Looking at calculations of free energy differences using thermodynamic integration in the literature, the typical error in the results are of the order of $10^{-3} N k_{\mathrm{B}} T$ up to $0.07 N k_{\mathrm{B}} T$ for hard spheres and hard sphere linked chain models. The er-

rors calculated from phase switch MC are orders of magnitude smaller. For the linked chain model, we showed that the error given for calculation of the Helmholtz free energy using thermodynamic integration would have led to an uncertainty of $\rho\sigma^3 = \pm 0.3$ in the transition density, compared to our uncertainty of ± 0.001; the need for phase switch MC is clear. Even with the improvement in computers, thermodynamic integration will always be limited by the ratio between the absolute free energies and the free energy difference of interest. Wilms et al. [117] compared TI and phase switch MC calculations of the same result and found the error from TI to be at least an order of magnitude larger than from the phase switch method, which shows that even improvements in computing capabilities cannot improve the uncertainty in TI calculations of free energy differences.

For our calculation of the transition in the CG model of cholesterol, we estimated that thermodynamic integration would have an error of ± 8K compared to our error of ± 1K This estimation used the errors quoted from calculations of hard sphere crystals and did not take into account the more complex system and larger system size for the cholesterol model; these issues would likely increase the error from thermodynamic integration even further.

Further work including this methodology into a large-scale, parallel, open source scientific code would allow for much greater use and availability. This would involve accounting for a wider range of possible constraints and possible topologies in systems. However, we have established the framework for this and only small changes to the calculation of the generalised coordinates would be necessary. Phase switch MC has previously been extended to fluid-solid [34] and binary phase transitions [55]; an extension of our framework for flexible molecules to include these would be very useful and enhance the range of applications greatly.

It is also worth investigating new methods to the sampling of our simulations. Schultz and Kofke [91] introduced an alternative method for isothermal-isobaric MC simulations to increase the efficiency of volume moves. This has not been tested for flexible molecules and the authors suggest that is will be most beneficial for hard potentials. This method also has the potential to be utilised alternatively as a novel biasing scheme.

Appendix A

Quaternions

When making a rotation in $\mathcal{R}(3)$ using 3 angles, e.g. Euler angles, one must always be aware of the presence of at least one singularity. This is often called a gimbal lock, when two axes become aligned, this causes the system to lose one degree of freedom. It is especially problematic when flying a spacecraft. Hence, the need for a description of rotations that is free of singularities. Quaternions are a representation of rotations without singularities and with the bonus of more computationally efficient algorithms.

Quaternions are a set, $\mathcal{H}$, of hyper-complex numbers of rank 4. The basis elements of this set are usually denoted as $1, i, j$ and k, where i, j and k are the imaginary parts. Every quaternion can be written as a linear combination of the basis set, $q = q_0 + q_1 i + q_2 j + q_3 k = (q_0, q_1, q_2, q_3)$, where q_0, q_1, q_2 and q_3 are real numbers. The basis elements obey the equations,

$$i^2 = j^2 = k^2 = ijk = -1. \tag{A.1}$$

All possible products of i, j and k can be determined from these equations.

A.1 Quaternion Algebra

Two quaternions are only equal if they have exactly the same components, $q = p$ if and only if,

$$\begin{aligned} q_0 &= p_0 \\ q_1 &= p_1 \\ q_2 &= p_2 \\ q_3 &= p_3 \end{aligned}$$

The quaternion conjugate can be written in the form

$$\bar{q} = (q_0, -q_1, -q_2, -q_3). \tag{A.2}$$

The sum of two quaternions is then

$$q + p = (q_0 + p_0, q_1 + p_1, q_2 + p_2, q_3 + p_3), \tag{A.3}$$

the norm of a quaternion is defined as

$$|q| = \sqrt{q\bar{q}} = \sqrt{q_0^2 + q_1^2 + q_2^2 + q_3^2} \tag{A.4}$$

the inverse (reciprocal) of a quaternion if given by

$$q^{-1} = \frac{\bar{q}}{|q|^2} \tag{A.5}$$

such that

$$q^{-1}q = qq^{-1} = 1. \tag{A.6}$$

When the quaternion is a unit vector, that is $|q| = 1$, then $\bar{q} = q^{-1}$.

Unlike real numbers, quaternion multiplication is non-commutative, e.g. $ij = k$, while $ji = -k$. This is comparable to the order of rotations being essential, as rotations made in a different order will give a different result.

A.2 Applying rotations

The rotation of a vector can be given as

$$v' = qvq^{-1} = qv\bar{q}, \tag{A.7}$$

The combination of rotations q and then p is then

$$p(qv\bar{q})\bar{p} = (pq)v(\bar{q}\bar{p}) = (pq)v(\bar{qp}) = Qv\bar{Q}, \tag{A.8}$$

so rotations can be compounded together via multiplication before computation of the rotation.

A.3 Minimum arc

We can calculate the normalised quaternion required to rotate vectors $\underline{v}_1$ onto $\underline{v}_2$ by

$$q_0 = \sqrt{(\underline{v}_1 \cdot \underline{v}_1)(\underline{v}_2 \cdot \underline{v}_2)} + \underline{v}_1 \cdot \underline{v}_2 \tag{A.9}$$

$$(q_1, q_2, q_3) = \underline{v}_1 \times \underline{v}_2. \tag{A.10}$$

To ensure the quaternion is normalised, the vectors $\underline{v}_{1,2}$ must be normalised.

A.4 Axis angle representation

The rotation by an angle θ about an axis $\underline{a}$ can be converted to a quaternion as follows,

$$q_0 = \cos\left(\frac{\theta}{2}\right) \tag{A.11}$$

$$(q_1, q_2, q_3) = \underline{a}\sin\left(\frac{\theta}{2}\right), \tag{A.12}$$

where $\underline{a}$ is a unit vector and θ is in radians.

Bibliography

[1] G S Abela and K Aziz. Cholesterol crystals rupture biological membranes and human plaques during acute cardiovascular events-a novel insight into plaque rupture by scanning electron microscopy. *Scanning*, 28(1):1–10, 2006.

[2] G S Abela, K Aziz, A Vedre, D R Pathak, J D Talbott, and J DeJong. Effect of Cholesterol Crystals on Plaques and Intima in Arteries of Patients With Acute Coronary and Cerebrovascular Syndromes. *Am. J. Cardiol.*, 103:959–968, 2009.

[3] R S Abendan and J A Swift. Dissolution on Cholesterol Monohydrate Single-Crystal Surfaces Monitored by in Situ Atomic Force Microscopy. *Cryst. Growth Des.*, 5(6):2146–2153, 2005.

[4] E R Andrew and B Peplinska. NMR study of solid cholesterol. *Mol. Phys.*, 70(3):505–512, 1990.

[5] J G Aston and G H Messerly. The Heat Capacity and Entropy, Heats of Fusion and Vaporization and the Vapor Pressure of n-Butane. *J. Am. Chem. Soc.*, 62(8):1917–1923, 1940.

[6] D Bach. Phospholipid/cholesterol model membranes: formation of cholesterol crystallites. *Biochim. Biophys. Acta - Biomembr.*, 1610(2):187–197, 2003.

[7] R E Belardinelli and V D Pereyra. Wang-Landau algorithm: A theoretical analysis of the saturation of the error. *J. Chem. Phys.*, 127(18):184105, 2007.

[8] R E Belardinelli, S. Manzi, and V. Pereyra. Analysis of the convergence of the 1/t and Wang-Landau algorithms in the calculation of multidimensional integrals. *Phys. Rev. E*, 78(6):067701, 2008.

[9] B A Berg and T Neuhaus. Multicanonical algorithms for first order phase transitions. *Phys. Lett. B.*, 267(2):249–253, 1991.

[10] B A Berg, U Hansmann, and T Neuhaus. Properties of interfaces in the two and three dimensional Ising model. *Phys. B Condens. Matter*, 90(2):229–239, 1993.

[11] K Bloch. *Sterol Structure and Membrane Function.* Conant Laboratories Harvard University Cambridge, Massachusetts, 1981.

[12] D Bluestein, Y Alemu, I Avrahami, M Gharib, K Dumont, J J Ricotta, and S Einav. Influence of microcalcifications on vulnerable plaque mechanics using FSI modeling. *J. Biomech.*, 41(5):1111–1118, 2008.

[13] R Boese, H Weiss, and D Blöser. The Melting Point Alternation in the Short-Chain n-Alkanes: Single-Crystal X-Ray Analyses of Propane at 30 K and of n-Butane to n-Nonane at 90 K. *Angew. Chem. Int. Ed. Engl.*, 38(7):988–992, 1999.

[14] H Bogren and K Larsson. An X-ray-diffraction study of crystalline cholesterol in some pathological deposits in man. *Biochim. Biophys. Acta*, 75(0):65–69, 1963.

[15] B R Brooks, R E Bruccoleri, B D Olafson, D J States, S Swaminathan, and M Karplus. CHARMM: A program for macromolecular energy, minimization, and dynamics calculations. *J. Comput. Chem.*, 4(2):187–217, 1983.

[16] A D Bruce, N B Wilding, and G J Ackland. Free energy of crystalline solids: A Lattice-Switch Monte-Carlo Method. *Phys. Rev. Lett.*, 79(16):3002–3005, 1997.

[17] A D Bruce, A N Jackson, G J Ackland, and N B Wilding. Lattice-Switch Monte-Carlo Method. *Phys. Rev. E.*, 61(1):906–919, 2000.

[18] M Cao and P A Monson. Solid-Fluid and Solid-Solid Equilibrium in Hard Sphere United Atom Models of n-Alkanes: Rotator Phase Stability. *J. Phys. Chem. B*, 113(42):13866–13873, 2009.

[19] A Catte, J C Patterson, D Bashtovyy, M K Jones, F Gu, L Li, A Rampioni, D Sengupta, T Vuorela, P Niemel, M Karttunen, S J Marrink, I Vattulainen, and J P Segrest. Structure of spheroidal HDL particles revealed by combined atomistic and coarse-grained simulations. *Biophys. J.*, 94(6):2306–2319, 2008.

[20] E R Chan, A Striolo, C McCabe, P T Cummings, and Sharon C Glotzer. Coarse-grained force field for simulating polymer-tethered silsesquioxane self-assembly in solution. *J. Chem. Phys.*, 127(11):114102, 2007.

[21] Z Cournia, A C Vaiana, G M Ullmann, and J C Smith. Derivation of a molecular mechanics force field for cholesterol. *Pure Appl. Chem.*, 76(1):189–196, 2004.

[22] Z Cournia, J C Smith, and G M Ullmann. A molecular mechanics force field for biologically important sterols. *J. Comput. Chem.*, 26(13):1383–1399, 2005.

[23] B M Craven. Crystal structure of cholesterol monohydrate. *Nature*, 260: 727–729, 1976.

[24] S R T Cromie and P Ballone. Structural motifs of cholesterol nanoparticles. *J. Chem. Phys.*, 131(1):034906, 2009.

[25] S R T Cromie, M G Del Pópolo, and P Ballone. Interaction of room temperature ionic liquid solutions with a cholesterol bilayer. *J. Phys. Chem. B*, 113 (34):11642–8, 2009.

[26] A G Cunha-Netto, A A Caparica, S Tsai, R Dickman, and D P Landau. Improving Wang-Landau sampling with adaptive windows. *Phys. Rev. E (Statistical, Nonlinear, Soft Matter Physics)*, 78(5):55701, 2008.

[27] A G Cunha-Netto, R Dickman, and A A Caparica. Two-dimensional lattice polymers: Adaptive windows simulations. *Comput. Phys. Commun.*, 180(4): 583–586, 2009.

[28] G M Day, W D S Motherwell, H L Ammon, S X M Boerrigter, R G Della Valle, E Venuti, a Dzyabchenko, J D Dunitz, B Schweizer, B P van Eijck, P Erk, J C Facelli, V E Bazterra, M B Ferraro, D W M Hofmann, F J J Leusen, C Liang, C C Pantelides, P G Karamertzanis, S L Price, T C Lewis, H Nowell, a Torrisi, H a Scheraga, Y a Arnautova, M U Schmidt, and P Verwer. A third blind test of crystal structure prediction. *Acta Crystallogr. B.*, 61(Pt 5):511–27, 2005.

[29] P M C de Oliveira, T J P Penna, and H J Herrmann. Broad histogram Monte Carlo. *Eur. Phys. J. B - Condens. Matter Complex Syst.*, 1(2):205–208, 1998.

[30] R Dickman and C K Hall. High density Monte Carlo simulations of chain molecules: Bulk equation of state and density profile near walls. *J. Chem. Phys.*, 89(5):3168–3174, 1988.

[31] M T Dove. *Introduction to Lattice Dynamics*. Cambridge Topics in Mineral Physics and Chemistry. Cambridge University Press, 1993.

[32] D J Earl and M W Deem. Markov chains of infinite order and asymptotic satisfaction of balance: application to the adaptive integration method. *J. Phys. Chem. B*, 109(14):6701–4, 2005.

[33] R M Epand, D Bach, N Borochov, and E Wachtel. Cholesterol crystalline polymorphism and the solubility of cholesterol in phosphatidylserine. *Biophys. J.*, 78(2):866–73, 2000.

[34] J R Errington. Solid-liquid phase coexistence of the Lennard-Jones system through phase-switch Monte Carlo simulation. *J. Chem. Phys.*, 120(7):3130–3141, 2004.

[35] F A Escobedo and J J de Pablo. Extended continuum configurational bias Monte Carlo methods for simulation of flexible molecules. *J. Chem. Phys.*, 102(6):2636–2652, 1995.

[36] A M Ferrenberg and R H Swendsen. New Monte-Carlo Technique for Studying Phase Transitions. *Phys. Rev. Lett.*, 61(23):2635–2638, 1988.

[37] L X Finegold. *Cholesterol in Membrane Models*. Taylor & Francis, 1992. ISBN 9780849342073.

[38] D Frenkel and A J C Ladd. New Monte-Carlo method to compute the free energy of arbitrary solids. Application to the fcc and hcp phases of hard spheres. *J. Chem. Phys*, 81(7):3188–3193, 1984.

[39] D Frenkel and B Smit. *Understanding Molecular Simulation: From Algorithms to Applications*. Academic Press, 2 edition, 2002. ISBN 9780122673511.

[40] M C Frincu, S D Fleming, A L Rohl, and J A Swift. The Epitaxial Growth of Cholesterol Crystals from Bile Solutions on Calcite Substrates. *J. Am. Chem. Soc.*, 126(25):7915–7924, 2004.

[41] M C Frincu, R E Sharpe, and J A Swift. Epitaxial Relationships between Cholesterol Crystals and Mineral Phases: Implication for Human Disease. *Cryst. Growth Des.*, 4(2):223–226, 2004.

[42] V Fuster, P R Moreno, Z A Fayad, R Corti, and J J Badimon. Atherothrombosis and High-Risk Plaque: Part I: Evolving Concepts. *J. Am. Coll. Cardiol.*, 46(6):937–954, 2005.

[43] N Garti, L Karpuj, and S Sarig. Phase transitions in cholesterol crystallized from various solvents. *Thermochim. Acta*, 35(3):343–348, 1980.

[44] W Guo and J A Hamilton. A Multinuclear Solid-State NMR Study of Phospholipid-Cholesterol Interactions. Dipalmitoylphosphatidylcholine-Cholesterol Binary System. *Biochemistry*, 34(43):14174–14184, 1995.

[45] W Guo, J D Morrisett, M E DeBakey, G M Lawrie, and J A Hamilton. Quantification In Situ of Crystalline Cholesterol and Calcium Phosphate Hydroxyapatite in Human Atherosclerotic Plaques by Solid-State Magic Angle Spinning NMR. *Arter. Thromb. Vasc. Biol.*, 20(6):1630–1636, 2000.

[46] K R Hadley and C McCabe. A coarse-grained model for amorphous and crystalline fatty acids. *J. Chem. Phys.*, 132(13):134505, 2010.

[47] K R Hadley and C McCabe. A Structurally Relevant Coarse-Grained Model for Cholesterol. *Biophys. J.*, 99(9):2896–2905, 2010.

[48] A T Hagler, E Huler, and S Lifson. Energy functions for peptides and proteins. I. Derivation of a consistent force field including the hydrogen bond from amide crystals. *J. Am. Chem. Soc.*, 96(17):5319–5327, 1974.

[49] M J R Hoch. An NMR study of molecular reorientation processes in solid nbutane. *J. Chem. Phys.*, 65(7):2522–2526, 1976.

[50] W G Hoover and F H Ree. Use of computer experiments to locate the melting transition and calculate the entropy in the solid phase. *J. Chem. Phys.*, 47: 4873–4878, 1967.

[51] L Hsu and C Nordman. Phase transition and crystal structure of the $37°C$ form of cholesterol. *Science*, 220(4597):604–606, 1983.

[52] L Hsu, J W Kampf, and C E Nordman. Structure and pseudosymmetry of cholesterol at 310K. *Acta Crystallogr. Sect. B*, 58(2):260–264, 2002.

[53] M J Hwang, T P Stockfisch, and A T Hagler. Derivation of Class II Force Fields. 2. Derivation and Characterization of a Class II Force Field, CFF93, for the Alkyl Functional Group and Alkane Molecules. *J. Am. Chem. Soc.*, 116(6):2515–2525, 1994.

[54] J P Incardona and S Eaton. Cholesterol in signal transduction. *Curr. Opin. Cell Biol.*, 12(2):193–203, 2000.

[55] A N Jackson and G J Ackland. Lattice-switch Monte Carlo simulation for binary hard-sphere crystals. *Phys. Rev. E*, 76(6):66703, 2007.

[56] A N Jackson, A D Bruce, and G J Ackland. Lattice-switch Monte Carlo method: Application to soft potentials. *Phys. Rev. E*, 65(3):36710, 2002.

[57] K Jayalakshmi, K Sonkar, A Behari, V K Kapoor, and N Sinha. Solid state 13 C NMR analysis of human gallstones from cancer and benign gall bladder diseases. *Solid State Nucl. Magn. Reson.*, 36(1):60–65, 2009.

[58] W L Jorgensen, D S Maxwell, and J Tirado-Rives. Development and Testing of the OPLS All-Atom Force Field on Conformational Energetics and Properties of Organic Liquids. *J. Am. Chem. Soc.*, 118(45):11225–11236, 1996.

[59] J Kaloustian, A Pauli, P de la Porte, H Lafont, and H Portugal. Thermal analysis of anhydrous and hydrated Cholesterol. *J. Therm. Anal. Calorim.*, 71(2):341–351, 2003.

[60] J Kim, J E Straub, and T Keyes. Statistical-Temperature Monte Carlo and Molecular Dynamics Algorithms. *Phys. Rev. Lett.*, 97(5):050601, 2006.

[61] F M Konikoff, D S Chung, J M Donovan, D M Small, and M C Carey. Filamentous, helical, and tubular microstructures during cholesterol crystallization from bile. Evidence that cholesterol does not nucleate classic monohydrate plates. *J. Clin. Invest.*, 90(3):1155–1160, 1992.

[62] L C Labowitz. A previously unreported phase transition in cholesterol at $37°C$ and its possible significance in arteriosclerosis. *Thermochim. Acta*, 3(5): 419–420, 1972.

[63] Y W Li, T Wüst, D P Landau, and H Q Lin. Numerical integration using Wang Landau sampling. *Comput. Phys. Commun.*, 177(6):524–529, 2007.

[64] C Liang, L Yan, J Hill, C S Ewig, T R Stouch, and A T Hagler. Force field studies of cholesterol and cholesteryl acetate crystals and cholesterol-cholesterol intermolecular interactions. *J. Comput. Chem.*, 16(7):883–897, 1995.

[65] S Lifson, A T Hagler, and P Dauber. Consistent force field studies of intermolecular forces in hydrogen-bonded crystals. 1. Carboxylic acids, amides, and the C:O...H- hydrogen bonds. *J. Am. Chem. Soc.*, 101(18):5111–5121, 1979.

[66] C R Loomis, G G Shipley, and D M Small. The phase behavior of hydrated cholesterol. *J. Lipid Res.*, 20(4):525–535, 1979.

[67] R Lustig. Surface and volume of three, four, six and twelve hard fused spheres. *Mol. Phys.*, 55(2):305–317, 1985.

[68] L Mainali, M Raguz, and W K Subczynski. Formation of cholesterol bilayer domains precedes formation of cholesterol crystals in cholesterol/dimyristoylphosphatidylcholine membranes: EPR and DSC studies. *J. Phys. Chem. B*, 117(30):8994–9003, 2013.

[69] A P Malanoski and P A Monson. The high density equation of state and solid-fluid equilibrium in systems of freely jointed chains of tangent hard spheres. *J. Chem. Phys.*, 107(17):6899–6907, 1997.

[70] A P Malanoski and P A Monson. Solid-fluid equilibrium in molecular models of n-alkanes. *J. Chem. Phys*, 110(1):664–675, 1999.

[71] A P Malanoski and P A Monson. Erratum "Solid-fluid equilibrium in molecular models of n-alkanes". *J. Chem. Phys.*, 118(2):995, 2003.

[72] J R Maple, M J Hwang, T P Stockfisch, U Dinur, M Waldman, C S Ewig, and A T Hagler. Derivation of Class II Force Fields. I. Methodology and Quantum Force Field for the Alkyl Functional Group and Alkane Molecules. *J. Comput. Chem.*, 15(2):162–182, 1994.

[73] S Mau and David A Huse. Stacking entropy of hard-sphere crystals. *Phys. Rev. E*, 59(4):4396–4401, 1999.

[74] G C McNeil-Watson, C Graham, and N B Wilding. Freezing line of the Lennard-Jones fluid: A phase switch Monte Carlo study. *J. Chem. Phys.*, 124 (6):64504, 2006.

[75] N Metropolis, A W Rosenbluth, M N Rosenbluth, A H Teller, and E Teller. Equation of State Calculations by Fast Computing Machines. *J. Chem. Phys.*, 21(6):1087–1092, 1953.

[76] A Morozov and S Lin. Accuracy and convergence of the Wang-Landau sampling algorithm. *Phys. Rev. E*, 76(2):026701, 2007.

[77] W G Noid. Perspective: Coarse-grained models for biomolecular systems. *J. Chem. Phys.*, 139(9):090901, 2013.

[78] P Padilla and S Toxvaerd. Self-diffusion in n-alkane fluid models. *J. Chem. Phys.*, 94(8):5650–5654, 1991.

[79] M Parrinello. Polymorphic transitions in single crystals: A new molecular dynamics method. *J. Appl. Phys.*, 52(12):7182, 1981.

[80] E Plesnar, W K Subczynski, and M Pasenkiewicz-Gierula. Comparative computer simulation study of cholesterol in hydrated unary and binary lipid bilayers and in an anhydrous crystal. *J. Phys. Chem. B*, 117(29):8758–69, 2013.

[81] J M Polson and D Frenkel. Calculation of solid-fluid phase equilibria for systems of chain molecules. *J. Chem. Phys.*, 109(1):318–328, 1998.

[82] J. M. Polson, E. Trizac, S. Pronk, and D. Frenkel. Finite-size corrections to the free energies of crystalline solids. *J. Chem. Phys.*, 112(12):5339, 2000.

[83] S Poyry, T Rog, M Karttunen, and I Vattulainen. Significance of Cholesterol Methyl Groups. *J. Phys. Chem. B*, 112(10):2922–2929, 2008.

[84] S Pronk and D Frenkel. Can stacking faults in hard-sphere crystals anneal out spontaneously? *J. Chem. Phys.*, 110(9):4589–4592, 1999.

[85] P Raiteri, J D Gale, D Quigley, and P M Rodger. Derivation of an accurate force-field for simulating the growth of calcium carbonate from aqueous solution: a new model for the calcite-water interface. *J. Phys. Chem. C*, 114(13): 5997–6010, 2010.

[86] K Refson and G S Pawley. The structure and orientational disorder in solid n-butane by neutron powder diffraction. *Acta Crystallogr. Sect. B*, 42(4): 402–410, 1986.

[87] D Reith, M Pütz, and F Müller-Plathe. Deriving effective mesoscale potentials from atomistic simulations. *J. Comput. Chem.*, 24(13):1624–36, 2003.

[88] J Ryckaert and A Bellemans. Molecular dynamics of liquid alkanes. *Faraday Discuss. Chem. Soc.*, 66(0):95–106, 1978.

[89] J Ryckaert and M L Klein. Translational and rotational disorder in solid n-alkanes: Constant temperature-constant pressure molecular dynamics calculations using infinitely long flexible chains. *J. Chem. Phys.*, 85(3):1613–1620, 1986.

[90] J Ryckaert, I R McDonald, and M L Klein. Disorder in the pseudohexagonal rotator phase of n-alkanes: molecular-dynamics calculations for tricosane. *Mol. Phys.*, 67(5):957–979, 1989.

[91] A J Schultz and D A. Kofke. Algorithm for constant-pressure monte carlo simulation of crystalline solids. *Phys. Rev. E*, 84(4):046712, 2011.

[92] B J Schulz, K Binder, M Müller, and D P Landau. Avoiding boundary effects in Wang-Landau sampling. *Phys. Rev. E*, 67(6):67102, 2003.

[93] J L Sheumaker and J K Guillory. Polymorphism in cholesterol. *Thermochim. Acta*, 5:355–356, 1973.

[94] H S Shieh, Hoard L G, and Nordman C E. Crystal structure of anhydrous cholesterol. *Nature*, 267:287–289, 1977.

[95] H.-S. S. Shieh, L. G. Hoard, and C. E. Nordman. The structure of cholesterol. *Acta Crystallogr. Sect. B*, 37(8):1538–1543, 1981.

[96] J I Siepmann and D Frenkel. Configurational bias Monte Carlo : a new sampling scheme for flexible chains. *Mol. Phys.*, 75(1):59–70, 1992.

[97] S W I Siu, K Pluhackova, and R A Böckmann. Optimization of the OPLS-AA Force Field for Long Hydrocarbons. *J. Chem. Theory Comput.*, 8(4): 1459–1470, 2012.

[98] G R Smith and Bruce. A study of the multi-canonical Monte Carlo method. *J. Phys. A. Math. Gen.*, 28(23):6623, 1995.

[99] W Smith and T R Forester. DL_POLY_2.0: A general-purpose parallel molecular dynamics simulation package. *J. Mol. Graph.*, 14(3):136–141, 1996.

[100] I Solomonov, M J Weygand, K Kjaer, H Rapaport, and L Leiserowitz. Trapping Crystal Nucleation of Cholesterol Monohydrate: Relevance to Pathological Crystallization. *Biophys. J.*, 88:1809–1817, 2005.

[101] K Sonkar, N Sinha, S de Gironcoli, and E Kucukbenli. Complete C13 NMR Chemical Shifts Assignment for Cholesterol Crystals by Combined CP-MAS Spectral Editing and ab initio CIPAW Calculations with Dispersion Forces. *J. Phys. Chem. A*, 116(14):3765–3769, 2012.

[102] H L Spier and K G van Senden. Phase transition of cholesterol. *Steroids*, 6 (6):871–874, 1965.

[103] M B Sweatman. New techniques for simulating crystals. *Mol. Simul.*, 35 (10-11):897–909, 2009.

[104] I T Todorov, W Smith, K Trachenko, and M T Dove. DL_POLY_3: new dimensions in molecular dynamics simulations via massive parallelism. *J. Mater. Chem.*, 16:1911–1918, 2006.

[105] G M Torrie and J P Valleau. Monte Carlo free energy estimates using non-Boltzmann sampling: Application to the sub-critical Lennard-Jones fluid. *Chem. Phys. Lett.*, 28(4):578–581, 1974.

[106] K van Putte, W Skoda, and M Petroni. Phase transition and CH3-rotation in solid cholesterol. *Chem. Phys. Lipids*, 2(4):361–371, 1968.

[107] A Vedre, D R Pathak, M Crimp, C Lum, M Koochesfahani, and G S Abela. Physical factors that trigger cholesterol crystallization leading to plaque rupture. *Atherosclerosis*, 203(1):89–96, 2009.

[108] C Vega and E G Noya. Revisiting the Frenkel-Ladd method to compute the free energy of solids: The Einstein molecule approach. *J. Chem. Phys.*, 127 (15):154113, 2007.

[109] C Vega, S Lago, and B Garzon. Virial coeffcients and equation of state of hard alkane models. *J. Chem. Phys.*, 100(3):2182, 1994.

[110] F Wang and D P Landau. Efficient, multiple-range random walk algorithm to calculate the density of states. *Phys. Rev. Lett.*, 86(10):2050–2053, 2001.

[111] J Wang and L W Lee. Monte Carlo algorithms based on the number of potential moves. *Comput. Phys. Commun.*, 127(1):131–136, 2000.

[112] J Wang and R H Swendsen. Transition Matrix Monte Carlo Method. *J. Stat. Phys.*, 106:245, 2002.

[113] P K Weiner and P A Kollman. AMBER: Assisted model building with energy refinement. A general program for modeling molecules and their interactions. *J. Comput. Chem.*, 2(3):287–303, 1981.

[114] N B Wilding. Critical-point and coexistence-curve properties of the Lennard-Jones fluid: A finite-size scaling study. *Phys. Rev. E.*, 52(1):602–611, 1995.

[115] N B Wilding. Computer Simulation of Fluid Phase Transitions. *Am. J. Phys.*, 69:1147, 2001.

[116] N B Wilding. A new simulation approach to the freezing transition. *Comput. Phys. Commun.*, 146(1):99–106, 2002.

[117] D Wilms, N B Wilding, and K Binder. Transitions between imperfectly ordered crystalline structures: A phase switch Monte Carlo study. *Phys. Rev. E*, 85(5):56703, 2012.

[118] L V Woodcock. Entropy difference between the face-centred cubic and hexagonal close-packed crystal structures. *Nature*, 385:141–143, 1997.

[119] Q Yan and J de Pablo. Fast Calculation of the Density of States of a Fluid by Monte Carlo Simulations. *Phys. Rev. Lett.*, 90(3):035701, 2003.

[120] P L Yeagle. Modulation of membrane function by cholesterol. *Biochimie*, 73 (10):1303–1310, 1991.

[121] P L Yeagle. *Structure of Biological Membranes*. Taylor & Francis, 2 edition, 2004. ISBN 9781420040203.

[122] C Zhou, T C Schulthess, S Torbrügge, and D P Landau. Wang-Landau Algorithm for Continuous Models and Joint Density of States. *Phys. Rev. Lett.*, 96(12):120201, 2006.

[123] R Ziblat, L Leiserowitz, and L Addadi. Crystalline Domain Structure and Cholesterol Crystal Nucleation in Single Hydrated DPPC:Cholesterol:POPC Bilayers. *J. Am. Chem. Soc.*, 132(28):9920–9927, 2010.